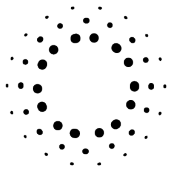

IFT - UNESP
INSTITUTO DE FÍSICA TEÓRICA

Doctorate Thesis IFT.T 06/2023

Mathematical models for ecological and evolutionary processes in biological invasions

Silas Poloni Lyra

Supervisor
Prof. Dr. Roberto André Kraenkel
Co-supervisor
Prof. Dr. Renato Mendes Coutinho

December 7, 2023

Lyra, Silas Poloni
L992m Mathematical models for ecological and evolutionary processes in biological invasions / Silas Poloni. – São Paulo, 2023
123 f.: il.

Tese (doutorado) – Universidade Estadual Paulista (Unesp), Instituto de Física Teórica (IFT), São Paulo
Orientador: Roberto André Kraenkel
Coorientador: Renato Mendes Coutinho

1. Equações de reação-difusão. 2. Biologia - Populações. 3. Matemática aplicada. I. Título

Sistema de geração automática de fichas catalográficas da Unesp. Biblioteca do Instituto de Física Teórica (IFT), São Paulo. Dados fornecidos pelo autor(a).

Dedico esta tese à
minha esposa Fernanda

Agradecimentos

Eu agradeço à minha esposa, Fernanda Moura, por todo o apoio e carinho durante toda a jornada acadêmica. Agradeço à minha mãe, por também me apoiar durante toda a jornada, não só acadêmica, mas da minha vida.

Aos meus melhores amigos, Ricardo, Bruno, Maycon e Neto, que durante a pandemia foram essenciais para que eu permanecesse alegre, mesmo em um momento tão difícil e solitário.

Eu agradeço aos meus amigos e colaboradores do Observatório Covid-19, que durante a pandemia desempenharam papel fundamental na divulgação científica, análise de dados da epidêmia e no esforço de modelagem para compreender o espalhamento da doença no Brasil durante os momentos mais críticos. Sou imensamente grato por ter tido a oportunidade de colaborar com todos.

Agradeço aos meus colabores mais próximos nominalmente: Ao meu orientador, Roberto Kraenkel, agradeço por sempre confiar em meu trabalho e me dar total liberdade e apoio em minhas ideias e investigações, e ao Renato Coutinho, por sempre me auxiliar, e a ambos por sempre estarem abertos para discutir o meu trabalho. Sem eles, o capítulo 2 dessa tese seria bem menos interessante.

Gostaria de agradecer a FAPESP pelo financiamento do doutorado e da BEPE, através dos processos 2018/24037-4 e 2020/15320-4.

A partir daqui, eu mudo o idioma para agradecer alguns amigos e colabores que conheci durante a BEPE.

I thank Prince, Jane, Cameron and Alice, for all the hospitality they offered me. Prince helped me find a place to live, and explained Canada 101 to me, Jane did all her best so I could meet new people, and Cameron and Alice where excellent new people I met. Thanks everyone for everything.

I also thank Frithjof Lutscher, who supervised me in my period abroad, for several discussions regarding the content of chapter 3, and a little bit of chapter 2 as well. Also, I'd like to thank him for trusting in my ideas and giving me all the support I needed in order to develop them.

Finally, several people helped me with chapter 3, by suggesting analyses and help with writing. Tom Hillen suggested looking at the perturbations of the multiplication operator, which led me to study C0 semi-group theory in detail, and this is now the 3rd theorem in chapter 3. Sebastian Schreiber gave significant feedback on the text. Finally, I thank Fields Institute for funding and organizing the "Workshop on New Mathematical Theory to Understand the Effects of Evolution on Range Expansion", and people that participated in it, a lot of chapter 3 was benefited from the event and discussions therein.

"Science, my lad, is made up of mistakes, but they are mistakes which it is useful to make, because they lead little by little to the truth."

Jules Verne,
A Journey to the Centre of the Earth

Resumo

Invasões biológicas são onipresentes no antropoceno. Diversos fatores influenciam como uma espécie invasora se espalha pelo novo território e as escalas espaço-temporais usuais dificultam a realização de experimentos. Assim, abordagens teóricas e quantitativas auxiliam a entender os principais fatores e estimar velocidades de invasão e mudanças de regime causadas pela espécie não nativa. Nessa tese, nós revisamos modelos matemáticos clássicos para invasões biológicas, focando em modelos de equações de reação e difusão e integrais a diferenças. Construindo sobre a teoria de equações de reação e difusão, nós analisamos um modelo de invasão de espécies consumidoras em habitats homogêneos e heterogêneos, formando redes de predação intraguilda com espécies locais. Determinamos velocidades de invasão desses consumidores em habitats homogêneos e condições para reversões competitivas em habitats heterogêneos, levando a regimes de coexistência e exclusão inesperados. Também construímos e analisamos modelos para populações estruturadas por fenótipos em termos de equações a integrais a diferenças. Mostramos que essas equações admitem soluções do tipo onda viajante e velocidades assimptóticas linearmente determinadas, e também estudamos distribuições fenotípicas na frente de invasão e como elas mudam com diferentes *trade-offs* entre fertilidade e dispersão e taxas de mutação. Por último, apontamos algumas perspectivas e conclusões do trabalho.

Palavras Chaves: Equações de reação e difusão, equações integrais a diferenças, biologia de populações,

Áreas do conhecimento: Física, Matemática, Ecologia; Sistemas dinâmicos, Matemática Aplicada, Ecologia Espacial;

Abstract

Biological invasions are ubiquitous in the Anthropocene. With many factors influencing how alien species spread into novel territory and large spatio-temporal scales often make experiments much more complicated. This way, theoretical quantitative approaches become a useful tool into understanding such factors and estimating spreading speeds and regime shifts caused by invading populations. In this thesis we review classical mathematical models for biological invasions in the form of reaction diffusion equations and integro-difference equations. Then, building upon reaction diffusion equations theory, we formulate models for consumer population invasions leading to intraguild predation interaction networks with resident species in both homogeneous and heterogeneous landscapes. We show speeds are linearly determinate, and that competitive reversals among intraguild prey and predator might occur in heterogenous landscapes, leading to unnexpected coexistence and exclusion regimes. Moving on, we also develop models for evolutionary processes in biological invasions, that have been show to take place in ecological timescale and significantly change spread phenomena. We show that discrete time recursions for trait structured populations can also exhibit traveling wave solutions and linearly determinate speeds, and determine the leading edge trait distributions for different growth-dispersal trade-offs and mutation rates. Finally, we outline some perspectives and conclusions of our work.

Keywords: Reaction-diffusion equations, Integro-difference equations, population biology

Knowledge fields: Physics, Mathematics, Ecology; Dynamical Systems, Applied Mathematics, Spatial Ecology

Contents

Chapter 1

An Introduction to Mathematical Models for Biological Invasions

Biological invasions are ubiquitous in the Anthropocene. With increasing international travel and commerce, the different parts of the globe have never been more connected. With that, humans are continuously inadvertently, accidentally or purposely introducing alien species in novel ecosystems and regions, causing possible regime shifts in local communities [1, 2]. More than that, human activities such as deforestation for farming or housing and usage of non-renewable energy, leading to global warming, can facilitate biological invasions, favoring non-native species in the invaded habitats [3, 4, 5, 6].

The early detection and prevention of biological invasions are rarely viable. Therefore, understanding the possible mechanisms that allow for an alien species to establish in a novel region, thereby identifying methods applicable to control their spread, have been the target of many studies [7]. The large temporal and spatial scales in which biological invasions take place, however, make experiments quite difficult. This way, developing quantitative theoretical approaches for species range expansion can help determine possible regime shifts the invasive species can cause and its attainable spreading speeds, and reveal what are the possible routes to control it [8, 9].

The challenges in a theoretical approach are many, nonetheless. There is a large amount of processes that can change how invasions take place and how species move through the landscape, such as species interactions [10, 11], landscape heterogeneity and habitat selection [12] and eco-evolutionary feedback loops [13]. This imposes challenges not only in precisely depicting the biological relevant aspects in a quantitative framework, but also on gaining intelligible information from it. This way, a good portion of recent work on the field of theoretical spatial ecology has been to develop new models and approaches to include such complex processes observed in nature into mathematical frameworks that provide results

that are simple enough to understand, but yet sufficiently informative of the phenomena they represent.

This thesis presents classical theory for biological invasions, and, using recent methods and advances, provides novel results and theory for how community structure, dispersal behavior and evolution may alter the course of species range expansion. For that, the thesis is divided in 4 chapters, and their content will be briefly summarized in the following paragraphs.

In this first chapter we will go over classical mathematical models for biological invasions. Although many formulations are possible, here we will focus on reaction-diffusion equations (RDEs) and integro-difference equations (IDEs), as both are the main formulations used in the remaining of the text. We start with single species models, and discuss some important definitions and theory for these models. We then move for multispecies models, to account for ecological interactions, and present some examples for it. We also cite important references that cover topics not covered in this chapter at the end of each section.

In chapter 2, we present a manuscript in final stages of preparation, containing the analysis of Intraguild Predation in homogeneous and heterogenous landscapes using an RDE framework. We calculate spreading speeds and show some of the possible regimes found in an homogeneous landscape. We also show how heterogenous landscapes can promote competitive reversals, that are modulated by consumer and resource dispersal and habitat preference, allowing for novel coexistence and exclusion mechanisms.

In chapter 3, using IDEs, we present a manuscript published in Journal of Mathematical Biology, where we formulate and analyze models for discrete and continuous trait structured populations, in order to study dispersal evolution during range expansion. We obtain expressions for spreading speeds and population trait distributions at the front of expansion, as well as show that spreading speeds are non-increasing with mutation rates among different traits.

Finally, in chapter 4 we present new routes of investigation for future research. We mainly focus on presenting models accounting for eco-evolutionary feedback loops in range expansion, such as mate-finding and mate selection, evolutionary arms race and dispersal evolution in predator-prey interactions, and the evolution of habitat selection. We also draw some conclusion of the work presented here.

1.1 Single Species Models

1.1.1 Framework Presentation

A single species model in RDE formulation assumes that individuals display Brownian movement, and that growth, death and movement occur simultaneously within the population and population generations overlap. In mathematical terms, we track the density of individuals $u \equiv u(x,t)$ in space, x, in time, t, as follows

$$\partial_t u = D\partial_x^2 u + f(u), \tag{1.1}$$

where D is the diffusion coeficient, f the density dependent growth function, and $(x,t) \in \mathbb{R} \times (0,T)$, $T > 0$ a maximum time of observation of the spreading population. In the case $f(u) = ru(1-u/C)$, this equation is called the Fisher-Kolmogorov equation, as it was simultaneously studied by Fisher [14] and Kolmogorov A et al. [15] to model the spread of advantageous genes. In this setting, u is to be understood not as a population density, but instead, the frequency of the mutant advantageous gene, such that $0 \leq u \leq 1 = C$, and r its selection gradient in respect to the resident gene. The applications of the equation to ecology and animal movement were soon to follow, as the effects of intraspecific competition are modeled by the same growth function, with r the intrinsic growth rate and C the carrying capacity [16].

IDE models assume that individuals have distinct growth and dispersal phases. Dispersal is not necessarily described by Brownian motion, i.e., different movement behaviors can be accounted for, and population generations do not overlap. Therefore, individuals of this population have exactly one dispersal phase, on reproduction phase, and then die out. We keep track of the t-th generation population density in space, $u_t(x)$, which is governed by the following difference equation

$$u_{t+1}(x) = \int_{-\infty}^{\infty} K(x,y)F(u_t(y))\mathrm{d}y, \tag{1.2}$$

where $K(x,y)$ is the movement kernel, a probability density function of an individual that left from $y \in \mathbb{R}$ arriving at $x \in \mathbb{R}$, and F is the growth function. Here, we will assume that the movement kernels do not depend on the explicit locations x, y, but instead in their relative distance, that is, $x-y$, such that $K(x,y) = K(x-y)$, following [17]. Functions F are the typical growth functions used in discrete time pop-

ulation models, such as the Beverton-Holt model, $F(u) = Ru/(1 + (R-1)u/C)$, where R is the intrinsic growth rate and C the carrying capacity [18, 19].

Both RDE and IDE formulations can be understood as discrete time projection operators, i.e,

$$u_{t+\Delta t}(x) = Q[u_t](x). \tag{1.3}$$

In the case of IDEs, the relation is quite straightforward, operator Q is the integral operator itself, and projects the solution an interval $\Delta t = 1$ forward. For RDEs, we would need to construct the exact projection operator that map solutions $u(x,t)$ into solutions in a posterior time, $u(x, t + \Delta t)$. However, important properties of the general projection operator can be stated as properties of the reaction diffusion equation itself. We will consider the problem of point release to illustrate these properties as well as provide an upper limit to how fast is population spread for a class of models.

1.1.2 Point release

Consider the class of RDE models that satisfy $f'(0) = r > 0$ and $f(u) \leq ru \; \forall u$. In the IDE case, the analogous class would be $F'(0) = R > 1$ and $F(u) \leq Ru \; \forall u$. In essence, these assumptions exclude models that account for Allee effects [20], and lead to the following inequalities:

$$\partial_t u = \partial_x^2 u + f(u) \leq \partial_x^2 u + ru, \tag{1.4}$$

and

$$u_{t+1}(x) = \int_{-\infty}^{\infty} K(x-y)F(u_t(y))\mathrm{d}y \leq R\int_{-\infty}^{\infty} K(x-y)u_t(y)\mathrm{d}y. \tag{1.5}$$

In a more general setting, we define the positive linear operator

$$P[a] > 0 \; \forall \; a > 0, \tag{1.6}$$

as a linearization of operator Q, i.e.,

$$P[u](x) = \lim_{\epsilon \to 0^+} \frac{1}{\epsilon} Q[\epsilon u](x), \tag{1.7}$$

such that

$$u_{t+1}(x) = Q[u_t](x) \leq P[u_t](x) \; \forall u_t, \tag{1.8}$$

is satisfied. We have that solutions of the non-linear problems cannot be, at any

moment in time, larger than the solutions of the auxiliary linear problems. This way, the linear models are good candidates to provide us with an upper limit to how fast a population may spread.

Linear reaction-diffusion equation

The linear reaction diffusion equation

$$\partial_t u = \partial_x^2 u + ru \tag{1.9}$$

with initial conditions $u(x,0) = \delta(x)$ and vanishing at $x \to \pm\infty$, has solution

$$u(x,t) = \frac{1}{\sqrt{4\pi Dt}} e^{rt} e^{-\frac{x^2}{4Dt}}. \tag{1.10}$$

If we set a population threshold $\bar{u}$ and track the position $\bar{x} \equiv \bar{x}(t)$ that this density is attained, i.e, $u(\bar{x},t) = \bar{u}$, we can estimate how fast this population advances in space by measuring the speed $\bar{x}/t$. A quick calculation yields

$$\frac{\bar{x}}{t} = \sqrt{4rD - \frac{4D}{t} \ln \sqrt{4\pi Dt}\bar{u}}. \tag{1.11}$$

In the limit $t \to \infty$, since $\lim_{t\to\infty} t^{-1} \ln \sqrt{t} = 0$, we have that the speed of spread is

$$c_L = \lim_{t\to\infty} \frac{\bar{x}}{t} = 2\sqrt{rD}. \tag{1.12}$$

Equation (1.12) is the classical expression for speed obtained in Fisher [14], Kolmogorov A et al. [15], using the method used by Skellam [16]. It tells us that, at the asymptotic limit, the population spreads at most with speed $c_L = 2\sqrt{rD}$.

Linear integro-difference equation

For the IDE linear model,

$$u_{t+1}(x) = R \int_{-\infty}^{\infty} K(x-y) u_t(y) \mathrm{d}y \tag{1.13}$$

we have that an initial condition $u_0(x) = \delta(x)$, leads to

$$u_1(x) = R\int_{-\infty}^{\infty} K(x-y)\delta(y)\mathrm{d}y, \tag{1.14}$$
$$u_1(x) = R(K*\delta)(x), \tag{1.15}$$
$$u_1(x) = RK(x), \tag{1.16}$$

where $(K*\delta)(x)$ denotes the convolution between K and δ. Similarly

$$u_2(x) = R\int_{-\infty}^{\infty} K(x-y)(RK(y))\mathrm{d}y = R^2(K*K)(x), \tag{1.17}$$
$$u_3(x) = R\int_{-\infty}^{\infty} K(x-y)R^2(K*K)(y)\mathrm{d}y = R^3(K^{*3})(x), \tag{1.18}$$

where K^{*n} denotes the convolution of K with itself n times (often called the $n-$fold convolution). Repeating this iterative process for longer times will lead to

$$u_t(x) = R^t K^{*t}. \tag{1.19}$$

Therefore, calculating the $t-$fold convolution of K yields the solution of the linear IDE model. However, calculating the $t-$fold convolution is not an easy task, and can be performed only for a few dispersal kernels.

Here, we show the calculation for the Gaussian kernel, but see section 5.2 in Lutscher [21], for the example of the Cauchy Kernel. The (zero mean) Gaussian kernel is

$$K(x-y) = K(z) = \frac{1}{\sqrt{2\pi\sigma^2}}\mathrm{e}^{-\frac{z^2}{2\sigma^2}}, \tag{1.20}$$

and since the convolution of two Gaussians with variances σ_1^2 and σ_2^2 result in a Gaussian with variance $\sigma_1^2+\sigma_2^2$, the $t-$fold convolution of $K(z)$ results in a Gaussian with variance $t\sigma^2$, i.e.,

$$u_t(x) = R^t K^{*t} = \frac{R^t}{\sqrt{2\pi t\sigma^2}}\exp\left(-\frac{x^2}{2t\sigma^2}\right). \tag{1.21}$$

The solution (1.21) is equivalent to the solution in equation (1.10), evaluated at $t\in\mathbb{Z}_+$ with $r=\ln(R)$ and $2D=\sigma^2$. This implies that the projection operator Q that maps solutions $u(x,t)$ into time-1 steps forward solutions, $u(x,t+1)$, of the linear RDE model (1.9) is precisely the linear IDE model (1.13) with Gaussian

kernel.

The speed of spread attained after a long time can be obtained in a similar manner as performed for the RDE case, yielding

$$c_G = \sqrt{2\sigma^2 \ln(R)}, \tag{1.22}$$

this way, IDE models with Gaussian kernels and linearly bounded growth functions cannot travel at speeds higher than c_G.

Here, we stablished a method, for both RDE and IDE models, to estimate an upper bound for the spreading speeds. That does not say that this is the speed at which the non-linear models will travel. In the following subsection, we will discuss how to obtain lower bounds for RDEs and IDEs via traveling exponential fronts.

1.1.3 Traveling exponential fronts

At the interface of colonized and non-colonized regions of a biological invasion, i.e., at the leading edge, the population densities are low enough, such that $u \approx 0$ and the growth functions can be approximated via Taylor expansion to $f(u) \approx f'(0)u$, and similarly for F in the IDE case, resulting in a linear equation at the front of invasion.

Traveling exponential fronts are expressed mathematically as

$$u^*(x - ct) = \mathrm{e}^{-s(x-ct)}, \tag{1.23}$$

where s is the shape parameter of the front, and c, the speed of the traveling front.

Reaction-Diffusion Equation Models

Plugging the exponential front profile (1.23) in the linear RDE model (1.9), with $r = f'(0) > 0$, results in

$$scu^* = s^2 Du^* + ru^* \tag{1.24}$$

$$c(s) = sD + \frac{r}{s}. \tag{1.25}$$

Equation (1.25) is the dispersion relation for the RDE model (1.9), and it relates wave front profiles with their speeds. Note that the expression for $c(s)$ is not

monotone in s. Fast fronts (high c) are either flat, since $\lim_{s\to 0} c(s) = \infty$, or very steep, since $\lim_{s\to\infty} c(s) = \infty$. The minimal spreading speed, $\hat{c}$, is attained at $s = \sqrt{r/D}$, yielding

$$\hat{c} = \min_{s>0} c(s) = 2\sqrt{rD}. \tag{1.26}$$

Note that this implies that traveling fronts can travel no slower than $\hat{c}$. However, we also know that linearly bounded RDE models' solutions cannot travel faster than c_L. This way, since $\hat{c} = c_L$, we have a strong reason to believe that at the asymptotic limit $t \to \infty$, a species modeled by (1.1), with f linearly bounded, travels exactly at speed $\hat{c} = c_L = 2\sqrt{rD}$.

Integro-Difference Equation Models

Combining the traveling exponential front (1.23) with the linear model (1.13) with $R = F'(0) > 1$, we have

$$e^{-s(x-c(t+1))} = R\int_{-\infty}^{\infty} K(x-y)e^{-s(y-ct)}dy, \tag{1.27}$$

$$e^{sc} = R\int_{-\infty}^{\infty} K(x-y)e^{s(x-y)}dy, \tag{1.28}$$

$$e^{sc} = R\int_{-\infty}^{\infty} K(z)e^{sz}dz, \tag{1.29}$$

$$e^{sc} = RM(s), \tag{1.30}$$

$$c(s) = \frac{1}{s}\ln RM(s), \tag{1.31}$$

where $M(s)$ is the moment generating function of movement kernel $K(z)$, and equation (1.31) is the dispersal relation for a linear IDE model.

Note that, by writing $M(s)$, we are making a subtle, but important, assumption on the movement kernel (and therefore on species movement behavior). The assumption is that $K(z)$ is exponentially bounded (or thin tailed), i.e., that $K(z)$ vanishes at $z \to \infty$ faster than the exponential e^{-sz}, so that $M(s)$ is finite at least for some $s > 0$.

By definition, $M(s)$ is increasing with s, and we can show that the expression for $c(s)$ can have at most one minimum and no maximum at all (see Weinberger [22] and Lutscher [21] for a complete proof). With this, we define the minimal spreading speed for the IDE case as

$$\hat{c} = \inf_{s>0} c(s) = \inf_{s>0} \left\{ \frac{1}{s} \ln(RM(s)) \right\}. \tag{1.32}$$

For the Gaussian kernel case, we have $M(s) = \mathrm{e}^{(s\sigma)^2/2}$, and the minimal speed is attained at $s = \sqrt{\ln(R)}/\sigma$, such that

$$\hat{c}_G = \sqrt{2\sigma^2 \ln(R)}, \tag{1.33}$$

that is, the minimal spreading speed is also the upper limit established by the linear solution, i.e., $\hat{c}_G = c_G$, and again, we have a strong reason to believe that $\hat{c}_G$ is the asymptotic spreading speed for the IDE problem with linearly bounded growth functions.

The property that the asymptotic spreading speed equals the one obtained from linearization, found in both RDE and IDE models (equations (1.1) and (1.2), respectively) has been termed linear determinacy. We say that whenever this property holds, the speeds are linearly determinate. In the next subsection, we briefly go over the theory developed by Aronson and Weinberger [23], Weinberger [22, 24] for traveling wave solutions of some single species systems.

1.1.4 Traveling waves

A traveling wave solution, in both RDE and IDE formulations, consists in spatial profile that has its shape unchanged, and is only displaced in space as time moves forward, similar to a traveling exponential front. In mathematical notation, we write a traveling wave solution for the RDE model in equation (1.1) as $u(x,t) = W(x - ct)$, and similarly for the IDE formulation in equation (1.2), where c is the speed this wave travels.

So far, we have been interested in tracking how fast the populations travel in the asymptotic time limit. We have not yet given a clear definition of what an asymptotic spreading speed is, and how to characterize it. However, for the remainder of the thesis, we will refer to such asymptotic spreading speeds in the following sense

Definition 1.1.1. *The asymptotic spreading speed of the recursion* $u_{t+1}(x) = Q[u_t](x)$, $x \in \mathbb{R}$, *with steady states* $u_t(x) = 0$ *and* $u_t(x) = u^* > 0$, *is a positive real value,* c^*, *such that, for all small but positive* ϵ, *we have*

$$\lim_{t\to\infty,|x|<(c^*-\epsilon)t} u_t(x) = u^* > 0, \tag{1.34}$$

$$\lim_{t\to\infty,|x|>(c^*+\epsilon)t} u_t(x) = 0. \tag{1.35}$$

This definition states that if an observer followed the population density with a speed slightly smaller than c^*, the observer would eventually be surrounded by individuals of this population. However, if the observer moved with a speed slightly larger than c^*, then the observer would eventually see no individuals of this population nearby.

Proving the existence of traveling wave solutions and of asymptotic spreading speeds for different projection operators has been the target of many scientific works. Here, we will state the results of Weinberger [22], in the form of a summarized version of their main theorems. Several advances in the theory follow the ideas of Weinberger [22] closely, hence, it is worthwhile to revisit it here.

We assume the projection operator Q has the following properties:

($A1$): The projection operator Q has only two steady states, namely $u_t = 0$ (unstable) and $u_t = u^* > 0$ (stable), i.e.,

$$Q[u] = u \text{ if, and only if, } u = 0 \text{ or } u = u^*. \tag{1.36}$$

($A2$): Q is monotone increasing (order preserving), i.e., for any pair $u, v \in C(\mathbb{R})$, where $C(\mathbb{R})$ is the Banach space of continuous positive functions in $x \in \mathbb{R}$, we have that

$$Q[u] \geq Q[v] \text{ if } u \geq v. \tag{1.37}$$

here, the notation $u \geq v$ denotes that for every $x \in \mathbb{R}$ we have $u(x) \geq v(x)$.

($A3$): We assume that Q is compact, this way, alongside the previous assumptions, it follows that $Q : C_{u^*}(\mathbb{R}) \to C_{u^*}(\mathbb{R})$, where $C_{u^*}(\mathbb{R}) = \{u \in C(\mathbb{R}) | 0 \leq u \leq u^*\}$, i.e., Q maps the Banach space of continuous positive functions bounded in $[0, u^*]$ into itself.

($A4$): Q is translation and rotation invariant, i.e., letting $T_c[u](x) = u(x + c)$ (the translation operator), and $R[u](x) = u(-x)$ (the reflection operator), we

have

$$T_c[Q[u]](x) = Q[T_c[u]](x), \text{ for any } c \in \mathbb{R}, \tag{1.38}$$

$$R[Q[u]](x) = Q[R[u]](x) \tag{1.39}$$

Both these assumptions imply that the landscape is homogenous and that movement in this landscape is unbiased.

(*A5*): Since Q is compact, translation and rotation invariant, the linearization P can be represented as the integral operator

$$P[u](x) = \int_{\mathbb{R}} u(x-y)\rho(y)\mathrm{d}y, \tag{1.40}$$

where $\rho(y)$ is a bounded and symmetric density. We assume that the dominant eigenvalue $\lambda(s)$ of the linearization P, defined by

$$P[\mathrm{e}^{-s\cdot}](x) = \lambda(s)\mathrm{e}^{-sx}, \tag{1.41}$$

is larger than unity and finite for some s. This implies that only thin tailed movement kernels are accounted for, and that $s^{-1}\ln\lambda(s)$ has a single minimum.

(*A6*): Q is linearly bounded, i.e., if P is a linearization of Q around the $u_t = 0$ fixed point, then

$$Q[u] \leq P[u] \;\forall\; u \in C_{u^*}(\mathbb{R}). \tag{1.42}$$

Because Q is monotone increasing, P is a positive linear operator. Biologically, this assumption excludes models that account for Allee effects[20].

Theorem 1.1.1. *[Weinberger [22]] Given a recursion defined by $u_{t+1}(x) = Q[u_t](x)$, with Q satisfying assumptions (A1)-(A6), and a bounded compact support initial condition, $0 \leq u_0(x) \leq u^*$. Then, Q has an asymptotic spreading speed, c^*, and it admits traveling wave solutions $u_t = W(x-ct)$ for every $c \geq c^*$, connecting the fixed points u^* to 0 in space. No traveling wave solutions exist for $c < c^*$. Moreover, the asymptotic spreading speed is linearly determinate, i.e.,*

$$c^* = \inf_{s>0}\left\{\frac{1}{s}\ln\lambda(s)\right\}. \tag{1.43}$$

Proof. See Weinberger [22] for a full detailed proof. Here, we will go over the general ideas of the proof. For the asymptotic spreading speed, essentially, we define the following order preserving operator

$$Q_c[a](x) = T_c[Q[a]](x) \tag{1.44}$$

and show that, for c^* as defined in (1.43) and a nonincreasing initial function $0 < a_0(x) < u^*$, the recursion

$$a_{t+1}(c;x) = \max\{a_0(x), Q_c[a_t](c;x)\} \tag{1.45}$$

yields a sequence of functions $a_t(x)$ that converges uniformly to u^* at $x \to \infty$ for $c < c^*$. While, for $c \geq c^*$, $a_t(x)$ converges to 0 at $x \to \infty$. So that c^* is properly an asymptotic spreading speed, as defined in 1.1.1.

To show the existence of traveling wave solutions, we invoke again operator Q_c and note that a traveling wave solution, $W(x - ct)$, follows

$$Q[W](x) = W(x - c) \tag{1.46}$$

and, therefore

$$Q_c[W](x) = Q[W](x + c) = W(x), \tag{1.47}$$

so W must be a fixed point of Q_c.

Consider now a traveling front $e^{s(c)x}$, $s(c)$ the shape parameter that yields a front with speed $c(s) = s^{-1} \ln \lambda(s)$. Since

$$P[e^{s(c)\cdot}](x) = \lambda(s)e^{s(c)x} = e^{s(c)(x-c(s))} = T_{-c(s)}[e^{s(c)\cdot}](x), \tag{1.48}$$

and $Q[e^{s(c)\cdot}](x) < P[e^{s(c)\cdot}](x)$, it follows that

$$Q[e^{s(c)\cdot}](x) < T_{-c(s)}[e^{s(c)\cdot}](x), \tag{1.49}$$

$$Q_c[e^{s(c)\cdot}](x) < e^{s(c)x}. \tag{1.50}$$

Defining

$$b_0^+(x) = \begin{cases} u^* & \text{if } x < 0, \\ u^* e^{s(c)x} & \text{if } x \geq 0, \end{cases} \tag{1.51}$$

we have

$$Q_{c(s)}[b_0^+](x) \leq b_0^+(x). \tag{1.52}$$

Since $Q_{c(s)}$ is order preserving, the recursion $b^+_{t+1}(x) = Q_{c(s)}[b^+_t](x)$ is decreasing in t, and therefore, by dominated convergence theorem, $Q_{c(s)}$ has a fixed point $W(x)$. Showing that this $W(x)$ is not trivial involves building a sequence $b^-_t(x)$ that is non-constant and non-decreasing in t, i.e., $b^-_{t+1}(x) = Q_{c(s)}[b^-_t](x) \geq b^-_t(x)$. This way, since $Q_{c(s)}$ is order preserving, for any $b^-_0 < b^+_0$ we have that

$$b^-_t \leq W(x) \leq b^+_t \; \forall \; t > 0. \tag{1.53}$$

Since b^-_t is non-constant and increasing, and b^+_t is decreasing, they must converge to a non-constant spatial profile $W(x)$. The argument works for any $c(s) > c^*$, and requires some small modifications on the initial $b^\pm_0$ for $c(s) = c^*$. This way, traveling wave solutions exist for any $c \geq c^*$. The fact that W connects fixed points u^* and 0 in space follow from similar arguments as the ones used in the existence of an asymptotic spreading speed, and jointly imply that no traveling wave solutions exist for any $c < c^*$. □

Example: Fisher-Kolmogorov equation

Let us now consider the example of the RDE model with logistic growth function, i.e.,

$$\partial_t u = D\partial^2_x u + ru(1 - u/C), \tag{1.54}$$

with C the carrying capacity, and r the intrinsic growth rate, and vanishing conditions at $x \to \pm\infty$. First, we proceed with similar calculations as those performed by Fisher [14] and Kolmogorov A et al. [15], later, we apply the theorem to measure the expected asymptotic speed.

The ansatz $u(x,t) = W(x - ct) = W(z)$ inserted in equation (1.54) yields the following ODE

$$D\frac{\mathrm{d}^2 W}{\mathrm{d}z^2} = -c\frac{\mathrm{d}W}{\mathrm{d}z} - rW(1 - W/C). \tag{1.55}$$

We can reduce the order of this equation via $V(z) = \dfrac{\mathrm{d}W}{\mathrm{d}z}$, leading equation (1.55) to the following system of coupled ODEs

$$\begin{cases} \dfrac{\mathrm{d}W}{\mathrm{d}z} &= V \\ \dfrac{\mathrm{d}V}{\mathrm{d}z} &= -\dfrac{c}{D}V - \dfrac{1}{D}rW(1 - W/C). \end{cases} \tag{1.56}$$

with Jacobian matrix

$$J(W,V) = \frac{1}{D}\begin{bmatrix} 0 & D \\ r(1-2W/C) & -c \end{bmatrix}. \tag{1.57}$$

The eigenvalues of $J(W,V)$, denoted as $\lambda_J^{\pm}$, are given by

$$\lambda_J^{\pm} \equiv \lambda_J^{\pm}(W) = -\frac{c}{2} \pm \frac{1}{2}\sqrt{c^2 - 4Dr(1-2W/C)}. \tag{1.58}$$

Since $rW(1-W/C)$ has roots 0 and C, the fixed points of (1.56) are

$$(W,V) = (0,0), \tag{1.59}$$
$$(W,V) = (C,0). \tag{1.60}$$

Note that $(W,V) = (C,0)$ is always a saddle point, since $\lambda_J^-(C) < 0 < \lambda_J^+(C)$. The fixed point at $(W,V) = (0,0)$ is a saddle point only if

$$c \geq 2\sqrt{Dr}, \tag{1.61}$$

otherwise $(W,P) = (0,0)$ is a vortex and allow for oscillations around zero, i.e., non-positive solutions. Therefore, the minimal speed of such traveling wave solutions is $\hat{c} \geq 2\sqrt{Dr}$.

To apply the theorem, we note that the equation (1.54) satisfies the assumptions (*A1*)-(*A6*) (see Cantrell and Cosner [25] chapter 3 for compactness and order preserving properties). We have the following linearization of F-KPP equation

$$\partial_t u = L[u] = D\partial_x^2 u + ru, \tag{1.62}$$

where L is the infinitesimal semi-group generator of

$$T(t) = \mathrm{e}^{Lt}. \tag{1.63}$$

The solutions at a time-one step forward can be obtained by $u(t+1,x) = T(1)u(t,x)$, so that $u_{t+1}(x) = \mathrm{e}^L[u_t](x) = P[u_t](x)$ generates the time-one linearized map, and allow us to calculate the speed. The dominant eigenvalues $\lambda(s)$ and $\gamma(s)$ of $P[\mathrm{e}^{s\cdot}](x)$ and $L[\mathrm{e}^{s\cdot}](x)$, respectively, are connected through

$$\lambda(s) = \mathrm{e}^{\gamma(s)}. \tag{1.64}$$

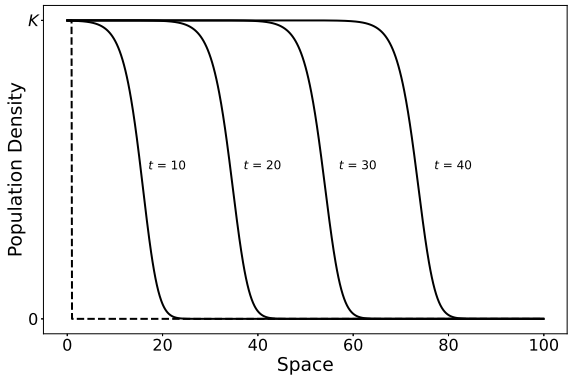

Figure 1.1: Traveling wave solution with speed $c^* = 2$. Parameters uded are $r = D = 1$

This way, the minimal and asymptotic spreading speed are

$$\hat{c} = c^* = \inf_{s>0} \left\{ \frac{\gamma(s)}{s} \right\}, \tag{1.65}$$

and by (1.25) we have that $\gamma(s) = s^2 D + r$, and therefore

$$c^* = 2\sqrt{Dr}, \tag{1.66}$$

as expected. Moreover, there are traveling wave solutions, $W(x - ct)$, for the F-KPP equation for every $c \geq c^*$. These traveling wave solutions can be seen in figure 1.1

Example: IDE with Beverton-Holt growth functions

We now analyze the discrete analogue of a RDE model with logistic growth, the IDE model with Beverton-Holt growth function. Note that, since the growth function is

$$F(u) = \frac{Ru}{(1 + (R-1)u/C)}, \tag{1.67}$$

with $R > 1$ the growth rate and C the carrying capacity, we have that $F(u) > F(v)$ whenever $u > v$, and also that $F(u) < Ru$, so growth is monotone increasing in u and linearly bounded. With an exponentially bounded, and symmetric (around zero average displacement) movement kernel, we have that

$$u_{t+1}(x) = Q[u_t](x) = \int_{-\infty}^{\infty} K(x-y) \frac{Ru(y)}{1 + (R-1)u(y)/C} \mathrm{d}y \tag{1.68}$$

satisfies all assumptions (*A1*)-(*A6*).

The linearized operator yields equation (1.13), and the asymptotic spreading speed is, therefore,

$$c^* = \inf_{s>0} \frac{1}{s} \ln RM(s). \tag{1.69}$$

For a Gaussian movement kernel, the expression is already covered in the text. To illustrate another method to calculate speed c^* from the formula above, we will use a parametric representation, as in Kot et al. [17]. First, the dispersion relation

$$e^{sc(s)} = RM(s), \tag{1.70}$$

can be interpreted as a c *vs* R, relation, parameterized by s. We note that, at the minimal value of $c(s)$ at $s = s^*$, we must have

$$\begin{aligned} \partial_s c(s^*) &= 0, & (1.71)\\ \partial_s \left\{ \frac{1}{s} \ln RM(s) \right\}_{s=s^*} &= 0, & (1.72)\\ \frac{1}{s} \left(c(s^*) - \frac{\partial_s M(s^*)}{M(s^*)} \right) &= 0. & (1.73) \end{aligned}$$

This way, at $s = s^*$, we must simultaneously have

$$c(s^*) = \frac{\partial_s M(s^*)}{M(s^*)} \tag{1.74}$$

and

$$R = \frac{e^{sc(s^*)}}{M(s^*)} = \frac{e^{s\frac{\partial_s M(s^*)}{M(s^*)}}}{M(s^*)}. \tag{1.75}$$

Both equations (1.74) and (1.75) can be solved for s^*, and yield the minimal speed.

Let us now apply the method for the Laplace kernel, defined as

$$K(z) = \frac{a}{2} e^{-a|z|}, \tag{1.76}$$

with $1/a$ the average dispersal distance. The variance of the Laplace dispersal kernel, σ^2, in terms of a is $\sigma^2 = 2/a^2$. We will stick to a since it is a shorter notation. The moment generating function of the Laplace kernel is

$$M(s) = \frac{a^2}{a^2 - s^2}. \tag{1.77}$$

Solving equations (1.74) and (1.75), yield

$$c(s^*) = -\frac{s^*}{a^2}g(s^*) \quad \text{and} \quad R = -\frac{2}{e^2}\frac{e^{-g(s^*)}}{g(s^*)}, \tag{1.78}$$

where $g(s) = -2a^2/(a^2 - s^2)$. Note that the equation for R can be rewritten as

$$g(s^*)e^{g(s^*)} = -\frac{2}{Re^2} = \varrho, \tag{1.79}$$

so $g(s^*)$ is the Lambert W_k function's k-th branch evaluated at $\varrho = -2/(Re^2)$, that is

$$\frac{2a^2}{a^2 - s^{*2}} = -W_k(\varrho), \tag{1.80}$$

therefore, the value of s^* is given by

$$s^* = a\sqrt{\frac{2}{W_k(\varrho)} + 1}. \tag{1.81}$$

Since $e^{-1} < \varrho < 0$, we have that both $k = 0$ and $k = -1$ branches of Lambert W_k functions are solutions. However, $-1 < W_0(\varrho) < 0$, such that $2/W_0(\varrho) + 1 < 0$ in this interval, and the solution for s^* with the $k = 0$ branch is not real valued. This way, the $k = -1$ branch provides the only viable solution, finally yielding

$$c^* = c(s^*) = -\frac{1}{a}W_{-1}(\varrho)\sqrt{\frac{2}{W_{-1}(\varrho)} + 1}. \tag{1.82}$$

Comparing the speeds obtained with Gaussian and Laplace dispersal kernels, we see that increasing variances always increases speed, as expected, however, the Laplace kernel always yields a higher asymptotic spreading speed than the Gaussian kernel with respect to variance(figure 1.2a). Similarly, speed increases in respect to intrinsic growth rates in both Laplace and Gaussian kernels, and is always larger for Laplace kernels as well (figure 1.2b)

1.1.5 Further Readings in Single Species problems

For the proof of theorem 1.1.1, we have used in multiple occasions the monotone property of operator Q (and of Q_c by extension). For systems that are not monotone we can perform a similar argument as long as we assume that the oper-

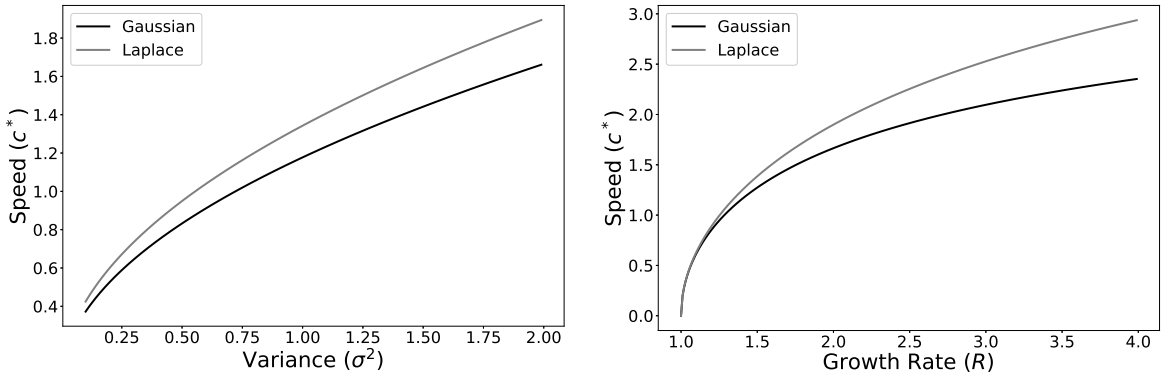

(a) $R = 2$ (b) $\sigma^2 = 2$

Figure 1.2: Asymptotic spreading speeds of the Beverton-Holt model. We use Gaussian (black lines) and Laplace (gray lines) dispersal kernels to illustrate quantitative differences in speed due different movement behaviors.

ator Q is bounded below and above by auxiliary monotone operators Q_- and Q_+, respectively, i.e., $Q_- \leq Q \leq Q_+$ at least in some neighborhood of the non-trivial fixed point $u^* = Q[u^*]$. We then have proper lower bounds c^*_- (correspondent to Q_-) and upper bounds c^*_+ (correspondent to Q^+) for the spreading speed of solutions of Q. Moreover, whenever $c^*_- = c^*_+ = c^*_\pm$ we must have that Q has an asymptotic spreading speed $c^* = c^*_\pm$, see Weinberger [24] for a more detailed proof, but the ideas follow the ones shown so far very closely.

The Ricker growth function, $F(u) = u\exp(r(1-u))$, provides one of those non-monotone cases for the IDE formulations. When there are no stable fixed points, in the parameter region $r > 2$, the solutions formed are not traveling wave solutions, and may present cycles in the core. For $0 < r < 2$ we have traveling wave solutions. In both cases, the fronts of invasion travel at a linearly determinate asymptotic spreading speed, given by (1.32), with $R = e^r$. For a more general theory of those systems, see Bourgeois et al. [26].

The results obtained in this sub-section do not apply to species with Allee effects. To deal with those, a complete different set of theory would need to be developed, and would probably require a section of this chapter dedicated solely to it. Since in the next chapters we only deal with problems that do not contain Allee effects, we skip these here, but point the reader to some important references. First, the theory for Allee effects in RDE formulation is usually modeled by the Nagumo equation [Nagumo et al. [27]], and for those, one can explicitly find a traveling spatial profile and calculate its speed under certain conditions [Hadeler and Rothe [28]]. For IDE models, a prototype Allee growth function can be built

to obtain an estimate for spreading speeds [Kot et al. [17]]. Finally, a more general theory for these systems is presented in [Lui [29]], where the exact necessary conditions for the existence of traveling wave solutions and asymptotic spreading speeds, and its estimates, are established.

The assumption that landscape is homogeneous is often not the case in nature. In order to account for possible landscape heterogeneity, mathematical models often consider that the habitats are periodic, and consist of two main types of patches, where species display distinct growth functions and/or dispersal behavior. Classically, the two types of patches are sources, where species can grow, and sinks/matrix, where species mortality rate surpasses growth. Among the first works to take such approach is Shigesada et al. [30], where, strangely, high dispersal in sink patches led to smaller spreading speeds (sometimes even failing invasion completely). Later, with theory for movement behavior on the interface of distinct patches developed in Ovaskainen and Cornell [31], Maciel and Lutscher [32] show that such behavior at the interface, reflecting habitat preferences, helps explain how and when highest dispersal in sink patches lead to slower speeds, while showing that it can also lead to higher speeds. From there, multiple works followed: Maciel and Lutscher [33] treat the problem with Allee effects in such landscapes, Yurk and Cobbold [34] develop an approximation technique that allows for easier computing of the dynamics and speeds in heterogeneous environments with interface behavior accounted for. Finally, Hamel et al. [35] formally shows the existence of traveling wave solutions in periodic habitats settings with patch preference behavior. A similar approach in terms of IDEs is found in [36, 37], but is far less present in literature, mainly because approximation methods are not available for this problems and computing speeds becomes slightly more involved.

We also let aside structured single species models, as, for example, sexually, age or stage structured population. The theory of sexually structured models is much more difficult, because often, the description of mate formation processes lead to Allee-like effects, although numerical results suggest the existence of traveling wave solutions and asymptotic spreading speeds (see Miller et al. [38]). For age/stage structured models, we require the order-preserving property of the projection operator, and the arguments are slightly more involved than the ones presented here, however, the ideas follow very closely (see Lui [39], Neubert and Caswell [40]). Since structured populations consist of interacting groups of a same species, separated by a given biological relevant structure, the framework for their analysis is much more similar to the one of interacting species, to follow in the

next section. In fact, one of the most important results on cooperative systems (given in Weinberger et al. [41]) is based on the theory of structured populations (developed in Lui [39]). Also, the same theory can be applied for trait-structured populations, which is the main topic of chapter 3, and will be covered in slightly more detail over there.

1.2 Interacting Species Models

Now, we focus on multiple species models. We first present the modeling framework and its linear analysis, with examples on interspecific competition an predator-prey communities, discussing some important theory developed for such models.

1.2.1 Framework Presentation

For multiple interacting species problems, we follow a similar modeling approach as the ones used in single species. For RDE models, we define the vector valued functions $\mathbf{u} \equiv \mathbf{u}(x,t) = (u_1, u_2, ..., u_n)^T$ as the community vector, where $u_i \equiv u_i(x,t)$ denotes the i-th species (or population) density, $i = 1, 2, ..., n$ in space x at time t. We describe each species as moving brownianly through space with a diffusion coefficient D_i, and each species grow according to a function $f_i(\mathbf{u})$. This yields the system of coupled RDEs

$$\partial_t u_i = \partial_x^2 D_i u_i + f_i(\mathbf{u}) \; \forall \; i, \tag{1.83}$$

or, in vector notation,

$$\partial_t \mathbf{u} = \partial_x^2 \mathbf{D}\mathbf{u} + \mathbf{f}(\mathbf{u}), \tag{1.84}$$

where $\mathbf{D} = \text{diag}(D_i)$ and $\mathbf{f}(\mathbf{u}) = (f_1(\mathbf{u}), f_2(\mathbf{u}), ..., f_n(\mathbf{u}))^T$.

In IDE formulation we follow similar definitions, that is, the community vector is denoted $\mathbf{u}_t(x) \equiv \mathbf{u}_t = (u_{t,1}, u_{t,2}, ..., u_{t,n})^T$, where $u_{t,i} \equiv u_{t,i}(x)$ is the i-th species density, $i = 1, 2, ..., n$ of generation t in space x. They each move with a kernel $K_i(x-y)$, and grow according to growth function $F_i(\mathbf{u}_t(y))$. This way, the IDE model is

$$u_{t+1,i}(x) = \int_{-\infty}^{\infty} K_i(x-y) F_i(\mathbf{u}_t(y)) \mathrm{d}y, \tag{1.85}$$

or, in vector notation,

$$\mathbf{u}_{t+1}(x) = \int_{-\infty}^{\infty} \mathbf{K}(x-y)\mathbf{F}(\mathbf{u}_t(y))\mathrm{d}y, \tag{1.86}$$

where $\mathbf{K}(x-y) = \mathrm{diag}(K_i(x-y))$ and $\mathbf{F}(\mathbf{u}_t) = (F_1(\mathbf{u}_t), F_2(\mathbf{u}_t), ..., F_n(\mathbf{u}_t))^T$.

Again, we can set this in a general framework by defining the recursion relations

$$u_{t+1,i}(x) = \mathcal{Q}_i[\mathbf{u}_t](x) \tag{1.87}$$

where $\mathcal{Q}_i : \mathcal{C}_{\bar{\mathbf{u}}}(\mathbb{R}) \to C_{\bar{u}_i}(\mathbb{R})$ projects the space of vector valued continuous and bounded functions

$$\mathcal{C}_{\bar{\mathbf{u}}}(\mathbb{R}) = \{\mathbf{u} = (u_1, u_2, ..., u_n) | u_i : \mathbb{R} \to [0, \bar{u}_i] \text{ is continuous for all } i\} \tag{1.88}$$

into $C_{\bar{u}_i}(\mathbb{R})$. Or, in vector valued functions formulation,

$$\mathbf{u}_{t+1}(x) = \mathcal{Q}[\mathbf{u}_t](x), \tag{1.89}$$

where $\mathcal{Q} = \mathcal{Q}_1 \oplus \mathcal{Q}_2 \oplus ... \oplus \mathcal{Q}_n$[1] is now an operator that projects $\mathcal{C}_{\bar{\mathbf{u}}}$ into itself. Note that we assumed that species i density is bounded in the positive interval $[0, \bar{u}_i]$, $\bar{u}_i < \infty$ for all i. In the case where recursion $\mathcal{Q}$ admits steady states $\mathbf{u}_k^* = \mathcal{Q}[\mathbf{u}_k^*]$, these upper bounds equal the steady states, i.e., $\bar{u}_i = u_{k,i}$, where we also assume that k steady states exist. In many cases, these communities might present stable oscillations, such as predator-prey cycles. In this setting, we still expect operators to preserve the densities inside a bounded interval, i.e., $0 \leq u_i(x) \leq \bar{u}_i \; \forall \; i$, and those usually revolve around an unstable steady state.

1.2.2 Linear Analysis

Now, of course, the exact properties of operator $\mathcal{Q}$ needed in order to establish the existence of traveling wave solutions and asymptotic spreading speeds are much harder to describe and prove in general terms. We usually assume that a resident community is invaded by an alien species, or a group of alien species, and linearize the system about the resident community fixed point. Then, we estimate minimal spreading speeds via such linearization.

Mathematically, we let a resident community be at a fixed point $\mathbf{u}_l^*$, where

[1] The notation $\mathbf{A} \oplus \mathbf{B}$ is used here in the standard sense of Kronecker sums

the subscript ι stands for the set $\iota = \{i \in \{1,2,...,n\} | u^*_{\iota,i} > 0\}$, that is, the set of indexes of all species present in equilibrium $\mathbf{u}^*_\iota$. Now, suppose a small density of individuals of an alien species ζ, $\zeta \in \{1,2,...,n\} \setminus \iota$, arrive at the landscape. They will grow and disperse, at the leading edge, according to

$$u_{t+1,\zeta}(x) = \mathcal{Q}_\zeta[\mathbf{u}_t](x) \approx \mathcal{Q}_\zeta[\mathbf{u}^*_\iota] + \mathcal{P}_{\zeta,\mathbf{u}^*_\iota}[u_{t,\zeta}](x) = \mathcal{P}_{\zeta,\mathbf{u}^*_\iota}[u_{t,\zeta}](x) \tag{1.90}$$

where $\mathcal{P}_{\zeta,\mathbf{u}^*_\iota}$ is the linearization of $\mathcal{Q}_\zeta$ around the alien species free fixed point. The notation for the linearization used, $\mathcal{P}_{\zeta,\mathbf{u}^*_\iota}[u_{t,\zeta}]$, implies we take the Fréchet derivative of $\mathcal{Q}_\zeta$ only in respect to $u_{t,\zeta}$, while keeping all other variations to $\mathbf{u}_t$ fixed.

Note now that the system is similar to that of a single species invading a new landscape. If we are interested in calculating its invasion speed, a good initial guess is to perform the very same calculation we did for a single species, i.e.,

$$\hat{c}_{\zeta\to\iota} = \inf_{s>0}\left\{\frac{1}{s}\ln(\lambda_{\zeta\to\iota}(s))\right\}, \tag{1.91}$$

where $\lambda_{\zeta\to\iota}(s)$ is the dominant eigenvalue of $\mathcal{P}_{\zeta,\mathbf{u}^*_\iota}[e^{-s\cdot}](x)$.

In the case of multiple species invading the landscape simultaneously, we expect that each of the ζ invading populations spread at speed $\hat{c}_{\zeta\to\iota}$, $\zeta \in \bar{\zeta} \subseteq \{1,2,...,n\} \setminus \iota$. However, now we might have different minimal speed values, since each species may spread at a different rate. We say that the invasion occurs jointly when $\inf_\zeta \hat{c}_{\zeta\to\iota} = \sup_\zeta \hat{c}_{\zeta\to\iota}$. In other cases, we might have the fastest population establishing ahead, and the slowest populations now each perceive the landscape as if it was already occupied by its fastest peers.

In cases were traveling wave solutions are formed, these solutions connect the ζ-species absent community fixed point, $\mathbf{u}^*_\iota$, to the post invasion fixed point, $\mathbf{u}^*_{\zeta\to\iota}$. When multiple species invade together, we can either have this transition occurring at once or in multiple steps, having the fastest species colonizing new regions of space first, followed by invasion of slower species.

1.2.3 Examples

Competing Species

Here, we will follow [41, 42]. We consider that species u_1 and u_2 are competing for a resource. Among the assumptions on $\mathcal{Q}$, we point out that the operator $\mathcal{Q}$ has

an unique coexistence steady state $\mathbf{u}^*_{\{1,2\}}$ (single species fixed points, $\mathbf{u}^*_{\{i\}}$, $i = 1, 2$ are still possible). We also assume that $\tilde{\mathcal{Q}}[(u_i, v_j)^T](x)$ is cooperative in u_i and v_j, where $\tilde{\mathcal{Q}}$ is obtained after the change of variables $v_j = u^*_{\{j\},j} - u_j$ in $\mathcal{Q}$. With such change, we measure the absence of species j, denoted as v_j, rather than its density itself. That is, competition is such that the absence of one of the species is beneficial to the other and vice-versa. This way, $\tilde{\mathcal{Q}}[\mathbf{a}] > \tilde{\mathcal{Q}}[\mathbf{b}]$ whenever $\mathbf{a} > \mathbf{b} > 0$ (it is order preserving). We also consider that, at the moment of invasion, the invader has a higher growth rate than the species invaded.

In a slightly more involved manner as performed for the monotone single species case, we can establish sufficient conditions for competitive systems to present linearly determinate speeds and traveling wave solutions. More details can be checked in Weinberger et al. [41].

To illustrate the applicability of the results for competing species, let us consider two examples. First, we study how a established resident population is invaded by a competitor. Later, we study how two competing species invade a landscape simultaneously

Resident Species *vs* Invading Competitor

We start with a classical Lotka-Voltera competition RDE model, and present the analogous IDE model for the phenomena. The two competing species $\mathbf{u} = (u_1, u_2)$ are described by the system of PDEs

$$\begin{cases} \partial_t u_1 &= D_1 \partial_x^2 u_1 + r_1 u_1 \left(1 - \dfrac{u_1 - a_{12} u_2}{C_1}\right), \\ \\ \partial_t u_2 &= D_2 \partial_x^2 u_2 + r_2 u_2 \left(1 - \dfrac{u_2 - a_{21} u_1}{C_2}\right), \end{cases} \tag{1.92}$$

where r_i, D_i and C_i are the intrinsic growth rate, the diffusion coefficient and the carrying capacity of species i, respectively. The coefficients $a_{i,j}$ measure the competitive negative impact that species j causes on species i, $(i, j = 1, 2)$.

The spaceless version of model (1.92) has four fixed points: The trivial one, $\mathbf{u}^*_0 = (0, 0)$, two of a single species present $\mathbf{u}^*_{\{i\}} = (C_1\delta_{1,i}, C_2\delta_{2,i})$, $i = 1, 2$, and the coexistence one $\mathbf{u}^*_{\{1,2\}} = (u_1^*, u_2^*)$, with

$$u_i^* = C_i \left(\frac{1 - \alpha_{ij}}{1 - \alpha_{ij}\alpha_{ji}}\right), \text{ for } i, j = 1, 2, \tag{1.93}$$

where $\alpha_{ij} = a_{ij}C_j/C_i$. The stability of these fixed points depend on the precise values of both α_{ij}, and will be discussed slightly ahead in terms of invasion dynamics.

Note that upon the substitution $v_i = C_i - u_i$, the system is cooperative in u_j and v_i, since

$$\partial_{v_i}\{\partial_t u_j\} = \frac{r_j a_{ji}}{C_j} u_j > 0 \text{ for } u_j > 0, \tag{1.94}$$

and similarly for the derivative of $\partial_t v_i$ in respect to u_j. This way, increments in v_i are beneficial to u_j and vice versa. We won't use v_i explicitly throughout the text, but keep in mind that the speed at which the absence of v_i advances in space is the same at which u_i regresses and vice versa.

We let species i be resident, and established at $u_i^* = C_i$ in the absence of j. A small density of species j individuals invades the landscape according to

$$\partial_t u_j = D_j \partial_x^2 u_j + r_j(1 - \alpha_{ji})u_j. \tag{1.95}$$

This is precisely the linearized single species RDE (1.9), with the substitution of r by $r_j(1-\alpha_{ji})$. This way, the minimal speed of the fronts of invasion

$$\hat{c}_{j\to i} = 2\sqrt{r_j D_j (1 - \alpha_{ji})}. \tag{1.96}$$

In fact, this minimal speeds of invasion are the asymptotic spreading speeds, i.e., $\hat{c}_{j\to i} = c^*_{j\to i}$, under the following sufficient, but not necessary, conditions [43, 42]

$$r_j(1-\alpha_{ji}) > 0, \qquad \frac{\alpha_{ij}\alpha_{ji} - 1}{\alpha_{ji} - 1} \leq \frac{r_j}{r_i}\left(2 - \frac{D_i}{D_j}\right),$$

$$\frac{D_i}{D_j} \leq 2.$$

Under the regime where the speeds are linearly determinate, note that $c^*_{j\to i} = 2\sqrt{r_j D_j(1-\alpha_{ji})} < 2\sqrt{r_j D_j}$, and therefore the presence of a competitor slows down the invasion of an alien species. Moreover, when $\alpha_{ji} > 1$ the invasion is halted, and the resident species i dominates and prevents invasion of j completely. This may occur under two distinct biological regimes: Either the resident species is competitively stronger than the invader and excludes it ($\alpha_{ij} < 1 < \alpha_{ji}$), or both are strong competitors ($1 < \alpha_{12}, \alpha_{21}$) and the resident species exerts founder's control.

When both α_{12} and α_{21} are smaller than 1, we have mutual invasibility of both species. The invader shifts the equilibrium of only resident species to the coexistence one. This way, if we have traveling wave solutions, $\mathbf{u}(x-ct)$, they connect the single resident species fixed point $\mathbf{u}_i^*$, at $x \to \infty$, to the coexistence one, $\mathbf{u}_{1,2}^*$, at the core of invasion (figure 1.3a).

The last possible case is the substitution of resident species. In the case $\alpha_{ji} < 1 < \alpha_{ij}$, not only invasion of species j is successful, but it also leads to the elimination of the resident species i. The traveling wave solutions connect single resident species fixed point $\mathbf{u}_i^*$, at $x \to \infty$, to the single invader species fixed point $\mathbf{u}_j^*$, at the core of invasion (figure 1.3b).

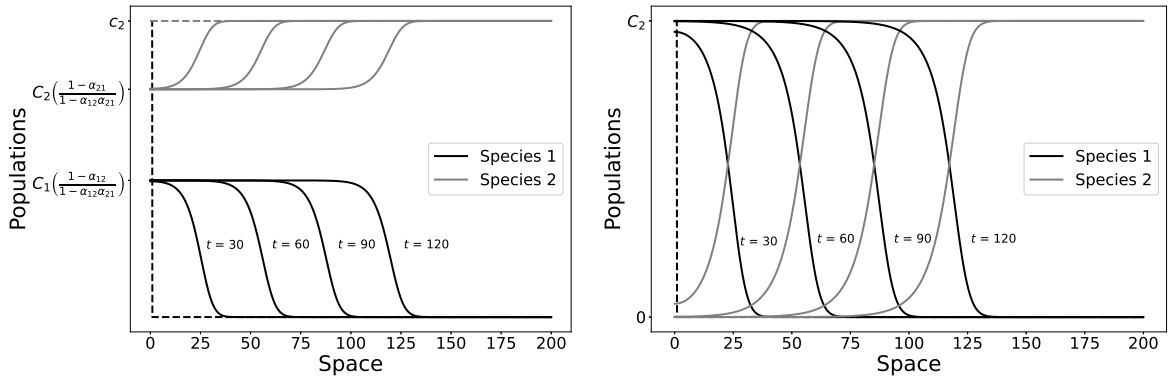

(a) $\alpha_{21} < 1$: Invasion leads to coexistence

(b) $\alpha_{21} > 1$: Invasion leads to exclusion

Figure 1.3: Invasion of a competitor species leading to either coexistence or exclusion of resident species

The analogous IDE model would be

$$u_{t+1,1}(x) = \int_{-\infty}^{\infty} K_1(x-y)F_1(u_{t,1}(y), u_{t,2}(y))\mathrm{d}y \tag{1.97}$$

$$u_{t+1,2}(x) = \int_{-\infty}^{\infty} K_2(x-y)F_2(u_{t,1}(y), u_{t,2}(y))\mathrm{d}y \tag{1.98}$$

where K_i are the movement kernels and F_i the growth functions. The F_i are in the form of a generalized of Beverton-Holt model. That is, the growth of species i is modelled by

$$F_i(\mathbf{u}) = \frac{R_i u_i}{1 + \frac{(R_i-1)}{C_i}(u_i + a_{ij}u_j)}, \tag{1.99}$$

where R_i are the intrinsic growth rates, C_i and a_{ij} are defined as in the RDE case. This particular form of F_i allows for the corresponding spaceless model (i.e., without dispersal) to have fixed points that follow the same expressions obtained for the RDE model.

The growth function of species j, linearized about the single resident species i fixed point $\mathbf{u}_i^* = (C_1\delta_{1,i}, C_2\delta_{2,i})$, yields

$$\partial_{u_j} F_j(\mathbf{u}_i^*) = \frac{R_j}{1 + \alpha_{ji}(R_j - 1)}, \tag{1.100}$$

with $\alpha_{ji} = a_{ji}C_i/C_j$, as before. The model for the invasive species at the leading edge is then

$$u_{t+1,j} = \frac{R_j}{1 + \alpha_{ji}(R_j - 1)} \int_{-\infty}^{\infty} K_j(x - y)u_{t,j}(y)\mathrm{d}y, \tag{1.101}$$

which is precisely the linear single species IDE (1.13) with R switched to $\partial_{u_j} F_j(\mathbf{u}_i^*)$. Therefore, we have that species j has the minimal speed

$$\hat{c}_{j\to i} = \inf_{s>0} \left\{ \frac{1}{s} \ln \left(\frac{R_j}{1 + \alpha_{ji}(R_j - 1)} M_j(s) \right) \right\}, \tag{1.102}$$

where $M_j(s)$ is the moment generating function of species j movement kernel, K_j. Under certain conditions (see Lutscher [21] chapter 12 or Lewis et al. [42]), we have that the asymptotic spreading speed is linearly determinate, i.e., $c^*_{j\to i} = \hat{c}_{j\to i}$.

Similarly to the RDE case, $\alpha_{ji} > 1$ implies species i prevents invasion of species j. Also, the case $\alpha_{ji} < 1$ allow for either invasion leading to coexistence with or exclusion of resident species, depending on the values of the pair α_{ij}, α_{ji} exactly as in the RDE case.

Two competitors invade the landscape simultaneously

For the case of simultaneous invasions, we consider the same RDE formulation used in the last example. Now consider that the landscape is uninvaded by neither of species, and that a small density $u_1, u_2 \ll 1$ of both species individuals arrive at said landscape. The front formed by this individuals can be written as $\mathbf{u}^*(x - ct) = \boldsymbol{\alpha}\mathrm{e}^{-s(x-ct)} = \boldsymbol{\alpha}\mathrm{e}^{-sz}$, where $\boldsymbol{\alpha}$ is a constant vector. The linearized equations around the 0 fixed point, with the traveling front form, yield

$$\begin{cases} c(s)\alpha_1 e^{-sz} &= \left(sD_1 + \frac{r_1}{s}\right)\alpha_1 e^{-sz} \\ c(s)\alpha_2 e^{-sz} &= \left(sD_2 + \frac{r_2}{s}\right)\alpha_2 e^{-sz} \end{cases} \tag{1.103}$$

The system can then be represented as an eigenvalue problem

$$c(s)\boldsymbol{\alpha} e^{-sz} = \mathbf{P}_{\{1,2\},0}\boldsymbol{\alpha} e^{-sz}, \tag{1.104}$$

where $\mathbf{P}_{\{1,2\},0}(s) = \text{diag}(sD_i + r_i/s)$ is the linearized projection operator, with eigenvalues $\gamma_i(s) = sD_i + r_i/s$ and we define

$$c^*_- = \min_i \inf_{s>0} \gamma_i(s) = \min_i 2\sqrt{r_i D_i} \tag{1.105}$$

and

$$c^*_+ = \max_i \inf_{s>0} \gamma_i(s) = \max_i 2\sqrt{r_i D_i} \tag{1.106}$$

as the fastest and slowest speeds of the problem.

Both species will invade the landscape together if $r_1 D_1 = r_2 D_2$, at speed $2\sqrt{r_1 D_1}$, as displayed in figure 1.4. Otherwise, the fastest species i, invades and colonizes new regions first and the slowest species perceives the landscape as already inhabited and invades at speed $\hat{c}_{j\to i}$. This latter case leads to 2 shifts in the landscape throughout space: first, the uninhabited areas are colonized by the fastest species, and $(0,0)$ goes to $(C_1\delta_i 1, C_2\delta_i)$ in a region of space, then, if the slowest species j is able to invade upon species i presence, then $(C_1\delta_i 1, C_2\delta_i)$ is shifted towards the equilibrium containing species j (figure 1.5).

Another possibility of simultaneous invasions is to have founders control leading to both species inhabiting two separated regions in space. Essentially, when $\alpha_{ij}, \alpha_{ji} > 1$, given proper initial conditions (the fastest species needs to be less abundant than the slowest one), neither the fastest species can push the slowest species back nor the slowest species advance in the fastest species presence (figure 1.6).

Predator-Prey

The theory for predator prey is slightly more sparse in literature, but [9] does a concise compilation of recent results and advances. Here we will navigate through literature on reaction diffusion equations models for such communities, and try to provide some details on mathematical methods used. However, here, we will constrain or focus on the RDE formulation, and refer to Lutscher [21] and

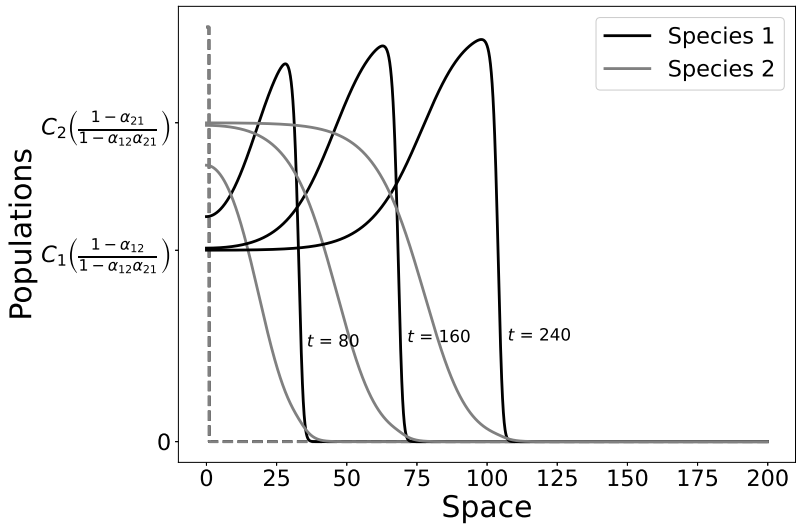

Figure 1.4: Simultaneous invasion of species 1 and 2 leading to coexistence at the core of invasion. $r_1 D_1 = r_2 D_2 = 1.5$

references therein for the IDE cases. This is for two reasons: First, predator prey dynamics have multiple modeling approaches in terms of discrete time models (Neubert and Kot [44] presents three modeling alternatives alone), which have different outcomes in terms of community stability. Secondly, the RDE approach itself has different coexistence regimes, such that covering all the different models in IDE formalism in addition to the RDE one would extend an already long chapter.

Resident prey and invader predator

We write the model for the prey u_v and predator u_w as

$$\begin{cases} \partial_t u_v &= D_v \partial_x^2 u_v + r u_v \left(1 - \dfrac{u_v}{C}\right) - g(u_v, u_w) u_v, \\ \\ \partial_t u_w &= D_w \partial_x^2 u_w + b g(u_v, u_w) u_v - m u_w, \end{cases} \tag{1.107}$$

where D_v, D_w is the diffusivity of prey and predator, respectively, r is the prey growth rate and C its carrying capacity. Predators attack rate upon prey is given by the function $g(u_v, u_w)$, and b is the conversion rate of captured prey into new predators, while m is predator mortality.

The choice of the specific form of g is usually Holling functional responses of type I or II [45, 46]. The type I functional response causes the coexistence fixed point of the spaceless version of (1.107) to be stable when viable. On the other hand, type II functional responses allow this coexistence fixed point to be either

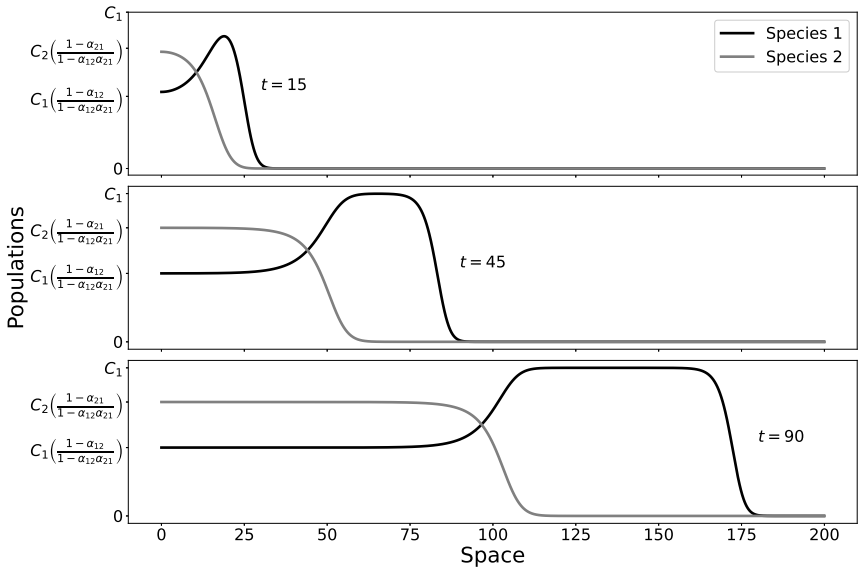

Figure 1.5: Simultaneous Invasions of species 1 and 2 with species 1 faster than species 2.

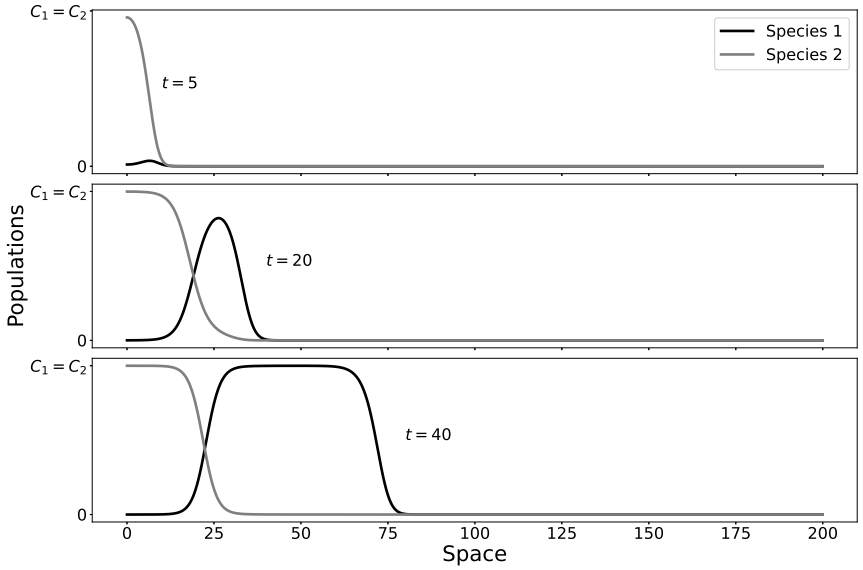

Figure 1.6: Simultaneous Invasions of species 1 and 2 with species 1 faster than species 2, but both compete strongly ($\alpha_{ij}, \alpha_{ji} > 1$). This leads to three distinct regions of space, one where only the slowest species inhabits, a small coexistence region, and a region where only the fastest species inhabits and advances in space.

stable or the center of oscillations. Here, for illustrative purposes, we will use type II Holling functions, since they allow for both coexistence qualitative behaviors (oscillatory or stable). We define

$$g(u_v, u_w) = \frac{au_w}{1 + hau_v}, \tag{1.108}$$

where a is the attack rate and h the handling time. With this, the coexistence fixed point, $\mathbf{u}^* = (u_v^*, u_w^*)$, is given by

$$u_v^* = \frac{m}{a\,(b - hm)}, \tag{1.109}$$

$$u_w^* = \frac{br\,(Cab - Cahm - m)}{Ca^2\,(b - hm)^2}. \tag{1.110}$$

Apart from the coexistence fixed point, we have the trivial extinction state, which is unstable, because prey is always able to grow. Also, we have the only prey fixed point, which is stable if $\partial_{u_w} g(C, 0) < m/bC$, i.e., predators must be able to grow from low densities to destabilize the prey only state.

Suppose prey is at its carrying capacity, C, throughout the landscape, and that a small density of predators is released at some point in space. We write the equation for the small invasion front u_w as

$$\partial_t u_w = D_w \partial_x^2 u_w + u_w(bC\partial_{u_w} g(C, 0) - m). \tag{1.111}$$

The minimal speed of these fronts is given by

$$\hat{c}_{w\to v} = 2\sqrt{D_w\,(bC\partial_{u_w} g(C, 0) - m)}, \tag{1.112}$$

which have been extensively shown to correspond the asymptotic spreading speeds, $c^*_{w\to v}$, via numerical investigations [47, 48, 49, 50]. For the formal theory of traveling wave solutions and linear determinacy of predator-prey reaction difusion equations, check [51, 52] Therefore, the invasion criteria is

$$\partial_{u_w} g(C, 0) > \frac{m}{bC}, \tag{1.113}$$

as expected.

Now, although the speed is linearly determinate and relatively simple to calculate, the behavior at the core of invasion is not as straightforward. Whenever

the coexistence fixed point is stable, traveling wave solutions formed connect the prey only fixed point to the coexistence one (figure 1.7). Whenever the fixed point is the center of oscillations in the non-spatially structured model, then, in the invasion process we can either have invasions leading to oscillatory regime right after the front (figure 1.8a), or the formation of a region of dynamical stability, where the coexistence fixed point seems stable in a region of space (figure 1.8b, also, see Petrovskii and Malchow [49] for more details).

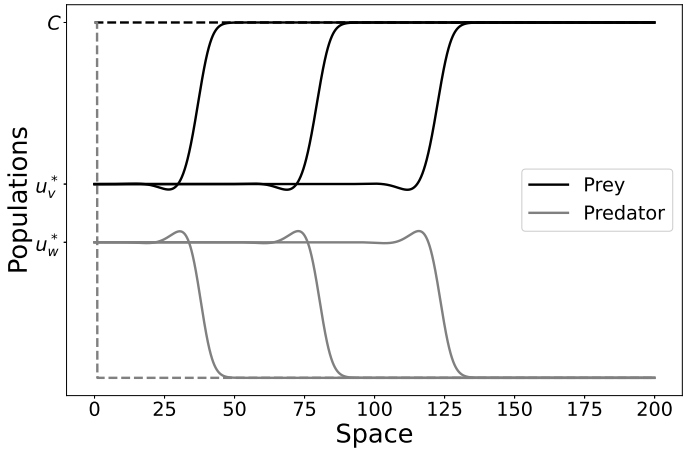

Figure 1.7: Predator invasions when the coexistence fixed point is stable at the core. Invasion simply shifts the prey only state to the coexistence one, with dumped oscillations if the coexistence state is a stable focus

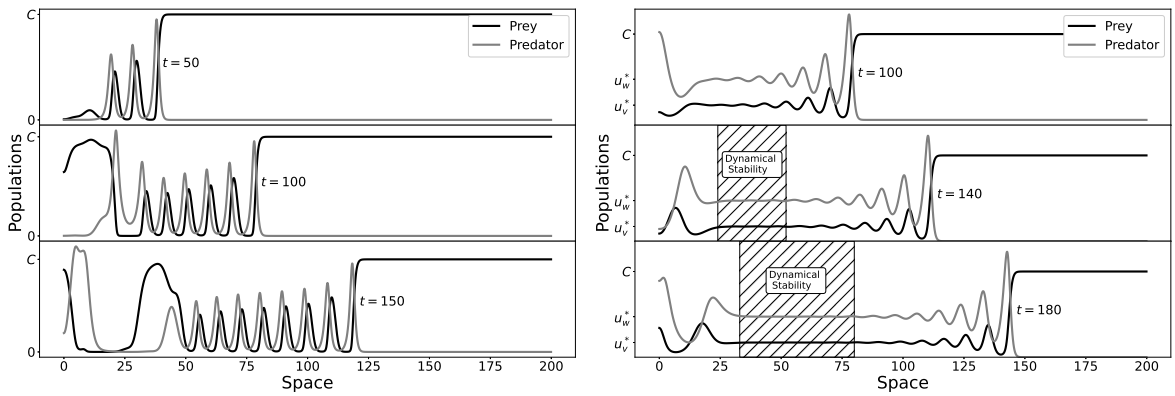

(a) Oscillations after front

(b) Dynamical stabilization

Figure 1.8: Predator invasions when the coexistence fixed point is unstable at the core. Different regimes are possible.

We can understand the formation of the dynamically stable region as two

regime shift fronts traveling at different speeds. First, predator invasion leads to a shift from prey only state to the coexistence one, however, since the coexistence one is unstable at the core, the unstable front travels through space at a speed ω^* smaller than that of the predator front, that is, $\omega^* < c^*_{w\to v}$. And in between the two fronts, dynamical stability is formed. Whenever the opposite holds, i.e., $\omega^* > c^*_{w\to v}$, we have only oscillatory regimes.

To measure the speed of the unstable front, we consider solutions the deviate little from the unstable coexistence fixed point (u^*_v, u^*_w), and see how fast such deviations spread. We denote $p_v(x,t) = u_v(x,t) - u^*_v$, and similarly for $p_w(x,t)$, to write $\mathbf{p} = (p_v, p_w)$. Applying p in equation (1.107) we get

$$\partial_t \mathbf{p} = \mathbf{D}\partial_x^2 \mathbf{p} + \tilde{\mathbf{J}}(u^*_v, u^*_w)\mathbf{p} \tag{1.114}$$

where $\tilde{\mathbf{J}}(u^*_v, u^*_w)$ is the Jacobian matrix (of the spatially unstructured model) calculated at the unstable fixed point. For simplicity in the calculations, we consider $D_v = D_w = 1$, such that $\mathbf{D} = \mathbf{I}$, the identity matrix.

Assuming that the unstable regime at the core advances and replaces the dynamical stability region at speed ω, we let solutions be given by $\mathbf{p} = \bar{\mathbf{p}}e^{s(x-\omega t)}e^{i\kappa t}$, with $\bar{\mathbf{p}}$ a constant vector and κ a constant to account for possible oscillatory behavior. Substituting this back into the equation (1.114) we find the dispersion relation

$$\omega(s) = \frac{1}{s}\mathrm{Re}(\lambda(s)), \tag{1.115}$$

where

$$\lambda(s) = s^2 + \frac{\tilde{T}}{2} + \frac{1}{2}\sqrt{\tilde{T}^2 - 4\tilde{\Delta}}, \tag{1.116}$$

with $\tilde{T} = \mathrm{tr}(\tilde{\mathbf{J}}(u^*_v, u^*_w))$ and $\tilde{\Delta} = \det(\tilde{\mathbf{J}}(u^*_v, u^*_w))$. And, as before, we expect that

$$\omega^* = \inf_{s>0} \omega(s). \tag{1.117}$$

Numerical investigations show that the dynamical stability usually forms when $\tilde{T} < 2\tilde{\Delta}$, such that the fixed point (u^*_v, u^*_w) is an unstable focus [48]. This way, we find

$$\omega^* = \sqrt{2\tilde{T}}, \tag{1.118}$$

and therefore, the condition for a region of dynamical stability to emerge is

$$\tilde{T} < bC\partial_{u_w} g(C,0) - m. \tag{1.119}$$

Finally, in parameter terms, condition (1.119) is (letting $C = a = 1$ - these essentially set population and time scales, respectively)

$$\frac{b+r}{b} < \frac{r(1+h)}{b-hm} + \frac{1}{m(1+h)}. \tag{1.120}$$

The same framework we used here has been used in Petrovskii and Malchow [53] to study the formation of chaotic regimes in this model. In fact regimes other than those shown here are also possible, but not on an invasion context (see Petrovskii and Malchow [49] for more details).

Is biological control of an invading species possible?

In this final example, we consider the following scenario: an invasion is detected at early stage, and we jointly release a natural and native predator of this invading species. We would like to know whether the predator can catch up to the invading species or at least slow the invasion down. To do this analysis, we present a slightly different technique, but which is essentially a linearization around the trivial fixed point.

We write $\mathbf{W}(z = x - ct) = (W_v(z), W_w(z))$ as traveling wave solutions and substitute it into equation (1.107), yielding

$$\begin{cases} c\frac{\mathrm{d}W_v}{\mathrm{d}z} + D_v\frac{\mathrm{d}^2W_v}{\mathrm{d}z^2} + rW_v\left(1 - \frac{W_v}{C}\right) - g(W_v, W_w)W_v &= 0, \\ \\ c\frac{\mathrm{d}W_w}{\mathrm{d}z} + D_w\frac{\mathrm{d}^2W_w}{\mathrm{d}z^2} + bg(W_v, W_w)W_v - mW_w &= 0. \end{cases} \tag{1.121}$$

Letting $\Psi_i = \frac{\mathrm{d}W_i}{\mathrm{d}z}$, and assuming $D_w = D_v = 1$ for simplicity in the calculations, we transform the problem into a 4 dimensional coupled first order ODE system:

$$\begin{cases} \dfrac{\mathrm{d}W_v}{\mathrm{d}z} &= \Psi_v \\ \dfrac{\mathrm{d}W_w}{\mathrm{d}z} &= \Psi_w \\ \dfrac{\mathrm{d}\Psi_v}{\mathrm{d}z} &= -c\Psi_v - rW_v\left(1-\frac{W_v}{C}\right) + g(W_v,W_w)W_v \\ \dfrac{\mathrm{d}\Psi_w}{\mathrm{d}z} &= -c\Psi_w - bg(W_v,W_w)W_v + mW_w. \end{cases} \tag{1.122}$$

Now, the Jacobian of this system is given by

$$\mathbf{J}(W_v,W_w) = \begin{bmatrix} \mathbf{0} & \mathbf{I} \\ -\tilde{\mathbf{J}} & -c\mathbf{I} \end{bmatrix}, \tag{1.123}$$

where $\tilde{\mathbf{J}} \equiv \tilde{\mathbf{J}}(W_v,W_w)$ is the jacobian matrix of the spatially unstructured version of the model and $\mathbf{I}$ the (2 by 2) identity matrix. The eigenvalues, $\lambda(W_v,W_w)$, of $\mathbf{J}$ are given by

$$\lambda(W_v,W_w) = -\frac{c}{2} \pm \frac{1}{2}\sqrt{c^2 - 2\left[\mathrm{tr}(\tilde{\mathbf{J}}) \pm \sqrt{\mathrm{tr}(\tilde{\mathbf{J}})^2 - 4\mathrm{det}(\tilde{\mathbf{J}})}\right]}. \tag{1.124}$$

Linearizing the system about the trivial fixed point, $(W_v,W_w) = (0,0)$, we expect that the eigenvalues are real valued, otherwise we would get oscillations around zero, leading to negative population densities. Therefore

$$c \geq \left[2\left(\tilde{T}_0 \pm \sqrt{\tilde{T}_0^2 - 4\tilde{\Delta}_0}\right)\right]^{\frac{1}{2}}, \tag{1.125}$$

where $\tilde{T}_0 = r - m$ and $\tilde{\Delta}_0 = -rm$ are the trace and determinant of $\tilde{\mathbf{J}}$ calculated at the trivial fixed point. This way, the inequality for c simplifies to

$$c \geq \sqrt{2(r - m \pm |r+m|)}. \tag{1.126}$$

We either have $c \geq 2\sqrt{r}$ or $c \geq 2i\sqrt{m}$. Since only the former has biological significance, the invasion of predator alongside prey has a minimal speed that equals that of prey invading alone (remember D_v was set to 1). Therefore, predators cannot slow down invasions, and, in fact, they can only catch up to prey if

$$c^*_{w\to v} \geq 2\sqrt{D_v r}, \tag{1.127}$$

$$D_w\left(b\frac{1}{1+h}-m\right) \geq D_v r, \tag{1.128}$$

$$\frac{b}{r}\frac{1}{1+h}-\frac{m}{r} \geq \frac{D_v}{D_w}, \tag{1.129}$$

where again we set $C = a = 1$.

The strict inequality in (1.129) only makes sense if the predator is catching up to prey, because it can only invade the landscape if the prey is present. Therefore, a predator that can catch up to prey, travels alongside it at speed $2\sqrt{D_v r}$ once it arrives at the leading edge. On the other hand, whenever the inequality above is not satisfied, simultaneous invasions of predator and prey lead to a growing region in space, of length $(2\sqrt{D_v r} - c^*_{w\to v})t$, where only prey is established at it's carrying capacity. As predator invades the landscape, it shifts the only prey state to the coexistence one.

1.2.4 Further Readings in Multiple Species problems

Here we only covered two types of species interactions, namely competition and predator-prey. Of course, there are many community modules in ecology, and many other interactions that we could study mathematically in similar manner as presented here.

The models of parasite and host are close to that of predator and prey, but for specific functional responses in continuous time see Roberts [54], while for discrete time models, the classical work of [55] is the main reference. Of course, such models must be coupled with the dispersal processes described here, and measuring spreading speeds should be quite straightforward, however, specific conditions for pattern formation, oscillatory and coexistence regimes apply Roberts [54], Wright and Hastings [56].

Facultative mutualistic interactions were also not covered in detail here, but the theory used for competition systems also apply in this case. In essence, the idea is to assume a resident established mutualistic partner, and an invasive mutualistic partner spreading into the resident species. Since the system is cooperative and both parts can grow in absence of its partner, the theory for cooperative systems apply directly, and speeds are linearly determinate under conditions detailed [41]. Briefly, the speed of spread the invader attains is higher than that it would

attain alone. When both mutualistic species invade together, the results change a little, because the mutual partners can either travel alone at different speeds when the mutualistic benefit is low (having the slowest being benefited by colonizing regions already occupied by its partner), or both travel together if the benefit is high enough, such that the slowest species can reach the fastest one (see [21] chapter 14). Obligate mutualisms, on the other hand, are much harder to analyze, because they present a form of strong Allee effects. The specific functional forms for models of mutualism interactions can be viewed at [57, 58], however, spatially structured are much less present in literature (but see Amor et al. [59]).

Systems with larger number of species and multiple simultaneous interactions are also less present in current literature for biological invasions. Studying spatially structured models for key interacting communities, such as exploitative competition [60], apparent competition [61] and intraguild predation [62, 63], can reveal important ways movement behavior and space can disrupt or promote alternative regimes, such as pattern formation and chaos.

For studies in heterogeneous landscapes Cobbold et al. [64], Andrade and Cobbold [65] provide an analysis of predator prey interactions in periodic landscapes, and the precise conditions for which cycles may emerge. For competition systems, see [66], where competitive reversals are found due to differences in habitat preferences.

Chapter 2

Intraduilg Predation in Homogeneous and Heterogeneous Landscapes

2.1 Introduction

Often, the introduction of new consumer species in a novel habitat can generate intraguild predation (IGP) interactions, a multi-species trophic network where exploitative competitors for a shared resource present a predator-prey relation [62, 67], and may lead to exclusion of native species, failure of invasion, or the formation of an IGP community [68, 69, 70, 71]. Alongside interspecific interactions, landscape heterogeneity play an important role on species spatial distributions, coexistence regimes and movement behavior [72, 12, 73], which in turn may also significantly change how invasions occur. Because so many factors can alter the course of range expansion events, spatially structured mathematical models have been vastly used to explore possible outcomes of biological invasions, and significant advances in the field allow us to estimate spreading speeds (see, for instance, Castillo-Chavez et al. [8]) and analyze heterogeneous landscapes in a simplified manner (see Yurk and Cobbold [34], Cobbold et al. [64]). Nonetheless, theoretical approaches for three species IGP communities haven't been studied in detail in this context, and can reveal regime shifts caused by the invasion of novel consumers, as well as the main factors behind it, such as the interplay of demographic traits and dispersal behaviors. In this work, we study a three species IGP model in different landscape settings and provide spreading speeds estimates, show some of the regimes found numerically, and provide some key factors that change community formation processes.

In a three species IGP network we have two consumers of a single biotic resource, with a predation relation among themselves, as displayed in figure 2.1 [63]. Such predation relation allows coexistence between both consumers, even in cases which otherwise would be unattainable [60, 74]. The precise conditions in which

coexistence is possible depend on how large is resource productivity/carrying capacity, and on the intraguild prey (IG prey) being a stronger exploitative competitor than intraguild predator (IG predator) [63]. Following Tilman and others [60], the latter translates into IG prey leading the resource to lower populational levels than IG predator (when each consumer is set with resource alone).

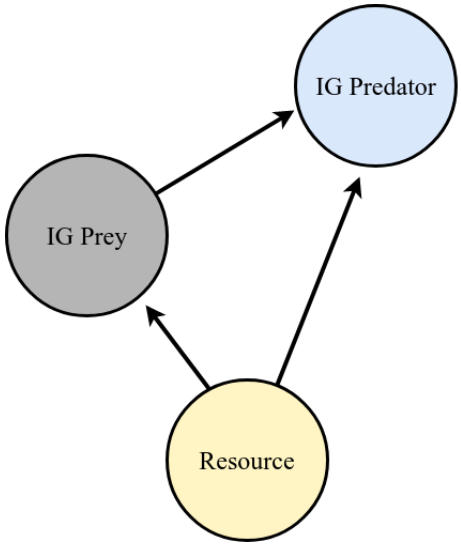

Figure 2.1: A three species intraguild predation network diagram

Among the mathematical approaches for intraguild predation, Holt and Polis [63] provides a concise theoretical foundation for the problem, and highlight many venues in which the theory can be pushed forward to explain other potential coexistence mechanisms, such as considering age structure, adaptive behaviors and spatial dynamics, such as dispersal and habitat heterogeneity. Concerning the latter, the classical works of Fisher [14], Kolmogorov A et al. [15] and Skellam [16] were the first of many works that followed and established reaction diffusion equations (RDE) as the main workhorses of spatial ecology. In this modeling framework, individuals of a given species are assumed to move with Brownian motion (hence diffusion), and population grows/decays according to the relevant biological processes governing demography, such as reproduction, death and intraspecific competition (hence reaction). With this theoretical approach, we have been able to estimate, for example, spreading speeds of invasive species [28, 22], and determine the existence of traveling wave solutions, i.e., spatial profiles that are maintained through time, but advance in space [24].

Accounting for inter-specific interactions in RDE frameworks has been the target of many studies, specially in competition and consumer-resource prob-

lems [75, 51, 50, 49, 76, 42, 43]. Since IGP consists of competition and predation, results from such models can provide some expectations for IGP as well. One characteristic RDE models for competition and predator-prey interactions display are the linear determinacy of spreading speeds (under certain conditions) [49, 48, 41, 42, 43]. This means that the speeds at which an invasive species spreads through the landscape depend solely on low invader density dynamics, where the alien species is still establishing, and resident community is still very close to its equilibrium. Another common finding in this two species systems is the formation of traveling wave solutions [41, 51, 52], which, for example, show the displacement of the resident single species state to a coexistence state as the invader species spreads through space. However, predator-prey dynamics can exhibit various spatial profiles other than traveling wave solutions such as pattern formation, dynamical stability and chaos, depending on the stability of the coexistence state [48, 76, 53, 47].

While RDE formulations for competition and consumer-resource are well described, spatially structured models for IGP are few, mainly because accounting for more than two species can often generate complex dynamics in space, and provide less informative results. With that, Bampfylde and Lewis [77] formulate a two species Lotka-Voltera competition model (with added terms for predation) to understand the dynamics of Intraguild Predation. They show that coexistence, extinction and bi-stable regimes are possible, which imply an invasive species may advance in space and exclude the resident species or coexist with it or, sometimes, regress and fail to invade the landscape.

Reaction diffusion equations have been also developed and applied to study heterogeneous landscapes in Shigesada et al. [30], with the landscape being composed of two patch types that are arranged periodically over the real line. Movement from one patch type to the other is such that flux and population densities are continuous, which do not address specifically possible patch preferences of the invasive and/or resident species that inhabit such landscape. To account for such preferences, Maciel and Lutscher [32] considers individual movement at the interfaces between different patches as being biased towards a preferred patch type, following [31]. This results in interface conditions that are discontinuous in density, but continuous in flux, with population densities potentially accumulating at edges of the preferred patch type.

A method to approximate the results of RDE models in periodic landscapes is presented in [34]. The main idea is to assume the dynamics inside a pair of patches

occur at a much smaller time scale than that of the whole landscape, allowing for the small scale processes to be averaged in the large scale. With this method, [66] investigated how movement behaviors can cause regime shifts in competing species, finding that reversals [1] can occur whenever the habitat preference of the weakest competitor allows for it to spend an optimal time in each of the habitats, increasing its effective carrying capacity while decreasing the negative effects from competition with the stronger competitor.

Albeit not being a RDE model, Amarasekare [79] studies the IGP in discrete space, and provides some insights for the problem of dispersal strategies and habitat selection. In her work, IG prey and predator move between three connected patches of varying resource productivity (resource is stationary). The investigations and results focus on the roles of IG prey and predator dispersal, showing that different strategies lead to different spatial distributions, e.g., fitness based dispersal leads to segregated coexistence, where IG prey stays on low resource productivity patches, and IG predator on high resource productivity ones.

Although some insightful results for IGP in space are present in literature, accounting for both resource population levels and dispersal is lacking, and can be a key process to understanding coexistence and exclusion regimes. Also, measuring speeds of invasion of a consumer species can unravel how fast possible regime shifts take place. Beyond that, we can verify the formation of spatial profiles such as traveling wave solutions and possible oscillatory regimes. Understanding the homogeneous landscape problem can also provide expectations for the large spatio-temporal scale for IGP in heterogeneous landscapes (following [34]), in which patch preference behavior of resource and consumers populations can be accounted for explicitly, and possibly mediate competitive reversals, which in IGP communities would mean shifting coexistence regimes into exclusion ones and vice-versa.

In this work, we consider a version of the classical IGP model by Holt and Polis [63] with added ecological diffusion terms to account for movement in a homogeneous and heterogeneous landscape. In section 2.2, we present the model in homogeneous landscapes, and measure spreading speeds as well as display some of the regimes found. In section 2.3, we present the corresponding model in heterogeneous/periodic landscapes, following [34, 64], we perform the homogenization technique, and drawing correspondence with our findings in the

[1] when the weaker competitor, by exhibiting a more efficient dispersal behavior than its competitor, can potentially exclude or coexist with it [78]

homogeneous landscape model, we determine conditions for mutual invasibility in the large spatio-temporal scales. Finally, in section 2.4, we discuss our results and present future venues of research.

2.2 Intraguild Predation in Homogeneous Landscapes

2.2.1 Model

We consider that population densities vary in continuous time, t, and space, x and denote IG prey density as $C_1 \equiv C_1(t,x)$, IG predator as $C_2 \equiv C_2(t,x)$, and the shared resource as $R \equiv R(t,x)$. In our model, every species move with "ecological" diffusion as in Ovaskainen and Cornell [31], Maciel and Lutscher [32], predation relations are linear, while consumers are subject to natural mortality and resource grows and reproduces according a density dependent growth function. The model equations are then

$$\begin{cases} \partial_t C_1 &= \partial_x^2(D_1 C_1) + b_1 C_1 R - \alpha C_1 C_2 - \delta_1 C_1, \\ \partial_t C_2 &= \partial_x^2(D_2 C_2) + b_2 C_2 R + \beta C_1 C_2 - \delta_2 C_2, \\ \partial_t R &= \partial_x^2(D_R R) + G(R) - a_1 C_1 R - a_2 C_2 R, \end{cases} \tag{2.1}$$

defined on $(t,x) \in (0,T) \times \mathbb{R}_+$. Where a_i is the attack rate of consumer i upon the resource, and b_i is the conversion rate of resource into new consumers of species i [2]. The natural mortality of consumer i is denoted δ_i and α is the attack rate of IG predator upon IG prey, while β its conversion rate. The diffusion coefficient of consumer i is D_i, while the diffusion coefficient of resource is D_i.

Finally, in equation (2.1), the function $G(R)$ describes how resource grows. We will assume that $G(R) \geq 0$ for $0 \leq R \leq R^*$ and that $G(R) < 0$ for $R > R^*$, such that $G(R^*) = 0$, i.e., resource population grows in the absence of consumers until it attains density R^*. Also, we assume that $R\partial_R G(R) < G(R)$ for $R > 0$, such that resource alongside a single consumer attain stationary states in the model without spatial structure. Throughout the text, we consider the logistic growth function, i.e, $G(R) = rR(1 - R/K)$, where K is the carrying capacity and r the intrinsic growth rate. However, other choices of growth functions that satisfy the conditions stated have similar qualitative results as we will display here, e.g., the chemo-stat growth function, i.e, $G(R) = \nu - rR$, where ν is the productivity of the system and r resource removing rate, which is often used to model abiotic

[2] in fact, b_i/a_i is the actual conversion rate, but we address b_i as it for short

resources [74].

Using the change of variables $\tau = rt$, $y = \sqrt{r/D_R}x$, $u_1 = (\beta/r)C_1$, $u_2 = (\alpha/r)C_2$ and $u_\rho = R/\sqrt{R_1^* R_2^*}$, where $R_i^* = \delta_i/b_i$ is the resource level under exclusive presence of consumer i, we set our equations to

$$\begin{cases} \partial_\tau u_1 &= d_1\partial_y^2 u_1 + \gamma m_1 u_1\left(u_\rho - \dfrac{1}{\gamma}\right) - u_1 u_2, \\ \partial_\tau u_2 &= d_2\partial_y^2 u_2 + \dfrac{m_2 u_2}{\gamma}(u_\rho - \gamma) + u_1 u_2, \\ \partial_\tau u_\rho &= \partial_y^2 u_\rho + f(u_\rho) - e_1 u_1 u_\rho - e_2 u_2 u_\rho, \end{cases} \tag{2.2}$$

where the new quantities are $\gamma = \sqrt{R_2^*/R_1^*}$, $e_1 = a_1/\beta$, $e_2 = a_2/\alpha$, $f(u_\rho) = G(\sqrt{R_1^* R_2^*}u_\rho)/(r\sqrt{R_1^* R_2^*})$, leading to a rescaled carrying capacity $K \leftarrow K/\sqrt{R_1^* R_2^*}$, $d_i = D_i/D_R$ and $m_i = \delta_i/r$. Coexistence regimes are only possible if $\gamma > 1$, which is then a competition outcome measure, i.e., whenever $\gamma > 1$ ($\gamma < 1$), IG prey (IG predator) is the stronger competitor.

2.2.2 Invasion Regimes and Community formation

Now, we consider Consumer-Resource and IGP communities formed upon introduction of either IG prey or IG predator into a landscape where either resource is established alone or alongside a resident consumer. In order to determine invasibility criteria, we consider a small invading population, such that the equations can be linearized around the invader-free fixed points. In the case of shifts between IG prey and IG predator, such that the former is excluded, the single consumer and resource fixed point is never a center (no sustained oscillations are possible), however, the coexistence fixed point can be either stable or a center of oscillations (see [63] for a detailed description)

Consumer invades Resource inhabited landscape

To start, we consider a landscape where resource is stablished at $u_\rho^* = \bar{u}_\rho$, $f(\bar{u}_\rho) = 0$, and a small density of IG prey, $u_1 \approx 0$, is invading. The leading edge is described by the linearized equation

$$\partial_\tau u_1 = d_1\partial_y^2 u_1 + u_1 m_1 \gamma\left(\bar{u}_\rho - \frac{1}{\gamma}\right), \tag{2.3}$$

which yields the minimal speed of invasion

$$\hat{c}_{1\to\rho} = 2\sqrt{d_1 m_1 \gamma \left(\bar{u}_\rho - \frac{1}{\gamma}\right)}. \tag{2.4}$$

similarly, IG predator (u_2) invading an resource inhabited landscape will have minimal speed

$$\hat{c}_{2\to\rho} = 2\sqrt{\frac{d_2 m_2}{\gamma}(\bar{u}_\rho - \gamma)}. \tag{2.5}$$

Since a single consumer invading a resource inhabited landscape has linearly determined speed [9, 50], we have that the asymptotic speeds of invasions equal the minimal ones, i.e., $c^*_{i\to\rho} = \hat{c}_{i\to\rho}$. Note that invasion speeds are only real valued for $\bar{u}_\rho > \gamma^{-1}$ in the case of IG prey, and $\bar{u}_\rho > \gamma$ in the case of IG predator. These set thresholds on parameters of $f(u_\rho)$. For the logistic growth function, we have $\bar{u}_\rho = K$. Then, for $K > K_{1\to\rho} = \gamma^{-1}$ ($K > K_{2\to\rho} = \gamma$), the landscape can be invaded by IG prey (IG predator).

An example of successful invasion is illustrated in figure 2.2a (2.2b) for IG prey (IG predator). Note that as IG prey (IG predator) spreads, the resource level shifts from the carrying capacity K to γ^{-1} (γ). Also, the solutions present the same spatial pattern at different times, i.e., they are traveling wave solutions of the consumer-resource problem, connecting the resource only fixed point at $y \to \infty$, to the resource-consumer fixed point at $y \to 0$.

IG predator invades IG prey and Resource inhabited landscape

When resource is established alongside one of the consumers, however, invasibility criteria change. We start with the case of resource and IG prey stable at levels $u^*_\rho = 1/\gamma$ and $u^*_1 = \gamma f(\gamma^{-1})/e_1$, and consider a small density of IG predator invaders, $u_2 \approx 0$. The linearized equation is

$$\partial_\tau u_2 = d_2 \partial_y^2 u_2 + u_2 \left(\frac{m_2}{\gamma}\left(\frac{1}{\gamma} - \gamma\right) + \frac{\gamma}{e_1} f(\gamma^{-1})\right), \tag{2.6}$$

yielding minimal speed

$$\hat{c}_{2\to(1,\rho)} = 2\sqrt{\frac{D_2\gamma}{e_1}\left(f(\gamma^{-1}) - \frac{m_2 e_1}{\gamma^2}\left(\gamma - \frac{1}{\gamma}\right)\right)}. \tag{2.7}$$

Under the assumption that the minimal speed of invasion is the asymptotic

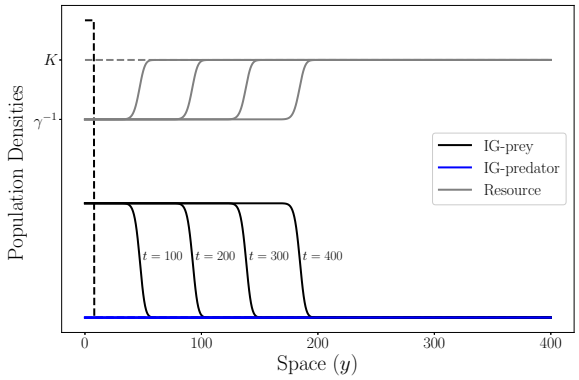

(a) IG prey invades a resource inhabited landscape.

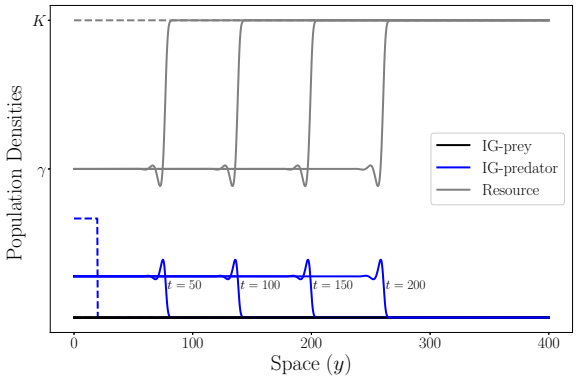

(b) IG predator invades a resource inhabited landscape.

Figure 2.2: Single consumer invading a resource only inhabited landscape, represented as solutions at different times t. Gray lines are Resource, while black (blue) lines are IG prey (IG predator), color matching dashed lines are initial conditions. Parameters are $2D_1 = 2D_2 = D_R = 0.6$ (space is not rescaled in the figure), $m_1 = 2m_2 = 2e_1 = e_2 = 1.2$ and $\gamma = 1.5$. In (a), $K = 0.87$, while in (b) $K = 3$. We use Neumann boundary conditions on both spatial domain extremities.

one, IG predator invades a landscape inhabited by resource and IG prey given

$$f(\gamma^{-1}) > f_{2\to(1,\rho)} = \frac{m_2 e_1}{\gamma^2}\left(\gamma - \frac{1}{\gamma}\right), \tag{2.8}$$

which in turn sets new thresholds for parameter values of f. For logistic growth, the carrying capacity must follow

$$K > K_{2\to(1,\rho)} = \frac{1}{\gamma(1 - \gamma f_{2\to(1,\rho)})}. \tag{2.9}$$

In the case $\gamma < 1$, condition (2.8) is always satisfied, so that IG predator always invades and competitively excludes IG prey. For $\gamma > 1$, in the parameter region $K_{1\to\rho} < K < K_{2\to(1,\rho)}$ we have that only IG prey is able to invade the landscape, while in $K > K_{2\to(1,\rho)}$, IG predator is able to invade the landscape, and, depending on the precise value of K, IG prey either coexists alongside IG predator (see figure 2.3a) or is excluded (figure 2.3b). Note that, for $\gamma > 1$, $K_{2\to(1,\rho)} < K_{2\to\rho}$, so the presence of a resident IG prey population facilitates IG predator invasion for these carrying capacity values.

In figures 2.3a and 2.3b we see spatial patterns being formed from $t = 50$ to $t = 100$, and maintained at longer times. In figure 2.3a, the traveling wave solution connects the IG prey and resource fixed point at $y \to \infty$ to the coexistence one in

$y \to 0$, while in figure 2.3b, it connects the IG prey and resource fixed point to the IG predator and resource fixed point.

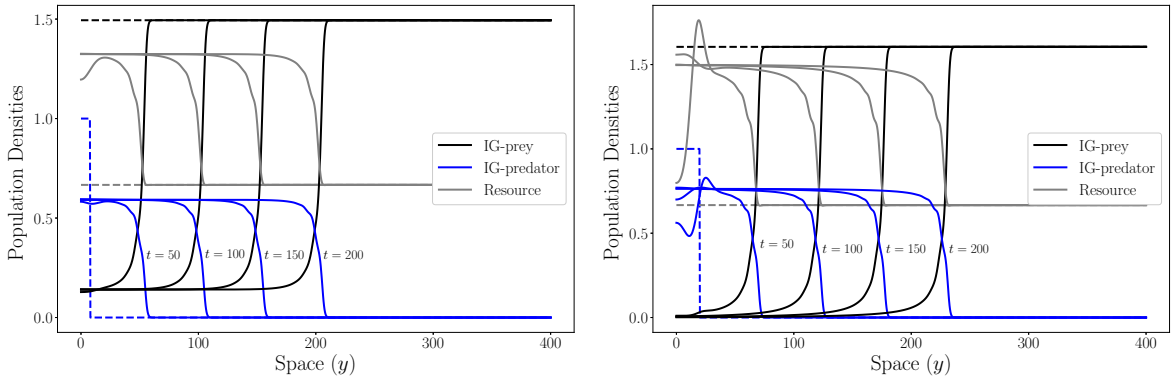

(a) Coexistence after IG predator invasion

(b) Exclusion of IG prey after IG predator invasion.

Figure 2.3: IG predator invading a IG prey and resource inhabited landscape, represented as solutions at different times t. Gray lines are Resource, while black (blue) lines are IG prey (IG predator), color matching dashed lines are initial conditions. Parameters are $2D_1 = 2D_2 = D_R = 0.6$, $m_1 = 2m_2 = 2e_1 = e_2 = 1.2$ and $\gamma = 1.5$. In (a), $K = 6.5$, while in (b) $K = 18$. We use Neumann boundary conditions on both spatial domain extremities and present only the right moving part of the solution.

IG prey invades IG predator and Resource inhabited landscape

Finally, we consider a landscape inhabited by resource and IG predator, at stable densities $u_\rho^* = \gamma$ and $u_2^* = \gamma^{-1} f(\gamma)/e_2$. A small density of IG prey, $u_1 \approx 0$, is described by the linearized equation

$$\partial_\tau u_1 = d_1 \partial_y^2 u_1 + u_1 \left(m_1 \gamma \left(\gamma - \frac{1}{\gamma} \right) - \frac{1}{\gamma e_2} f(\gamma) \right), \tag{2.10}$$

and has minimal speed

$$\hat{c}_{1\to(2,\rho)} = 2\sqrt{\frac{D_1}{\gamma e_2} \left(m_1 e_2 \gamma^2 \left(\gamma - \frac{1}{\gamma} \right) - f(\gamma) \right)}, \tag{2.11}$$

yielding yet another threshold for f in which IG prey is able to invade the landscape, given by

$$f(\gamma) < f_{1\to(2,\rho)} = m_1 e_2 \gamma^2 \left(\gamma - \frac{1}{\gamma} \right). \tag{2.12}$$

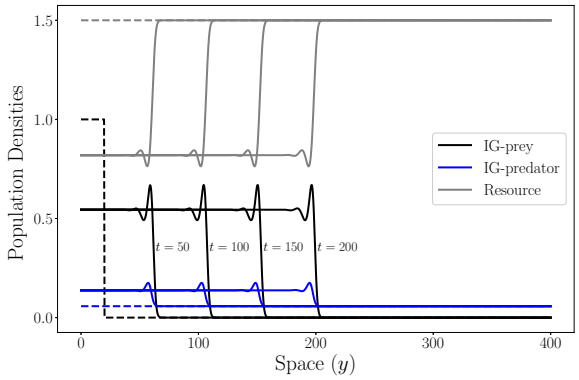

Figure 2.4: IG prey invading a IG predator and resource inhabited landscape, represented as solutions at different times t. Gray lines are Resource, while black (blue) lines are IG prey (IG predator), color matching dashed lines are initial conditions. Parameters are $2D_1 = 2D_2 = D_R = 0.6$, $m_1 = 2m_2 = 2e_1 = e_2 = 1.2$ and $\gamma = 1.5$, $K = 1.6$. Traveling wave solutions connect the resident IG predator and resource fixed point to the coexistence one. We use Neumann boundary conditions on both spatial domain extremities and present only the right moving part of the solution.

The threshold for carrying capacity is

$$K < K_{1\to(2,\rho)} = \frac{\gamma}{1-\gamma^{-1}f_{1\to(2,\rho)}}. \tag{2.13}$$

For $\gamma < 1$, i.e., when IG prey is not the best competitor, its minimal invasion speed is never real valued. Assuming that the minimal speed is the asymptotic one, we have that IG prey is never able to invade. For $\gamma > 1$, $K_{2\to(1,\rho)} < K < K_{1\to(2,\rho)}$ is a mutual invasibility region, i.e., IG prey can invade an IG predator occupied landscape and vice-versa, leading to a region of coexistence between both consumers (see figure 2.4). The region $K > K_{1\to(2,\rho)}$ IG prey can no longer invade an IG predator occupied landscape, and, in turn, IG predator invasions lead to IG prey exclusion, as previously shown in figure 2.3b. Also for $\gamma > 1$, we have $K_{2\to(1,\rho)} < K_{2\to\rho}$, and IG prey can never competitively exclude a resident IG predator population uppon invasion.

When the coexistence fixed point is unstable and display maintained oscillations, the system can display dynamical stabilization [48, 49]. In figure 2.5, as the front of invasion advances with speed $c_{i\to(j,\rho)}$, the interface between the dynamical stability region and oscillatory regime at the core of invasion also advances in space, but with a smaller speed than the front, such that the length of the dynamical stability region is increasing throughout invasion, similar to what is found in

Malchow and Petrovskii [48].

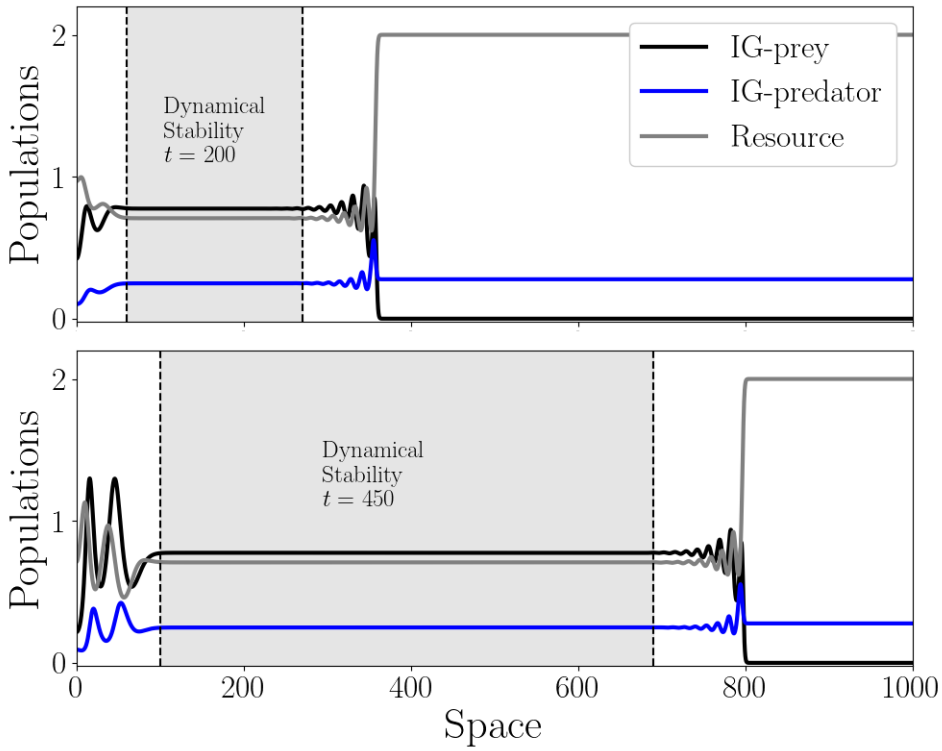

Figure 2.5: IG prey invasion leading to dynamical stability (light gray colored region) at $t = 200$ (top) and $t = 450$ (bottom. Parameters used are $K = 3$, $\gamma = 2$ and $e_2 = 2e_1 = m_1 = 2m_2 = 1.2$, $D_1 = D_2 = D_R = 0.5$

2.2.3 Asymptotic Invasion Speeds

We assumed that the minimal invasion speeds correspond to the asymptotic ones. Measuring the invasion speeds numerically (dots in figures 2.6a-2.6d) reveals that, for the explored region of parameter space, this is indeed the case, i.e., the asymptotic invasion speeds equal the minimal ones (solid lines in figures 2.6a-2.6d).

Note that increasing carrying capacity (figure 2.6a) increases IG predator invasion speed while decreases IG prey invasion speed, as expected, since we have a lower threshold for IG predator invasion in terms of carrying capacity ($K_{2\to(1,\rho)}$) and an upper treshold for IG prey invasion ($K_{1\to(2,\rho)}$). Increasing the invading species diffusivity (figure 2.6b) increases both consumers invasion speeds, as expected.

Invasion speeds behavior in respect to m_i and e_i is not that trivial. Note

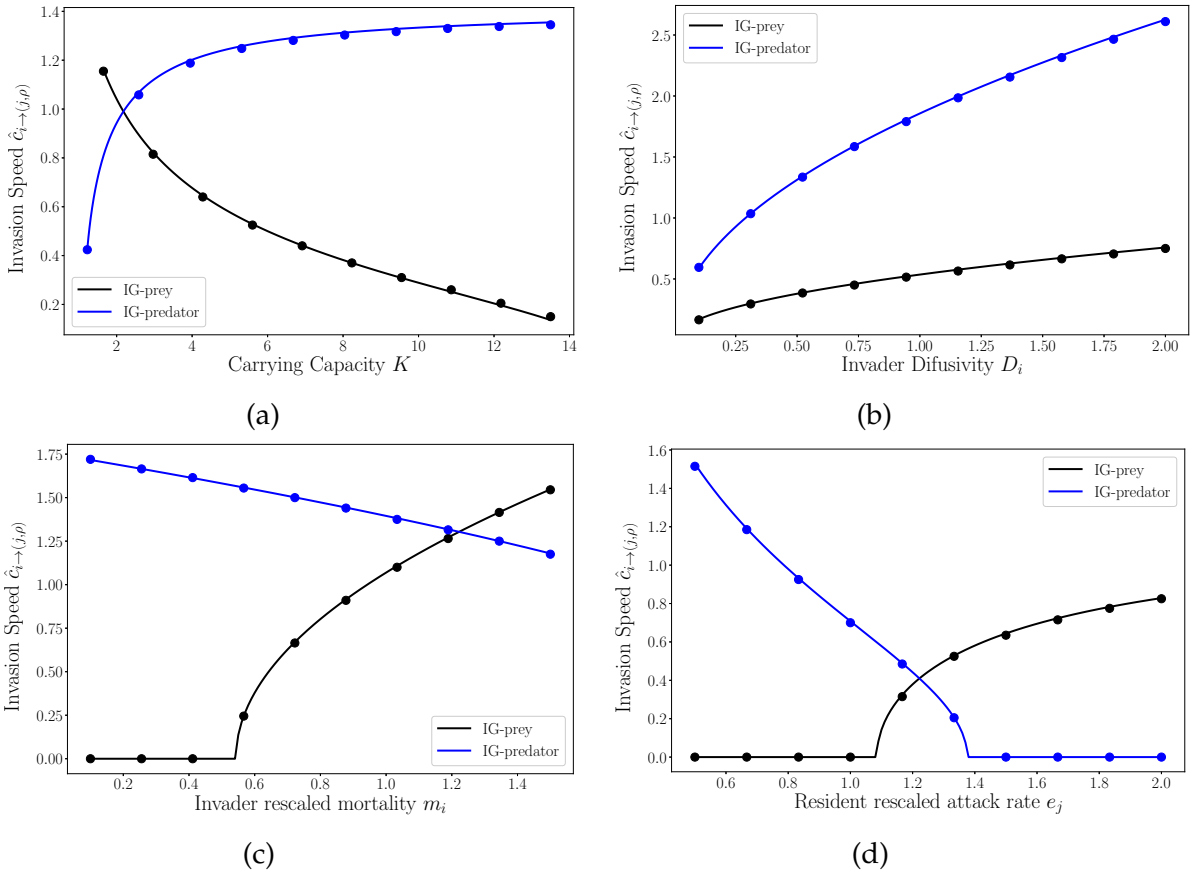

Figure 2.6: Numerical (dots) and linearly obtained (lines) invasion speeds for IG prey (black) and IG predator (blue). We always analyze the cases of invasion uppon a consumer-resource community. Parameters used, with the exception of the varying ones in each of their respective figures, are $D_1 = D_2 = D_R = 0.5$, $\gamma = 1.5$, $m_2 = 2m_1 = 2e_1 = e_2 = 1.2$, $K = 3$

that increasing rescaled mortalities m_i and resident consumer attack rates upon resource e_j produce opposite behaviors on IG prey and IG predator. The main reason lies in the fact that, at the leading edge, the net effect of competition for resource is positive (negative) in IG prey (IG predator). Since the net effect of competition in consumer i is proportional to m_i, increases in m_1 increase IG prey invasion speed, while the opposite holds for IG predator. Since m_i are scaled by $1/r$, simultaneously increasing both m_i can be seen as decreasing resource growth rate, low r favor IG prey, while high r favor IG predator (akin to the effect of increasing carrying capacity).

A similar discussion can be made in terms of e_i and the net effect of intraguild

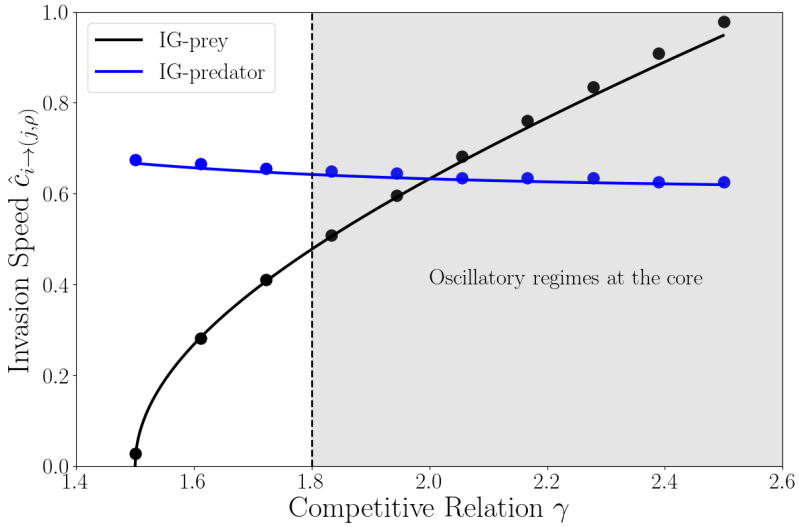

Figure 2.7: Assymptotic Invasion Speeds for different values of γ. In the region $\gamma > 1.8$ (roughly) dynamic stabilization regimes are possible. The numerically obtained speed (dots) match expressions (2.7) and (2.11) (lines). Parameters used are $K = 5$ and $e_2 = 2e_1 = m_1 = 2m_2 = 1.2$, $D_1 = D_2 = D_R = 0.5$

predation at the leading edge. While increasing e_1 decreases the total available IG prey for the consumption of an invading IG predator, thus, reducing its invasion speed, increasing e_2 decreases the total amount of IG predator, reducing predation pressure on an invading IG prey and allowing it to spread with faster speeds.

To illustrate the effects of invasion leading to both regimes on the spreading speeds, we calculate numerical spreading speeds (dots in figure 2.7) and compare them to the ones obtained from linearization (solid lines in figure 2.7) in a parameter region where the coexistence fixed point is unstable (region $\gamma > 2$ in figure 2.7). We observe that, although traveling wave solutions are not being formed, the spreading speeds are still linearly determined and expressions (2.7) and 2.11 provide accurate estimates. This was expected, since it also holds in the case of dynamical stabilization regimes of predator-prey models [48].

2.3 Intraguild Predation in Heterogeneous Landscapes

2.3.1 Model

We follow [32, 34, 64] closely. We let the space be composed of two types of patches, 1 and 2, of sizes l_1 and l_2 respectively, displaced periodically on the real line. We denote the desities of IG prey inside patches of the j-th type as C_{1j}, while

for IG predators and Resource we use C_{2j} and R_j, respectively. The dynamics of these populations on a patch of type j are given by

$$\begin{cases} \partial_t C_{1j} &= \partial_z^2(D_{1j}C_{1j}) + \mathcal{F}_{1j}, \\ \partial_t C_{2j} &= \partial_z^2(D_{2j}C_{2j}) + \mathcal{F}_{2j}, \quad z \in T_j \\ \partial_t R_j &= \partial_z^2(D_{Rj}R_j) + \mathcal{F}_{Rj}, \end{cases} \tag{2.14}$$

where T_j is the set of points within patches of type j, i.e.,

$$T_1 = \{z \in \mathbb{R} \mid m(l_1+l_2) < z < m(l_1+l_2)+l_1 \ \forall\, m \in \mathbb{Z}\}, \tag{2.15}$$

$$T_2 = \{z \in \mathbb{R} \mid m(l_1+l_2)-l_2 < z < m(l_1+l_2) \ \forall\, m \in \mathbb{Z}\}, \tag{2.16}$$

and $\mathcal{F}_{ij} \equiv \mathcal{F}_{ij}(C_{1j}, C_{2j}, R_j)$, $i = 1, 2, R$, are the growth functions of species i at a patch of type j. Following our model in homogeneous space 2.1 and letting intraguild predation relations occur in both patches we have

$$\mathcal{F}_{1j}(C_{1j}, C_{2j}, R_j) = b_{1j}C_{1j}R_j - \alpha_j C_{1j}C_{2j} - \delta_{1j}C_{1j} \tag{2.17}$$

$$\mathcal{F}_{2j}(C_{1j}, C_{2j}, R_j) = b_{2j}C_{2j}R_j + \beta_j C_{1j}C_{2j} - \delta_{2j}C_{2j} \tag{2.18}$$

$$\mathcal{F}_{Rj}(C_{1j}, C_{2j}, R_j) = G_j(R_j) - a_{1j}C_{1j}R_j - a_{2j}C_{2j}R_j, \tag{2.19}$$

with symbols maintaining their definition as in (2.1), but now containing an extra index, j, to denote the patch type in which they are valid. The same is true for the difusion coeficcients D_{ij}. Also, we keep G_j, $j = 1, 2$, as a logistic growth function [3], with intrinsic growth rate r_j and carrying capacity K_j. For the description of parameters and their correspondence to the homogeneous model (2.1), check table 2.1.

At the interface z_m of patches of type 1 and 2, we assume continuous flux, but discontinuous densities, to account for habitat preference [31, 32], leading to

$$\begin{cases} C_{11}(z_m^+, t) &= k_1 C_{12}(z_m^-, t) \\ D_{11}\partial_z C_{11}(z_m^+, t) &= D_{12}\partial_z C_{12}(z_m^-, t) \end{cases} \tag{2.20}$$

where $z_n = n(l_1+l_2) + \zeta_n l_1$, $\zeta_n = 1$ ($\zeta_n = 0$) if n is odd (even), and k_1 is the IG prey density effective patch preference. We proceed similarly for C_2 and R to write

[3] Here, the choice of logistic growth function reflects a living resource species that actively moves and selects between different patches

their interface conditions and define the patch preferences, k_2 and k_R, for the IG predator and the resource, respectively.

We follow [32] to set

$$k_i = \frac{D_{i2}}{D_{i1}} \frac{\alpha_i}{1-\alpha_i}, \tag{2.21}$$

where $\alpha_i \in (0,1)$ is the probability of species i, $i = 1, 2, R$, to move from the interface into a type 1 patch.

It is helpful to write the model (2.14) in a shorter notation. We define the piecewise constant (in z) functions $D_i(z) = D_{ij}$, $z \in T_j$ and $\mathcal{F}_i(z,\cdot) = \mathcal{F}_{ij}(\cdot)$, $z \in T_j$, to write

$$\begin{cases} \partial_t C_1 &= \partial_z^2(D_1(z)C_1) + \mathcal{F}_1(z,\cdot), \\ \partial_t C_2 &= \partial_z^2(D_2(z)C_2) + \mathcal{F}_2(z,\cdot), \\ \partial_t R &= \partial_z^2(D_R(z)R) + \mathcal{F}_R(z,\cdot). \end{cases} \tag{2.22}$$

Of course, (2.22) is only equivalent to (2.14) when interface conditions (2.20) are accounted for. However, this notation allows us to quickly address population densities C_1, C_2 and R in the landscape level (across multiple different patches).

2.3.2 Homogenization Technique

We proceed with a multiscale analysis and approximation method following Yurk and Cobbold [34], we will briefly outline the method, but refer to the original study for more details. Also, we will describe the methods in terms of a single species, C_1, but the proceedings are the same for C_2 and R, and are to be taken simultaneously.

We define the large scale x and the small scale $z = x/\ell$, with $\ell = l_1 + l_2 \ll 1$ in the large scale, and assume that population densities depend on both x and z, leading to $C_1 \equiv C_1(x,z,t)$, the IG prey density in both. Expanding such solutions in ℓ, we get

$$C_1(x,z,t) = \sum_{q=0}^{\infty} \ell^q C_1^{(q)}(x,z,t), \tag{2.23}$$

and assuming x and z are independent we have $\partial_z \to \partial_x + \frac{1}{\ell}\partial_z$. When substituting the expanded solution and the change of variables to (2.14) with interface conditions (2.20), we find a system of coupled equations, that can be solved for $C_1^{(0)}, C_1^{(1)}, C_1^{(2)}$.

The leading order of the expansion, $C_1^{(0)}$, is given by

$$C_1^{(0)}(x,z,t) = \frac{\hat{C}_1(x,t)}{h_1(z)}, \tag{2.24}$$

where $h_1(z) = 1$ ($h_1(z) = k_1$) for $z \in T_1$ ($z \in T_2$). Applying the same procedure to C_2 and R, we arrive in a similar expression for $C_2^{(0)}$ and $R^{(0)}$, with $h_2(z)$ and $h_R(z)$ defined in the same fashion as $h_1(z)$. Since $h_i(z) > 0\ \forall i,\ z$, the population densities are strongly dependent on $\hat{C}_1$, $\hat{C}_2$ and $\hat{R}$, which are obtained by solving

$$\begin{cases} \partial_t \hat{C}_1 &= \hat{l}_1^2 \langle D_1 \rangle^{(H)} \partial_x^2 \hat{C}_1 + \langle \mathcal{F}_1 \rangle (\hat{C}_1, \hat{C}_2, \hat{R}), \\ \partial_t \hat{C}_2 &= \hat{l}_2^2 \langle D_2 \rangle^{(H)} \partial_x^2 \hat{C}_2 + \langle \mathcal{F}_2 \rangle (\hat{C}_1, \hat{C}_2, \hat{R}), \\ \partial_t \hat{R} &= \hat{l}_R^2 \langle D_R \rangle^{(H)} \partial_x^2 \hat{R} + \langle \mathcal{F}_R \rangle (\hat{C}_1, \hat{C}_2, \hat{R}), \end{cases} \tag{2.25}$$

where, $\hat{l}_i$, $\langle D_i \rangle^{(H)}$ and $\langle \mathcal{F}_i \rangle$, are the scaled spatial periods, diffusion coefficients and growth functions of species i in the large scale, respectively. Namely, the scaled periods are given by

$$\hat{l}_i = \frac{\ell}{\ell_i}, \quad \text{with} \quad \ell_i = l_1 + \frac{l_2}{k_i}, \tag{2.26}$$

while the diffusion coefficients are the harmonic mean between the diffusion coefficients of each habitat, i.e.,

$$\langle D_i \rangle^{(H)} = \frac{\ell_i}{\frac{l_1}{D_{i1}} + \frac{k_i l_2}{D_{i2}}} \tag{2.27}$$

and the growth functions are the arithmetic mean of $\mathcal{F}_{ij}$, i.e.,

$$\langle \mathcal{F}_i \rangle (\hat{C}_1, \hat{C}_2, \hat{R}) = \frac{1}{\ell_i} (l_1 \mathcal{F}_{i1}(\hat{C}_1, \hat{C}_2, \hat{R}) + l_2 \mathcal{F}_{i2}(\hat{C}_1/k_1, \hat{C}_2/k_2, \hat{R}/k_R)). \tag{2.28}$$

Rearranging the terms in $\langle \mathcal{F}_j \rangle$, we find that system (2.25) can be written in the same form as (2.1), i.e.

$$\begin{cases} \partial_t \hat{C}_1 &= \partial_x^2 (\hat{D}_1 \hat{C}_1) + \langle b_1 \rangle \hat{C}_1 \hat{R} - \langle \alpha \rangle \hat{C}_1 \hat{C}_2 - \langle \delta_1 \rangle \hat{C}_1, \\ \partial_t \hat{C}_2 &= \partial_x^2 (\hat{D}_2 \hat{C}_2) + \langle b_2 \rangle \hat{C}_2 \hat{R} + \langle \beta \rangle C_1 C_2 - \langle \delta_2 \rangle C_2, \\ \partial_t \hat{R} &= \partial_x^2 (\hat{D}_R \hat{R}) + \langle G \rangle (\hat{R}) - \langle a_1 \rangle \hat{C}_1 \hat{R} - \langle a_2 \rangle \hat{C}_2 \hat{R}. \end{cases} \tag{2.29}$$

We organize the definition and correspondence between the heterogeneous landscape homogenized parameters in model (2.29) and the homogeneous landscape parameters in model (2.1) in table 2.1.

With the parameters defined in table 2.1, we rescale time, space and population

densities as follows:

$$\begin{gathered} U_1 = \frac{\langle\beta\rangle}{\langle r\rangle}\hat{C}_1 \qquad\qquad U_2 = \frac{\langle\alpha\rangle}{\langle r\rangle}\hat{C}_2 \qquad\qquad U_R = \frac{\hat{R}}{\sqrt{\hat{R}_1^*\hat{R}_2^*}}, \\ t' = \langle r\rangle t \qquad\qquad x' = \sqrt{\frac{\langle r\rangle}{\hat{D}_R}}x \end{gathered} \tag{2.30}$$

where

$$\hat{R}_i^* = \frac{\langle\delta_i\rangle}{\langle b_i\rangle} = \frac{l_1\delta_{i1} + l_2\delta_{i2}/k_i}{\frac{l_1\delta_{i1}}{R_{i1}^*} + \frac{l_2\delta_{i2}}{R_{i2}^* k_i k_R}}, \tag{2.31}$$

is the (approximate) resource level when established with only consumer i in an heterogeneous landscape. R_{ij}^* has a similar definition as $\hat{R}_i^*$ (and R_i^* in (2.1)), but only with respect to the patch type j, i.e., $R_{ij}^* = \delta_{ij}/b_{ij}$, $j = 1, 2$ and $i = 1, 2$.

After some algebra, system (2.29) can be written as

$$\begin{cases} \partial_{t'}U_1 &= \sigma_1\partial_{x'}^2 U_1 + \Gamma M_1 U_1\left(U_R - \dfrac{1}{\Gamma}\right) - U_1U_2, \\ \partial_{t'}U_2 &= \sigma_2\partial_{x'}^2 U_2 + \dfrac{M_2U_2}{\Gamma}(U_R - \Gamma) + U_1U_2, \\ \partial_{t'}U_R &= \partial_{x'}^2 U_R + \Phi(U_R) - E_1U_1U_R - E_2U_2U_R, \end{cases} \tag{2.32}$$

which is precisely in the same form of equation (2.2). The new quantities are

$$\begin{gathered} M_i = \frac{\langle\delta_i\rangle}{\langle r\rangle}, \quad E_1 = \frac{\langle a_1\rangle}{\langle\beta\rangle}, \quad E_2 = \frac{\langle a_2\rangle}{\langle\alpha\rangle}, \\ \sigma_i = \frac{\hat{D}_i}{\hat{D}_R}, \quad \Gamma = \sqrt{\frac{\hat{R}_2^*}{\hat{R}_1^*}}, \quad \Phi(U_R) = \frac{\hat{G}(\sqrt{\hat{R}_1^*\hat{R}_2^*}U_R)}{\langle r\rangle\sqrt{\hat{R}_1^*\hat{R}_2^*}}, \end{gathered} \tag{2.33}$$

where we rescale the carrying capacity to $\hat{K} \leftarrow \hat{K}/\sqrt{\hat{R}_1^*\hat{R}_2^*}$.

2.3.3 Mutual Invasibility Conditions

Since models (2.32) and (2.2) are in the same form, we expect mutual invasibility of IG prey and IG predator to take place in the same correspondent parameter regions as found for the homogeneous landscapes. This way, we expect mutual invasibility only for $\Gamma > 1$, i.e., when the homogenized competitive measure shows that IG prey is the stronger competitor, and within a range of effective

Table 2.1: Symbol correspondence for parameters on models (2.1), (2.14) and (2.25).

Parameter/Variable	**Homogeneous Landscape**	**Heterogeneous Landscape** (small scale)	**Heterogeneous Landscape** (homogenized)
Population Densities	C_1, C_2, R	C_{1j}, C_{2j}, R_j	$\hat{C}_1, \hat{C}_2, \hat{R}$
(Effective) Diffusion	D_i	D_{ij}	$\hat{D}_i = \hat{l}_i^2 \langle D_i \rangle^{(H)}$
Resource growth	$G(R) = rR(1-R/K)$	$G_j(R_j) = r_j R_j(1-R_j/K_j)$	$\hat{G}(\hat{R}) = \langle r \rangle \hat{R}(1-\hat{R}/\hat{K})$
Intrinsic growth rate	r	r_j	$\langle r \rangle = \frac{l_1 r_1 + l_2 r_2/k_R}{\ell_R}$
Carrying capacity	K	K_j	$\hat{K} = \frac{\langle r \rangle \ell_R^2}{l_1 r_1/K_1 + l_2 r_2/(K_2 k_R^2)}$
Death rate	δ_i	δ_{ij}	$\langle \delta_i \rangle = \frac{l_1 \delta_{i1} + l_2 \delta_{i2}/k_i}{\ell_i}$
Attack rate	a_i	a_{ij}	$\langle a_i \rangle = \frac{l_1 a_{i1} + l_2 a_{i2}/(k_R k_i)}{\ell_R}$
Conversion rate	b_i	b_{ij}	$\langle b_i \rangle = \frac{l_1 b_{i1} + l_2 b_{i2}/(k_R k_i)}{\ell_i}$
IGP attack rate	α	α_j	$\langle \alpha \rangle = \frac{l_1 \alpha_1 + l_2 \beta_2/(k_1 k_2)}{\ell_1}$
IGP conversion rate	β	β_j	$\langle \beta \rangle = \frac{l_1 \beta_1 + l_2 \beta_2/(k_1 k_2)}{\ell_2}$

carrying capacities $\hat{K}$.

The condition $\Gamma > 1$, in full form, becomes

$$\gamma_1 \gamma_2 > \left(\frac{\tilde{\theta}_2 k_2 k_R + \tilde{\delta}_2 l/\tilde{\theta}_2}{k_2 + \tilde{\delta}_2 l} \right) \left(\frac{\tilde{\theta}_1 k_1 k_R + \tilde{\delta}_1 l/\tilde{\theta}_1}{k_1 + \tilde{\delta}_1 l} \right)^{-1}, \tag{2.34}$$

where $l = l_2/l_1$ is the ratio of patch sizes, $\tilde{\delta}_i = \delta_{i2}/\delta_{i1}$ is the ratio of species i death rates in patch 2 and patch 1, $\tilde{\theta}_i = \sqrt{R_{i2}^*/R_{i1}^*}$, the ratio between resource levels in presence of species i in different patch types. Finally, $\gamma_j = \sqrt{R_{2j}^*/R_{1j}^*}$ is the competition outcome measure in patches of type j.

Whenever the right-hand side of inequality (2.34) is smaller than unity, mutual invasibility is facilitated and can occur even if $\gamma_j < 1$, $j = 1, 2$, i.e., competitive reversals in favor of IG prey are possible. At the same time, whenever the right-hand side is larger than unity, mutual invasibility is hindered, and may not occur

even if $\gamma_j > 1$, $j = 1, 2$, i.e., competitive reversals in favor of IG predator are also possible. When the right-hand side is precisely unity, the condition reduces to $\gamma_1 > \gamma_2^{-1}$, that is, whenever IG prey is not competitively stronger in one of the patches, it has to overcompensate this effect in the other patch.

The possible competitive reversal scenarios found on inequality (2.34) depend heavily on all three species patch preferences, k_i, $i = 1, 2, R$, how patchy the landscape is, given by l, as well as consumer traits ($\tilde{\theta}_i$ and $\tilde{\delta}_i$). To simplify this relation and gain some insight on how habitat preferences govern this inequality, we assume $\gamma_1 = \gamma_2 = \gamma$, which also implies $\tilde{\theta}_1 = \tilde{\theta}_2 = \tilde{\theta}$, and define $q_R = \tilde{\theta}^2 k_R$ and $\eta_i = \tilde{\delta}_i / k_i$. With this, condition (2.34) becomes

$$\gamma^2 > \left(\frac{q_R + \eta_2 l}{1 + \eta_2 l}\right)\left(\frac{1 + \eta_1 l}{q_R + \eta_1 l}\right) = w(q_R, l, \eta_1, \eta_2). \tag{2.35}$$

Note that $w(q_R = 1, \cdot) = 1$, i.e., whenever $q_R = 1$, we recover the conditions found in an homogeneous landscape. Moreover,

$$\text{sign}(\partial_{q_R} w) = \text{sign}\,(\eta_1 - \eta_2) \tag{2.36}$$

such that if $\eta_1 > \eta_2$, then w is monotonically increasing in q_R, and monotonically decreasing otherwise. Because q_R is monotone in $\tilde{\theta}$ and k_R, w is also monotone in these parameters. Since $w(q_R = 1, \cdot) = 1$, if w is monotonically increasing in q_R (figure 2.8a), then for $q_R > 1$ we have hindered mutual invasibility conditions, because $\gamma^2 > w(q_R, \cdot) > 1$, i.e., γ must be larger than what is expected in an homogeneous landscape. For $q_R < 1$ we have facilitated mutual invasibility conditions, because $\gamma^2 > w(q_R, \cdot)$ with $w(q_R, \cdot) < 1$, i.e., γ can be smaller than what is expected in an homogeneous landscape. The opposite holds when w is monotonically decreasing (figure 2.8b).

The ecological interpretation of inequality (2.35) and equation (2.36) is as follows: $\eta_i = \tilde{\delta}_i / k_i$ relates species i patch preference, k_i, and how much larger is its death rate in pathces of type 2 compared to type 1, $\tilde{\delta}_i$. Whenever there is a difference between IG prey and IG predator in this relation, then mutual invasibility is hindered or facilitated depending on how unbalanced is resource consumption between different patches, θ, and resource patch preference k_R.

To understand solely the effects of patch preferences, let $\tilde{\delta}_1 = \tilde{\delta}_2$, $\tilde{\theta} = 1$ and consider the following example: IG prey prefers patches of type 1, such that $k_1 > 1$, and IG predator prefers patches of type 2, such that $k_2 < 1$, this way, w is monotonically decreasing. The region $k_R > 1$ (resource prefers patches of type 1)

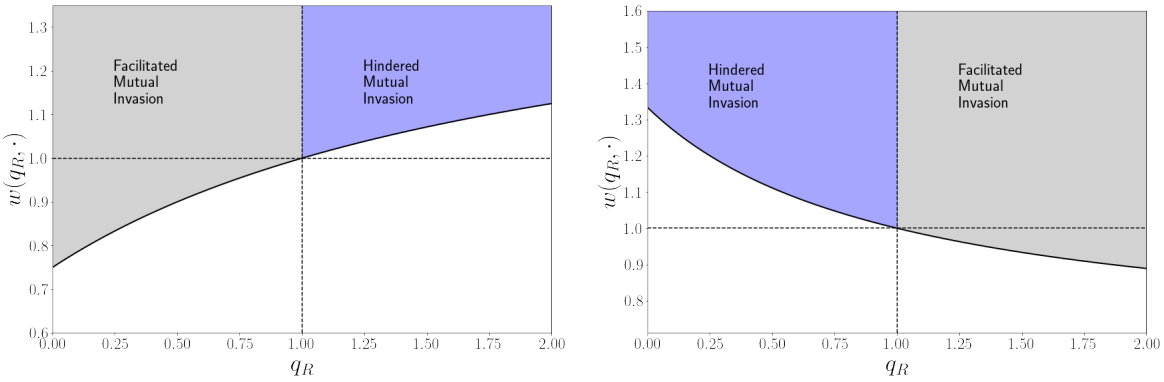

(a) w is monotonically increasing: $\eta_1 > \eta_2$

(b) w is monotonically decreasing: $\eta_1 < \eta_2$

Figure 2.8: Regimes of facilitated and hindered mutual invasions, depending on how the quantities $\frac{\tilde{\delta}_i}{k_i}$, $i = 1, 2$ relate.

leads to a competitive reversal in favor of IG prey whenever $w < \gamma^2 < 1$, while the region $k_R < 1$ (resource prefers patches of type 2) leads to competitive reversals in favor of IG predator whenever $w > \gamma^2 > 1$. The outcomes of the example are reversed when $k_1 < 1 < k_2$, i.e., IG prey and IG predator patch preferences are switched. This way, whichever consumer has their patch preferences aligned with resource species' patch preference can cause competitive reversals.

Similarly, we can understand competitive reversal scenarios only considering the death rate ratios, $\tilde{\delta}_i$, and uneven resource consumption between patches, $\tilde{\theta}$, through the following example: Let $k_1 = k_2$ and $k_R = 1$ and consider IG prey have a smaller death rate in patches of type 1 than in patches of type 2, and the opposite for IG predator, such that $\tilde{\delta}_2 < 1 < \tilde{\delta}_1$. With that, w is monotonically increasing in $\tilde{\theta}$. For $\tilde{\theta} < 1$, i.e., resource is less consumed in patches of type 1, we may have competitive reversals in favor of IG prey whenever $w < \gamma^2 < 1$, while $\tilde{\theta} > 1$ favors IG predator if $w > \gamma^2 > 1$. That way, whenever the patch where IG prey dies less is also the one where resource is less consumed, we have facilitated mutual invasibility, while hindered conditions apply when we have the opposite.

We could also discuss similar effects that occur between k_1, k_2 and $\tilde{\theta}$, as well as between $\tilde{\delta}_1, \tilde{\delta}_2$ and k_R, but the outcome would be quite similar. In a general manner, whenever the conditions favor IG prey (IG predator) in some way, the mutual invasibility conditions are facilitated (hindered). To formally write these parameter regions, we define $\delta\eta = \eta_1 - \eta_2$ and write the facilitated, $\mathcal{H}_f$, and hindered, $\mathcal{H}_h$, mutual invasion conditions as quadrants in the parameter space $(q_R, \delta\eta) \in \mathbb{R}_+ \times \mathbb{R}$ defined by

$$\mathcal{H}_f = \{(q_R, \delta\eta) \in \mathbb{R}_+ \times \mathbb{R} | q_R < 1 \text{ and } \delta\eta > 0 \text{ or } q_R > 1 \text{ and } \delta\eta < 0\}, \quad (2.37)$$

$$\mathcal{H}_h = \{(q_R, \delta\eta) \in \mathbb{R}_+ \times \mathbb{R} | q_R > 1 \text{ and } \delta\eta > 0 \text{ or } q_R < 1 \text{ and } \delta\eta < 0\}. \quad (2.38)$$

The ratio among patch sizes, l, does not appear in any of the relations discussed so far, but it does play an important role. Again, we focus on the case $\gamma_1 = \gamma_2 = \gamma$, just to simplify expressions and gain some insight.

We have $\Gamma^2 = \gamma^2/w$, and we note that

$$\lim_{l\to 0} \Gamma(l, \cdot) = \lim_{l\to\infty} \Gamma(l, \cdot) = \gamma, \quad (2.39)$$

i.e., whenever the landscape is almost homogeneous ($l_1 \gg l_2$ or $l_2 \ll l_1$), we recover the homogeneous mutual invasion conditions.

A quick inspection on the derivative $\partial_l \Gamma^2$ reveals that

$$\text{sign}(\partial_l\{\Gamma^2\}) = \text{sign}\left[(q_R - 1)\delta\eta\left(\frac{\eta_1\eta_2}{q_R}l^2 - 1\right)\right], \quad (2.40)$$

so $\partial_l\Gamma$ switches sign just once, at $l^* = \sqrt{\frac{q_R}{\eta_1\eta_2}}$, which is therefore the only extremum point of Γ w.r.t l, and limits (2.39) imply Γ is bounded by its extremum, $\Gamma(l = l^*, \cdot)$, and γ. Note that l^* is the maximum point of $\Gamma(l, \cdot)$ whenever $(q_r, \delta\eta) \in \mathcal{H}_f$, and by limits in (2.39) we have $\gamma < \Gamma(l, \cdot) \leq \Gamma(l = l^*, \cdot)$. Therefore, if $\gamma > 1$, mutual invasion regimes are possible for any l. In a similar fashion, l^* is a minimum point of $\Gamma(l, \cdot)$ whenever $(q_r, \delta\eta) \in \mathcal{H}_h$, and the limits in (2.39) imply $\Gamma(l = l^*, \cdot) \leq \Gamma(l, \cdot) < \gamma$. Therefore, if $\gamma < 1$ mutual invasion regimes are not possible for any l. This reads that whenever IG prey (resp. IG predator) is the superior competitior and is benefited by facilitated (resp. hindered) mutual invasion conditions, mutual invasions can (resp. do not) take place regardless of how patchy the landscape is.

Now, assuming that l^* is a maximum point, in order to have $\Gamma(l = l^*, \cdot) > 1$, we must have

$$\gamma^2 > \frac{\frac{\tilde{\delta}_1}{k_1}q_R + \frac{\tilde{\delta}_2}{k_2} - 2\sqrt{q_R\frac{\tilde{\delta}_1}{k_1}\frac{\tilde{\delta}_2}{k_2}}}{\frac{\tilde{\delta}_1}{k_1} + \frac{\tilde{\delta}_2}{k_2}q_R - 2\sqrt{q_R\frac{\tilde{\delta}_1}{k_1}\frac{\tilde{\delta}_2}{k_2}}} = w(q_R, l^*, \eta_1, \eta_2). \quad (2.41)$$

However, $w(q_R, l^*, \eta_1, \eta_2) < 1$ for $(q_R, \delta\eta) \in \mathcal{H}_f$. By continuity of $\Gamma(l, \cdot)$, whenever

$$w(q_R, l^*, \eta_1, \eta_2) < \gamma^2 < 1, \quad (2.42)$$

we have competitive reversals in favor of IG prey around a neighborhood of l^* and mutual invasions are possible, i.e., in order to have $\Gamma > 1$ even when $\gamma < 1$, the proportion of patch type lengths must be close to l^*.

The precise extent of l values at which competitive reversals occur is obtained by solving $\Gamma(l = \bar{l}, \cdot) = 1$, which yields $\bar{l}_\pm = \bar{l}_0 \pm \sqrt{\bar{l}_0^2 - l^{*2}}$, where

$$\bar{l}_0 = -\frac{1}{2\eta_1\eta_2}\left(\eta_1\frac{(\gamma^2 - q_R)}{(\gamma^2 - 1)} + \eta_2\frac{(\gamma^2 q_R - 1)}{(\gamma^2 - 1)}\right). \tag{2.43}$$

Note that roots $\bar{l}_\pm$ become negative whenever $\gamma > 1$ and $(q_R, \delta\eta) \in \mathcal{H}_f$. In this regime mutual invasion become possible for any l, as expected.

By assuming that l^* is a minimum, i.e., that hindered mutual invasion conditions take place, we arrive at complementary results. We have

$$w(q_R, l^*, \eta_1, \eta_2) > 1 \text{ for } (q_R, \delta\eta) \in \mathcal{H}_h, \tag{2.44}$$

and whenever

$$1 < \gamma^2 < w(q_R, l^*, \eta_1, \eta_2), \tag{2.45}$$

competitive reversals occur in favor of IG predator. Mutual invasions are only possible outside the range $[\bar{l}_-, \bar{l}_+]$, i.e., when the landscape is more homogeneous/less patchy. Also, if $\gamma < 1$ and $(q_R, \delta\eta) \in \mathcal{H}_h$, both $\bar{l}_\pm$ become negative and mutual invasibility is not possible, as expected.

Whenever competitive reversals occur, $(q_R, \delta\eta)$ determines in which direction the reversals are and the roots $l_\pm$ delimit the heterogeneity levels of the landscape necessary for it. Still, mutual invasibility regions only take place within a range of effective carrying capacities, $\hat{K}$. We proceed as in the homogeneous case and define

$$\Phi_{1\to(2,R)} = M_1 E_2 \Gamma^2 \left(\Gamma - \frac{1}{\Gamma}\right), \tag{2.46}$$

$$\Phi_{2\to(1,R)} = \frac{M_2 E_1}{\Gamma^2}\left(\Gamma - \frac{1}{\Gamma}\right), \tag{2.47}$$

and with these, the threshold values in $\hat{K}$ become

$$\hat{K}_{1\to R} = \frac{1}{\Gamma}, \tag{2.48}$$

$$\hat{K}_{1\to(2,R)} = \frac{\Gamma}{1-\Gamma^{-1}\Phi_{1\to(2,R)}}, \tag{2.49}$$

$$\hat{K}_{2\to(1,R)} = \frac{1}{\Gamma(1-\Gamma\Phi_{2\to(1,R)})}, \tag{2.50}$$

$$\hat{K}_{2\to R} = \Gamma. \tag{2.51}$$

The mutual invasibility region is delimited by $\hat{K}_{2\to(1,R)} < \hat{K} < \hat{K}_{1\to(2,R)}$, which only exists if $\Gamma > 1$. We investigate these regions in the plane $(\hat{K}, l)$ by plotting the different threshold values $\hat{K}_{\cdot}$. To illustrate the precise effects of competitive reversals, we focus again on $\gamma_1 = \gamma_2 = \gamma$.

First, let us consider the case of competitive reversals in favor of IG prey, we consider $w(q_R, l*, \eta_1, \eta_2) < \gamma < 1$ and $(q_R, \delta\eta) \in \mathcal{H}_f$, to plot figure 2.9. At the limits $\log(l) \to \pm\infty$, the landscape is more homogeneous and heavily composed of a single patch type, and regime shifts from increasing levels of carrying capacity occur only from resource alone (pastel colored) to IG predator and resource communities (blue colored). Note that the $l \in [\bar{l}_-, \bar{l}_+]$ region, when the landscape become more patchy, we have $\Gamma > 1$ in the upper plot, corresponding to the l region where IG prey can establish alone with resource (gray colored) and mutual invasions can occur (cyan colored) in the lower plot. All curves are increasing in $\log(l)$ because $k_R < 1/2$, so resource strongly prefers patches of type 1, which length's proportion decrease with increasing l.

To compare the approximation in 2.9 with numerical results, we plot the maximum population densities in figure 2.10. For that, we let 10 pairs of patches 1 and 2 of equal size ($l_1 = l_2 = 1$) in order to investigate whether mutual invasibility regimes were indeed observed, and vary the carrying capacities in each patch equally. The thresholds found via homogenization technique are quite close to the ones observed numerically, and mutual invasibility showed to lead to coexistence between IG prey and IG predator.

Now, in the case $1 < \gamma < w(q_R, l*, \eta_1, \eta_2) >$ and $(q_r, \delta\eta) \in \mathcal{H}_h$, we have figure 2.11. The regions of mutual invasibility (cyan colored) and IG prey dominance (gray colored) only exist outside the range $[\bar{l}_-, \bar{l}]$, where $\Gamma > 1$ in the top plot. Inside the interval $[\bar{l}_-, \bar{l}]$, only IG predator is able to invade granted resource carrying capacity is high enough (blue colored), where $\Gamma < 1$, while for low values

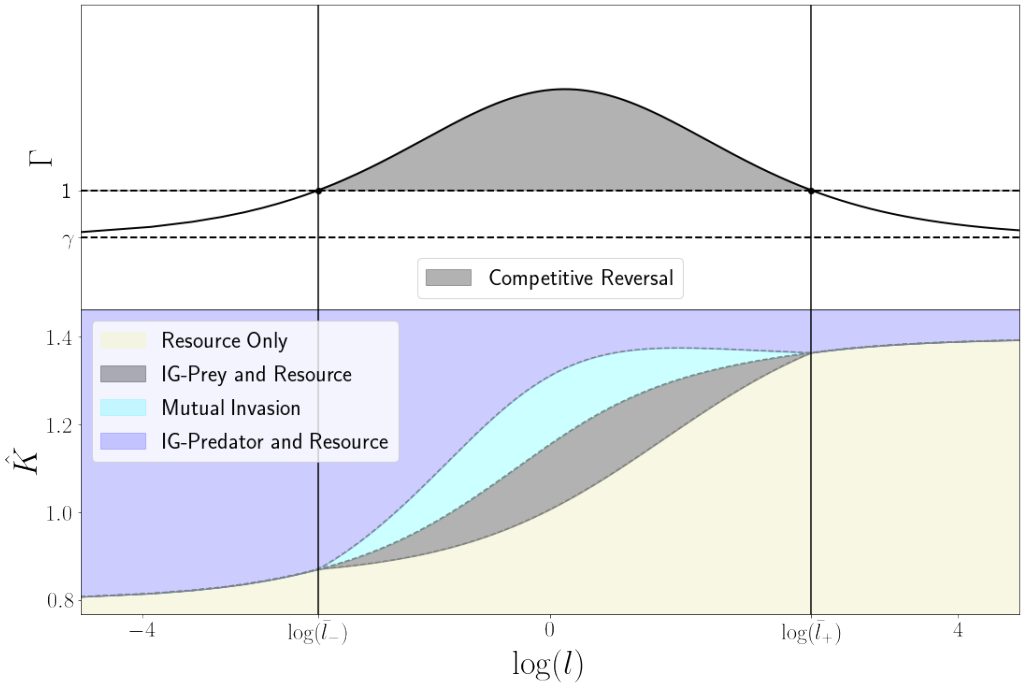

Figure 2.9: **Top**: Γ as a function of $\log(l)$. The gray colored region indicates a competitive reversals in favor of IG prey. **Bottom**: Invasibility regimes for different values of $\hat{K}$. The blue region is bounded bellow by $\hat{K}_{1\to(2R)}$ for $l \in [\bar{l}_-, \bar{l}_+]$, and by $\hat{K}_{2\to R}$ for other values of l, cyan region is comprised by $[\bar{l}_-, \bar{l}_+] \times [\hat{K}_{2\to(1R)}, \hat{K}_{1\to(2R)}]$, gray region is comprised by $[\bar{l}_-, \bar{l}_+] \times [\hat{K}_{1\to(R)}, \hat{K}_{2\to(1R)}]$, the pastel region is the complementary in the $(\hat{K}, \log(l))$ parameter space. **Parameters used**: $\alpha_1 = \alpha_2 = 0.25$, $\beta_1 = \beta_2 = 0.45$, $b_{11} = b_{12} = 0.8$, $b_{21} = 0.85 b_{22} = 0.6$, $\delta_{11} = \delta_{12} = 0.7$ $\delta_{21} = 0.85\delta_{22} = 0.5$, $r_1 = r_2 = 1$, $2D_1 = D_2 = 2D_R = 1.4$, $\alpha_1 = \alpha_R = 1 - \alpha_2 = 0.45$

of carrying capacity only resource is established in the landscape (pastel colored). This depicts a competitive reversal in favor of IG predator.

Again, we compare the approximation in 2.11 with numerical results in figure 2.12. For that, we let 10 pairs of patches 1 and 2 of equal size ($l_1 = l_2 = 1$) in order to investigate whether exclusion regimes were indeed observed, and vary the carrying capacities in each patch equally, as before. The IG predator threshold found via homogenization technique is quite close to the one observed numerically.

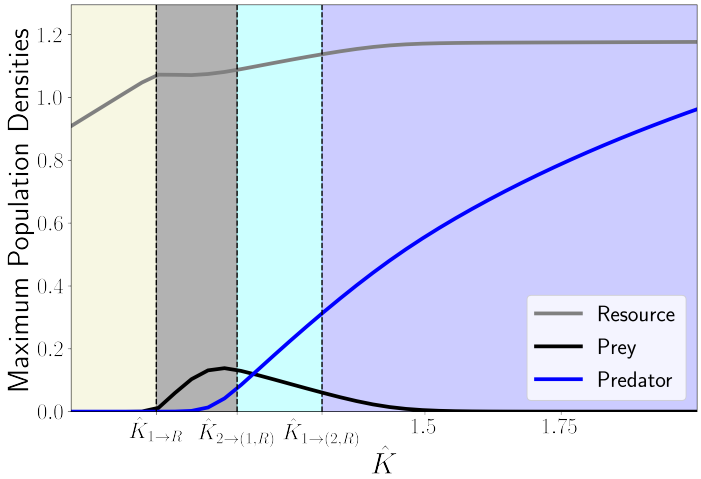

Figure 2.10: Numerically obtained maximum population densities for $l = 1$. The colored regions and parameters used are the same as in figure 2.9.

2.4 Discussion

In this work we analyzed of Intraguild Predation communities in homogeneous and heterogeneous landscapes, studying consumer species invasion dynamics. In an homogenous landscape, we recover invasibility conditions as expected in Holt and Polis [63], while also numerically verified that speeds of invasion are linearly determinate. In heterogeneous environments, using an approximation technique, we found competitive reversals between IG prey and IG predators modulated by multiple factors.

In an homogeneous landscape, we have four possible invasion regimes for $\gamma > 1$. First, neither of the consumers are able to invade, given $K < K_{1\to\rho}$, then, for $K \in [K_{1\to\rho}, K_{2\to(1,\rho)}]$ we have that only IG prey invades, and for $K \in [K_{2\to(1,\rho)}, K_{1\to(2,\rho)}]$ there is mutual invasibility/ coexistence, finally, for $K > K_{1\to(2,\rho)}$ only IG predator is able to invade the landscape. For $\gamma < 1$, we only find two regimes, either no consumer invades for $K < K_{2\to\rho}$, or IG predator invades for $K > K_{2\to\rho}$, excluding IG prey whenever it is also present in the landscape. This is the classical result of Holt and Polis [63], now revisited in the form of invisibility analysis of spatially structured populations.

Our numerical analysis of the homogeneous landscape model suggests that the different speeds of invasion are linearly determined for a large range of parameter values, this was somewhat expected, because invasion in consumer-resource

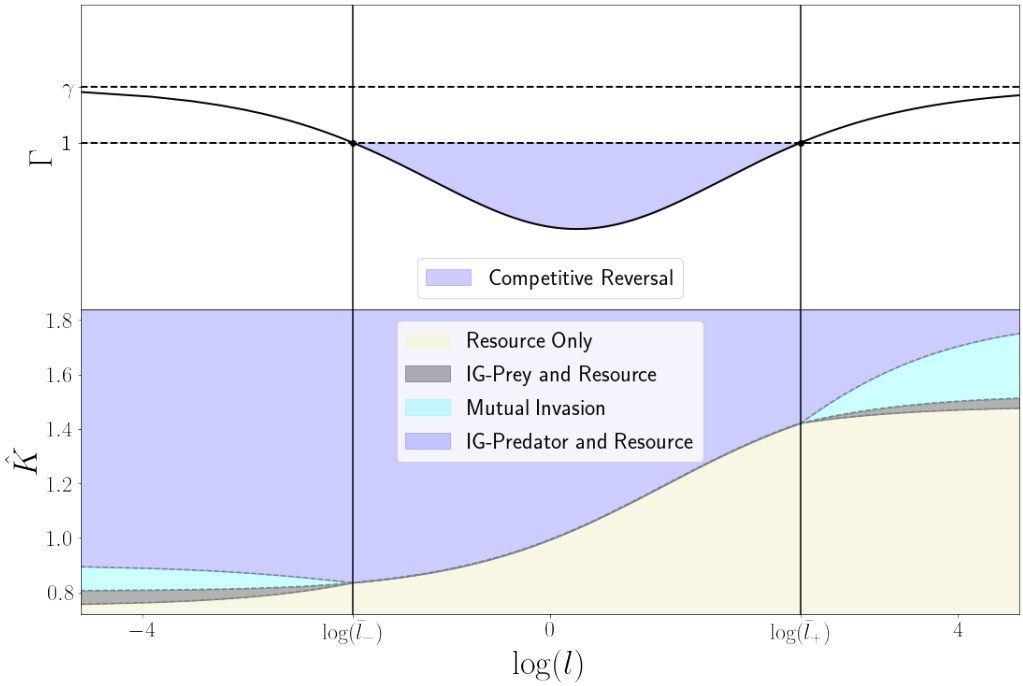

Figure 2.11: **Top**: Γ as a function of $\log(l)$. The gray colored region indicates a competitive reversals in favor of IG prey. **Bottom**: Invasibility regimes for different values of $\hat{K}$. The blue region is bounded bellow by $\hat{K}_{1\to(2R)}$ for $l \in [\bar{l}_-, \bar{l}_+]$, and by $\hat{K}_{2\to R}$ for other values of l, cyan region is comprised by $[\bar{l}_-, \bar{l}_+] \times [\hat{K}_{2\to(1R)}, \hat{K}_{1\to(2R)}]$, gray region is comprised by $[\bar{l}_-, \bar{l}_+] \times [\hat{K}_{1\to(R)}, \hat{K}_{2\to(1R)}]$, the pastel region is the complementary in the $(\hat{K}, \log(l))$ parameter space. **Parameters used**: $\alpha_1 = \alpha_2 = 0.25$, $\beta_1 = \beta_2 = 0.45$, $b_{11} = b_{12} = 0.8$, $b_{21} = 0.85 b_{22} = 0.6$, $\delta_{11} = \delta_{12} = 0.7$ $\delta_{21} = 0.85\delta_{22} = 0.5$, $r_1 = r_2 = 1$, $2D_1 = D_2 = 2D_R = 1.4$, $\alpha_1 = \alpha_R = 1 - \alpha_2 = 0.45$

models show linearly determinate speed as well [49, 80, 9]. We show that whenever a successful invasion leads to a shift from the resident community fixed point to a different stable fixed point (in the not spatially structured model sense), we usually have traveling wave solutions connecting these fixed points. We also show that dynamical stability regions can be formed when the coexistence fixed point is unstable, but leave the precise conditions in which to such dynamical stability occur for future research, possibly using the same analysis as in [48], which gets slightly more complicated in a three species system.

We have chosen linear functional responses for predator-prey dynamics, for both consumer-consumer or consumer-resource predation. However, if consumer-resource relations are type II Holing functions [45], the single consumer and resource equilibria can be unstable and present oscillations, allowing for coexis-

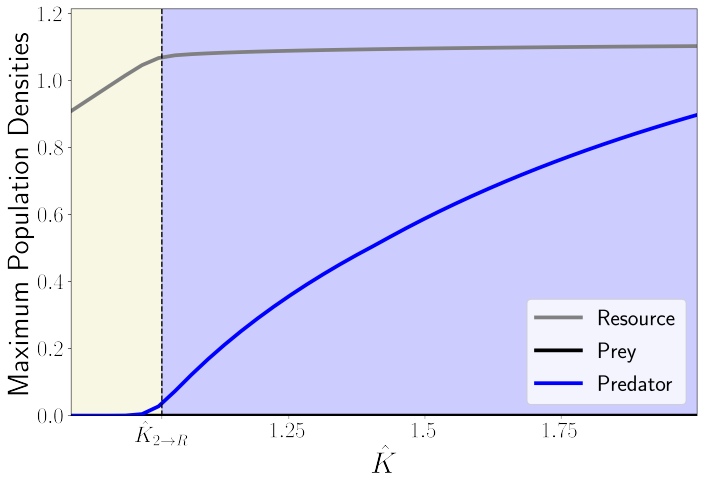

Figure 2.12: Numerically obtained maximum population densities for $l = 1$. The colored regions and parameters used are the same as in figure 2.11.

tence among two consumers without intraguild predation relations [74, 81]. The invasibility analysis in this scenario, however, gets much more complicated, and is a possible venue for future research.

The same invasibility regions found in homogeneous landscapes are found in periodic landscapes as well. However, they depend on multiple factors, and competitive reversals might occur. Competitive reversals have also been observed in models for interference competition in periodic landscapes in Maciel et al. [82], and depend exclusively on patchiness, l, and competitor species movement behaviors. Here we show that, in exploitative competition, resource patch preference is a key factor in order for competitive reversals to occur, either favoring IG prey or IG predator, whichever is more aligned with resources' patch preference or has a lower mortality rate therein, thereby facilitating or hindering mutual invasibility regimes. Competitive reversals can also occur if resource is unevenly consumed between patches. When resource is much less consumed where one of the consumers has a lower mortality rate, that consumer is benefited and can possibly overcome the fact of being the worst competitor. Similarly, competitive reversals occur if either of the consumers has a higher patch preference for the patch where resource is less consumed.

The observed competitive reversals show a mechanism of bottom-up regulation of Intraguild Predation communities, based on movement behavior of resource population [83]. This allows us to question if top-down regulations, based on predator patch preference, are possible in apparent competition interactions. Con-

sider an invasive generalist predator that induces apparent competition between species of the resident community. In homogeneous landscapes, we expect the classical results of [63], where prey species coexist at lower densities or that one excludes the other. In heterogeneous landscapes, however, consumer patch preference may shift expected exclusion regimes into coexistence ones and vice-versa, while also shifting exclusion of one prey species to the other. This can be possibly verified in a similar framework as displayed here, following [31, 32] to describe species interface behavior and [34, 64] to obtain approximate results, highlighting possible future venues where this framework can be applied.

Our work shows that a landscape composed by different patch types with similar lengths/areas, where species can interact and live, can be either detrimental or beneficial for biodiversity in intraguild predation communities, and has several implications in the context of biological invasions or reintroduction. By mutual invasion facilitation, we have possible coexistence regimes which would be otherwise unattainable. For hindered mutual invasion conditions, expected coexistence regimes might collapse, and IG predator may become dominant even if IG prey is the best competitor and carrying capacities are adequate in each of the patch types isolated.

Chapter 3

Integro-difference Models for Evolutionary Processes in Biological Invasions

3.1 Introduction

The ecological consequences of biological invasions, as well as how fast and far invading populations can spread, have been, and increasingly so, a focus of scientific attention [7]. More recently, different evolutionary processes of range expansions have been shown to play an important role in how such invasions occur (see Miller et al. [13] for a recent review on the topic). The fact that invading individuals differ in their dispersal abilities (by morphological or behavioral traits), as well as reproductive and/or competitive capacities, sets the stage for different evolutionary forces and ecological interactions to jointly alter the course of invasion [84, 85, 86]. Novel empirical observations about range expansions quickly lead to new modeling efforts because spatio-temporal scales and potential risks prevent large-scale experiments. Most of the mathematical theory is based on reaction diffusion equations (see Bouin et al. [87, 88], Keenan and Cornell [89], Morris et al. [90], to cite a few), while integrodifference equation (IDE) formulations are rare (Schreiber and Beckman [91], Lutscher et al. [92] are the few examples). IDE models are better suited to describe species with clearly distinct dispersal and growth phases; they also can account for different, non-Gaussian, movement behaviours [21]. Here, we will formulate and analyze a single-species trait-structured population IDE model. We will also explore numerically how different eco-evolutionary processes can change asymptotic spreading speeds and trait distributions at the leading edge.

One of the expected emerging processes to result from individual dispersal variation is spatial sorting, described in Shine et al. [85], Miller et al. [13] as an evolutionary process through which the most dispersive individuals in an expanding population are concentrated at the leading edge. In the absence of any other

forms of selection, these most dispersive individuals are the first colonizers of new, unexplored, regions and tend to mate with their equally dispersive peers therein, breeding, on average, offspring with dispersion traits larger than those of the overall population across the whole landscape. This process will repeat itself through many generations of the invading population, leading to the aforementioned effect on population distribution at the leading edge. The key elements through which spatial sorting occurs are dispersal heterogeneity within the population, genetic inheritance of these dispersal traits and the absence of any source of selection against these most dispersive individuals [85].

During range expansion, population density varies spatially and therefore sources of selection may differ between locations ('spatial selection'). For example, at the invasion front, densities are low so that there is little intra-specific competition, hence higher growth rates and dispersal ability are favoured (at least in the absence of an Allee effect [92]). By contrast, at the core of the population, density and intra-specific competition are high so that better competitive ability is favoured. Spatial selection may therefore create trade-offs between dispersal, growth and competitive abilities [86]. This leads to an interesting pattern of evolutionary forces throughout space, as, in the core, spatial selection for dispersal is much less important than selection for competitiveness, while in the front of an invasion the opposite holds. However, other forces of selection can impose heavy costs on the development of dispersal in favour of demographic traits [93].

On the mathematical side, the analysis of various models to understand population spread phenomena has evolved much since the pioneering work of Fisher [14], Kolmogorov A et al. [15]. The classical work of Weinberger [24] provides a more complete analysis of these single-species models, revealing that asymptotic spreading speeds and travelling wave solutions exist for these problems, and that the speed is, in many cases, linearly determinate, i.e., depends on the low-density dynamics at the invasion front. Lui [39] and Neubert and Caswell [40] extended this analysis for stage-structured populations, such as adult and juveniles life stages. Weinberger et al. [41], Lewis et al. [9] included inter-species biotic interactions.

Another type of structure which has recently been explored in mathematical models for population spread are traits: individuals within a species differ from each other by some demographic and/or dispersal trait. Alfaro et al. [94, 95, 96] explored the effects of demographic traits alone in reaction-diffusion equations. They found that, under some conditions, populations can adapt to spatio-temporally

changing optimal trait values. They showed that these equations support travelling wave solutions that spread at a constant speed. Bouin et al. [87] analyzed a reaction-diffusion model where individual dispersal is a continuously distributed trait. The authors found that such individual variation can allow for faster (accelerated in some scenarios) invasions and that the trait distribution at the leading edge is skewed towards higher dispersal. Qualitatively, these results persist even when high dispersal carries a mortality cost [88]. Other reaction–diffusion models considered finitely many morphs and trade-offs between dispersal and reproduction and found that anomalous spreading speeds may appear [97, 90, 89].

Few integrodifference equations account for individual variation in dispersal and reproduction. Marculis et al. [98] assumed that individuals invest their resources in either reproduction or dispersal, thereby creating an inherent trade-off between these traits. The authors found the optimal resource allocation strategy between dispersal and growth that maximized spread rates. Schreiber and Beckman [91] considered dispersal and growth rate as two independent traits and allowed for mutation between them. They showed that individual variation in dispersal leads to increased asymptotic spreading speeds, while variation in growth rates increases speed only if these traits are highly heritable.

We formulate IDE models with discrete and continuous trait space, analyze their behavior and explore how different evolutionary processes, such as spatial sorting, spatial and natural selection, alter the course of invasion and change population trait distributions. We connect our results with expectations of existing evolutionary theory.

In section 3.2, we present and describe two range-expansion models that include individual variability in reproduction and dispersal and account for mutations between different traits/types. Subsection 3.2.1 describes the formulation in continuous trait space, while 3.2.2 does the same in discrete trait space, that is, for a finite number of different types. In section 3.3, we prove the existence of travelling wave solutions and the formula for travelling wave speeds for both models. We show that increasing mutations typically decreases the spreading speed in section 3.4. Finally we present results on how asymptotic spreading speeds and trait distributions depend on trade-offs between mobility and growth in section 3.5. In section 3.6, we discuss model outcomes and interpretation from the evolutionary and ecological perspective, as well as provide future directions to expand the theory.

3.2 Model

In this section, we describe our discrete-time models for population spread in continuous physical space and continuous or discrete trait space, both formulated in terms of integrodifference equations. We give examples of the operators and functions necessary for the construction of such models, and discuss briefly how to interpret different modelling choices according to different biological processes. We keep the definitions broad, such that the formulation remains as general as possible.

From one generation to the next, individuals reproduce locally. Through mutation, the offspring may have a trait value different from their parent, that is, reproduction is clonal, but cloning is not necessarily perfect. Offspring then disperse in space, whereby their dispersal pattern depends on their trait value. Individuals are semelparous; i.e., they have a single reproductive phase in their life-time. Hence, their life-cycle is given by birth, dispersal, reproduction, and death, successively, with those events being synchronous within the population.

3.2.1 Continuous Trait Space

The density of individuals with continuous trait θ, at position x, in the t-th generation is denoted as $N_t(\theta, x)$. The following equation projects the density of individuals forward from one generation to the next through the operator Q:

$$N_{t+1}(\theta, x) = Q[N_t](\theta, x) = \int_{-\infty}^{\infty} K(\theta; x - y) \left\{ \int_{\Theta} L(\theta, \omega) F(\omega, N_t(\omega, y)) \mathrm{d}\omega \right\} \mathrm{d}y. \tag{3.1}$$

In this equation, $F(\omega, N)$ is the growth function of individuals with trait ω, usually written as $F(\omega, N) = NG(\omega, N)$, where $G(\omega, N)$ is the density dependent per capita growth rate. $L(\theta, \omega)$ is the mutation kernel, representing the probability that a parent of trait ω has an offspring of trait θ. We assume that the trait space is compact and write $\Theta = [\theta_{\min}, \theta_{\max}]$. Choosing a compact trait space is important for mathematical reasons that will become clear in the next section. From a biological point of view, choosing the trait space to be compact does not seem to be a major limitation. For example, if the trait is related to dispersal ability such as variance of the dispersal kernel (see below), then zero is a natural minimum and the scale of a continent seems a natural maximum. We return to this

discussion below when we consider deleterious traits. By choosing the growth function independent of spatial location, we have assumed that the environment is spatially homogeneous. For that reason, we consider dispersal to depend on the signed distance between points but not on their absolute location. Therefore, we can write the movement kernel, $K(\theta; x - y)$, as a probability density function of the location x of an individual with trait θ after dispersal, given that it was at location y before dispersal. Since we are interested in the effects of evolution and mutation on population spread rates, we choose physical space to be unbounded, i.e., $x, y \in \mathbb{R}$.

Since $K(\theta, \cdot)$ is a probability distribution, we require $K(\theta, \cdot) \geq 0$ and

$$\int_{-\infty}^{\infty} K(\theta, y)\mathrm{d}y = 1 \; \forall \; \theta, \tag{3.2}$$

which implies that dispersal in space incurs no loss to the population. We shall always assume that $K(\theta, \cdot)$ is exponentially bounded. For the mutation kernel, we require that $L(\cdot, \cdot) \geq 0$, and in general we only require that

$$\int_{\Theta} L(\theta, \omega)\mathrm{d}\theta \leq 1 \; \forall \; \omega. \tag{3.3}$$

If the integral is equal to unity for all ω, no individuals are lost due to mutations. If the integral is strictly less than unity for at least some ω, then some individuals are lost from trait space (and hence from the population) by mutation. Therefore, those mutations are deleterious, in fact, they are lethal.

3.2.2 Discrete Trait Space

When there are only finitely many types, we write θ_i for the trait value with $i = 1, \ldots, n$. We may assume that the trait values are ordered such that $\theta_j > \theta_i$ whenever $j > i$. The densities of different types at physical location x are given by the vector

$$\mathbf{N}_t(x) = (N_{1,t}(x), N_{2,t}(x), ..., N_{n,t}(x))^T, \tag{3.4}$$

where $N_{i,t}(x)$ is the density of individuals of type i in generation t. We denote vectors and matrices in bold letters, and write $\mathbf{V}^T$ for the transpose of a vector or matrix $\mathbf{V}$.

We collect the growth functions of the different types in a column vector, that is

$$\mathbf{F}(\mathbf{N}) = (F_1(\mathbf{N}), F_2(\mathbf{N}), ..., F_n(\mathbf{N}))^T, \tag{3.5}$$

where the F_i is the growth function of type i. Instead of a mutation kernel, we now have a mutation matrix $\mathbf{L} = l_{ij}$, where l_{ij} is the probability that parents of type j have offspring of type i. Each of the types move according to its trait; the respective movement kernels are organized in the diagonal matrix

$$\mathbf{K}(x-y) = \text{diag}((K_1(x-y), K_2(x-y), ..., K_n(x-y)), \tag{3.6}$$

with K_i the dispersal kernel of type i. With this notation, our model is written as

$$\mathbf{N}_{t+1}(x) = \tilde{Q}[\mathbf{N}_t](x) = \int_{-\infty}^{\infty} \mathbf{K}(x-y)\mathbf{L}\mathbf{F}(\mathbf{N}_t(y))\mathrm{d}y. \tag{3.7}$$

As in the continuous case, we must have $\mathbf{K} \geq 0$ and

$$\int_{-\infty}^{\infty} K_i(z)\mathrm{d}z = 1 \ \forall i. \tag{3.8}$$

The condition on the mutation matrix, $\mathbf{L}$, is now

$$\sum_{i=1}^{n} l_{ij} \leq 1 \ \forall \ j, \tag{3.9}$$

which is equivalent to

$$(\mathbf{1}^T\mathbf{L}) \leq \mathbf{1}^T \tag{3.10}$$

where $\mathbf{1}$ is the vector with all elements equal to 1. Again, equality holds when no loss from mutations is considered.

Remark 3.2.1. *We can formally discretize the mutation kernel, $L(\theta, \omega)$, from the continuous trait-space model by using delta distributions on n trait values, i.e.,*

$$L(\theta, \omega) = \sum_{i=1}^{n}\sum_{j=1}^{n} l_{ij}\delta(\theta - \theta_i)\delta(\omega - \theta_j). \tag{3.11}$$

We thereby obtain the discrete trait-space model in equation (3.7) from the continuous one in equation (3.1)

3.2.3 Modelling Examples

We give several examples of dispersal and mutation kernels as well as growth functions, and we indicate how different trait values can enter these functions.

Dispersal Kernels

When the trait is dispersal ability, a simple choice is to use the variance of the dispersal kernel as the trait value. In the case of a Gaussian or Laplace kernel, this leads to

$$K_G(\theta, x-y) = \frac{1}{\sqrt{2\pi\theta^2}} \exp\left(-\frac{(x-y)^2}{2\theta^2}\right), \tag{3.12}$$

$$K_L(\theta, x-y) = \frac{1}{\sqrt{2\theta^2}} \exp\left(-\sqrt{\frac{2}{\theta^2}}|x-y|\right). \tag{3.13}$$

Larger values of θ correspond to higher individual dispersal ability.

We can always represent our trait space $\Theta = [\theta_{\min}, \theta_{\max}]$, with $\theta_{\min} > 0$, as $\tilde{\Theta} = [0,1]$ by the affine transformation

$$\theta = (\theta_{\max} - \theta_{\min})\tilde{\theta} + \theta_{\min}, \tag{3.14}$$

where $\tilde{\theta} \in \tilde{\Theta} = [0,1]$. Note that $\tilde{\theta} = 0$ then corresponds to the minimal value of the parameter θ and not (necessarily) to $\theta = 0$. Throughout the text, whenever such movement kernels appear we will use this representation and drop the tildes.

We can also consider a behavioural trait, for instance, the probability of choosing between two types of movement kernels, say $K_1(x-y)$ and $K_2(x-y)$. Then, for $\theta \in \Theta = [0,1]$, we write

$$K(\theta, x-y) = \theta K_1(x-y) + (1-\theta)K_2(x-y). \tag{3.15}$$

Individuals with trait $\theta = 0$ move solely with dispersal kernel K_2, while individuals with trait $\theta = 1$ move solely with kernel K_1, and all the strategies in between are mixed. This type of dispersal kernel is often used to represent dispersal heterogeneity in a population, and is reported to best fit dispersal data of some tree species that display both short distance and a long distance dispersal simultaneously [99]. Such mixed kernels can reveal important aspects on how the asymptotic spreading speed changes according to different movement behaviours,

see, for instance, Stover et al. [100] and Lutscher [21] chapter 12.

Mutation Kernels

A simple way of modeling mutation is to consider a probability of mutation, μ, and a probability of perfect cloning, $1-\mu$. Then we obtain the mutation kernel

$$L(\theta,\omega) = (1-\mu)\delta(\theta-\omega) + \mu T(\theta,\omega), \tag{3.16}$$

where $\delta(\cdot)$ is the Dirac delta distribution and $T(\cdot,\omega)$ is a probability distribution function.

The analogous formulation for discrete traits is

$$\mathbf{L} = (1-\mu)\mathbb{1} + \mu\mathbf{T}, \tag{3.17}$$

where $\mathbf{T}$ is a column stochastic matrix.

A similar approach for describing mutations was taken by [91], but the authors assumed that the probability of mutating to some trait was independent of the parent's trait. Hence, they used a fixed distribution $T(\theta,\omega) \equiv T(\theta)$, a model class that encompasses Kingman's "House of Cards" model [101] as well as models considering rank-1 mutation matrices.

When there is no loss through mutation, i.e., no deleterious mutations, then L and $\mathbf{L}$ cannot be symmetric. Such conservative mutation kernels are also considered in [102] in an integro-differential equation. However, the trait considered there has no direct relation with individual dispersal ability.

Another possibility to describe mutation is as a truncated probability distribution for $\theta-\omega$, the distance between parent and offspring traits. If there are no deleterious mutations, we write

$$L(\theta,\omega) = \frac{f(\theta-\omega)}{\int_\Theta f(\theta-\omega)\mathrm{d}\theta'}, \tag{3.18}$$

where $f(\cdot)$ is any probability distribution. Note that here, mutation rarity is measured as the spread of $f(\cdot)$, such as standard deviation or variance, as opposed to (3.16), where mutation is regarded as the probability of imperfect cloning.

To allow for deleterious mutations in a kernel such as (3.18), we can disregard the normalization factor in the denominator. Deleterious mutations, therefore, can be studied in a general manner by letting

$$\int_\Theta L(\theta,\omega)\mathrm{d}\theta \;=\; g(\omega) < 1. \tag{3.19}$$

Given a mutation kernel with deleterious mutation, we can re-scale to obtain a kernel without deleterious mutations but a modified growth function. When we define $\Lambda(\theta,\omega) = L(\theta,\omega)/g(\omega)$, we get

$$\begin{aligned} N_{t+1}(\theta,x) &= \int_{-\infty}^{\infty} K(\theta; x-y) \int_\Theta L(\theta,\omega) F(\omega, N_t(\omega,y))\mathrm{d}\omega\mathrm{d}y, && (3.20)\\ &= \int_{-\infty}^{\infty} K(\theta; x-y) \int_\Theta \Lambda(\theta,\omega) g(\omega) F(\omega, N_t(\omega,y))\mathrm{d}\omega\mathrm{d}y, && (3.21)\\ &= \int_{-\infty}^{\infty} K(\theta; x-y) \int_\Theta \Lambda(\theta,\omega) \Phi(\omega, N_t(\omega,y))\mathrm{d}\omega\mathrm{d}y, && (3.22) \end{aligned}$$

where $\Phi(\omega,N) = g(\omega)F(\omega,N)$ is the re-scaled growth function. Since $g(\omega) < 1$, we have $\Phi(\omega,N) \leq F(\omega,N)$. We see that deleterious mutations produce losses in growth that are unequally distributed in trait space. Such a rescaling also introduces a dependence of the growth function on the shape parameters of the mutation kernel. For example, consider the Gaussian mutation kernel

$$L(\theta-\omega;\mu) = \frac{1}{\sqrt{2\pi\mu^2}} \exp\left(-\frac{(\theta-\omega)^2}{2\mu^2}\right), \tag{3.23}$$

where μ is the standard deviation ghat controls how rare mutations are. The re-scaled growth function (with $\Theta = [0,1]$ as explained above) is

$$\begin{aligned} \Phi(\omega,N;\mu) &= F(\omega,N) \int_0^1 L(\theta-\omega;\mu)\mathrm{d}\theta, && (3.24)\\ &= \frac{F(\omega,N)}{2}\left(\mathrm{erf}\left(\frac{1-\omega}{\sqrt{2\mu^2}}\right) - \mathrm{erf}\left(\frac{\omega}{\sqrt{2\mu^2}}\right)\right). && (3.25) \end{aligned}$$

Therefore, for $\mu \approx 0$, individuals at the edges of trait space lose about half their growth, while growth at the centre of trait space remains almost unchanged. As μ increases, $\Phi(\omega,N;\mu)$ decreases, i.e., as mutations become more common, so do deleterious mutations. The species overall becomes less viable. In general terms, high mutation rates lead to increased measures of spread of the mutation kernel, which in turn lead to smaller $g(\omega)$, which reflects directly in the species' growth

function $\Phi(\omega, N)$.

In discrete trait space, the re-scaling is achieved by introducing a diagonal matrix, $\mathbf{\Gamma} = \text{diag}(\Gamma_{ii})$, where $\Gamma_{ii} = \sum_j L_{ij} \leq 1$, or, in matrix notation,

$$\mathbf{1}^T \mathbf{L} = \mathbf{1}^T \mathbf{\Gamma}. \tag{3.26}$$

Then the loss of individuals from type-i parents due to mutation is $1 - \Gamma_{ii}$. Then, as in the continuous case, we define the re-scaled mutation matrix $\mathbf{\Lambda} = \mathbf{L}\mathbf{\Gamma}^{-1}$ and the re-scaled growth functions become $\mathbf{\Phi}(\mathbf{N}) = \mathbf{\Gamma}\mathbf{F}(\mathbf{N})$.

Demographic Traits

We can also consider traits related to reproduction or intra-specific competition. The following example is based on a generalized Beverton-Holt model. Consider

$$F(\theta, N(\theta, x)) = \frac{R(\theta)N(\theta, x)}{1 + Y[N](\theta, x)}, \tag{3.27}$$

where $R(\theta)$ is the low-density growth rate of trait θ and Y is an operator that represents competition for resources. Different choices of Y can model different biological phenomena. The simplest form is

$$Y[N](\theta, x) = k(\theta)N(\theta, x), \tag{3.28}$$

where competition is limited between individuals of the same trait, but can vary from trait to trait by the function $k(\theta)$. That is, each trait has its own niche and niches of different traits do not overlap. When niches overlap, we can write

$$Y[N](\theta, x) = k(\theta) \int_\Theta b(\theta, \omega)N(\omega, x)\mathrm{d}\omega. \tag{3.29}$$

Now, individuals of trait ω compete with individuals of trait θ within their respective niches. This competition is described by some function $b(\theta, \omega)$. If the niches of traits θ and ω overlap strongly (weakly) then both $b(\theta, \omega)$ and $b(\omega, \theta)$ are large (small). More details on modelling of intra-specific competition between different phenotypes can be found, for instance, in Doebeli [103]. We can think of $b(\theta, \omega)$ as the continuous limit of a competition matrix, $\mathbf{B} = b_{ij}$, where b_{ij} gives the competition strength between types i and j within type i niche, such as in competitive Lotka-Volterra models for multiple species [104].

One particular focus in our work is on trade-offs between mobility and growth. For that, we consider a single trait that affects both, dispersal and growth. For

example, if we choose a dispersal trait θ as above, we can set the corresponding low-density growth rate as

$$R(\theta) = (R_{\max} - R_{\min}) \left(\frac{\theta_{\max} - \theta}{\theta_{\max} - \theta_{\min}} \right)^{\alpha} + R_{\min}, \quad \theta \in [\theta_{\min}, \theta_{\max}], \tag{3.30}$$

where $R_{\min}$ is the minimal growth rate, attained at $\theta = \theta_{\max}$ (where dispersal is maximal), $R_{\max}$ is the maximal growth rate, attained at $\theta = \theta_{\min}$ (where dispersal is minimal) and α a shape parameter. If $R_{\min} < 1$, there is a strong trade-off between dispersal and reproduction (when the most dispersive traits are not viable on their own), otherwise ($R_{\min} > 1$), the trade-off is weak. The shape parameter α controls whether the curve is convex ($\alpha > 1$) or concave ($\alpha < 1$). This function is also used in Marculis et al. [98], in a similar trade-off context, in order to determine optimal strategies of resource investment between growth and movement.

3.3 Spreading Speeds and Trait Distributions

Here, we present the theory that allows us to measure spreading speeds and determine the trait distributions at the leading edge. We use existing theory from stage-structured populations by Liang and Zhao [105] in the continuous case and by Lui [39], Neubert and Caswell [40] in the discrete case.

In what follows, we denote the scalar field $S = (\Theta \times \mathbb{R})$ as the continuous trait and physical spaces, that is, the domain of the densities $N_t(\theta, x)$. We write $C(S)$ for the Banach space of continuous functions on S and $C_f(S) = \{u \in C(S) \mid 0 \leq u \leq f\}$ for the set of positive continuous functions on S, bounded from above by a given $f(\theta, x)$.

3.3.1 Continuous Trait Space

We make the following assumption on the movement and mutation kernels as well as the growth function.

(*AC1*): $K(\theta, z)$, is continuous in $\theta \in \Theta$ and movement is unbiased, i.e.,

$$K(\theta, z) = K(\theta, -z) \; \forall \; \theta \in \Theta. \tag{3.31}$$

(*AC2*): For every $\theta \in \Theta$, $K(\theta, z)$ is exponentially bounded, that is, the moment generating function

$$M(\theta, s) = \int_{-\infty}^{\infty} K(\theta, z) e^{sz} \mathrm{d}z \tag{3.32}$$

is finite for some $s > 0$ and for all $\theta \in \Theta$. Since $K(\theta, \cdot)$ is a probability density function for all θ, $M(\theta, s)$ is strictly positive.

(*AC3*): $F(\omega, N)$ is continuous and monotone increasing in N and is linearly bounded for all ω, i.e.,

$$R(\omega)N > F(\omega, N) \; \forall \, \omega, \tag{3.33}$$

where $R(\omega) = \partial_N F(\omega, 0) > 0 \; \forall \omega$.

(*AC4*): There are two steady states, $N_t(\theta, x) = 0$ and $N_t(\theta, x) = N^*(\theta) > 0$, such that

$$N^*(\theta) = \int_\Theta L(\theta, \omega) F(\omega, N^*(\omega)) \mathrm{d}\omega. \tag{3.34}$$

(*AC5*): The operator

$$\mathcal{L}[u](\theta) = \int_\Theta L(\theta, \omega) u(\omega) \mathrm{d}\omega \tag{3.35}$$

is irreducible. A sufficient condition for that is achieved by assuming that $L(\theta, \omega)$ is bounded above by a constant $\tilde{L}$, and also that it is strictly positive on a neighbourhood of the line $\theta - \omega = 0$, i.e,

$$L(\theta, \omega) < \tilde{L}, \; \theta, \omega \in \Theta \quad \text{and} \quad 0 < L(\theta, \omega) \text{ if } |\theta - \omega| < \epsilon. \tag{3.36}$$

This grants that any parent with trait ω can have descendants of any other trait θ given sufficient generations. We will also assume that $L(\theta, \omega)$ is continuous in $(\theta, \omega) \in \Theta^2$.

(*AC6*): The dominant eigenvalue of

$$\mathcal{L}[Ru](\theta) = \int_\Theta L(\theta, \omega) R(\omega) u(\omega) \mathrm{d}\omega \tag{3.37}$$

is larger than unity. This implies that the species is able to grow from small densities.

With this set of assumptions, we state our first theorem, which is a summarized version of theorems in [105] applied to our case.

Theorem 3.3.1. *Given the recursion $N_{t+1}(\theta, x) = Q[N_t](\theta, x)$ and an initial condition $N_0(\theta, x)$ with compact support, if Q satisfies assumptions (AC1)–(AC6), then there is an asymptotic spreading speed c^* for Q. Moreover, there are travelling wave solutions, $N_t(\theta, x) = W(\theta, x - ct)$, for every $c \geq c^*$ and no such solutions otherwise. Also, the system is linearly determinate with asymptotic speed given by*

$$c^* = \inf_{s>0} \left\{ \frac{1}{s} \ln(\lambda_s) \right\}, \tag{3.38}$$

where λ_s is the dominant eigenvalue of the linearized operator

$$P_s[q](\theta) = M(\theta, s) \int_\Theta L(\theta, \omega) R(\omega) q(\omega) \mathrm{d}\omega, \tag{3.39}$$

where $q = q(\omega)$ is a trait distribution.

Finally, the dominant eigenfunction of P_{s^*} is the population trait distribution at the leading edge, where s^* is the value of s at which the asymptotic speed is attained.

Proof. The operator has the stationary states $N^*(\theta)$ and 0. It is translation and reflection invariant and it is also order preserving, continuous and compact in $C_{N^*}(S)$. The linear operator P_s is also compact and has a simple positive dominant eigenvalue [106]. Thus, the recursion relation $N_{t+1}(\theta, x) = Q[N_t](\theta, x)$ satisfies all the conditions in remark 4.5 from Liang and Zhao [105]. Therefore, by that remark, there exists an asymptotic spreading speed and travelling wave solutions, and the speed is linearly determinate.

The claim that the dominant eigenvector of P_{s^*} is the population distribution at the leading edge can be checked by writing a solution of the linearized problem as a linear combination of eigenfunctions, $q_{i,s}$, of the linearized operator P_s. Let

$$N_t(\theta, x, s) = \sum_i \beta_i q_{i,s}(\theta) \lambda_{i,s}^t e^{-sx} \tag{3.40}$$

be such a linear combination and a solution, with shape parameter s, of the linearized operator

$$N_{t+1}(\theta, x) = P[N_t](\theta, x) = \int_{-\infty}^{\infty} K(\theta, x - y) \int_\Theta L(\theta, \omega) R(\omega) N_t(\omega, y) \mathrm{d}\omega \mathrm{d}y. \tag{3.41}$$

Let $\lambda_s = \lambda_{1,s}$ be the dominant eigenvalue of P_s and $q_s(\theta) = q_{1,s}(\theta)$ its respective

eigenfunction, then evaluating the limit below we get

$$\lim_{t\to\infty}\frac{N_t(\theta,x,s)}{\lambda_s^t}=\lim_{t\to\infty}e^{-sx}\sum_i\beta_i q_{i,s}(\theta)\left(\frac{\lambda_{i,s}}{\lambda_s}\right)^t=e^{-sx}\beta_1 q_s(\theta). \tag{3.42}$$

In the asymptotic limit, however, such solutions travel at speed c^*, with shape parameter $s=s^*$. Hence, the asymptotic population trait distribution at the leading edge is given by the dominant eigenfunction $q_{s^*}(\theta)$. □

3.3.2 Discrete Trait Space

The assumptions on the dispersal and mutation kernels as well as the growth functions in case of a finite trait space are analogous to the assumptions for the continuous case above.

(*AD1*): The kernels $K_i(z)$, $i=1,2,\ldots,n$, are continuous and movement is unbiased.

(*AD2*): The kernels $K_i(z)$, $i=1,2,\ldots,n$, are exponentially bounded. This implies that the matrix of moment generating functions

$$\mathbf{M}_s=\operatorname{diag}(M_1(s),M_2(s),\ldots,M_n(s)) \tag{3.43}$$

has finite entries for some $s>0$. Since $K_i(\cdot)$ are probability density functions, the $M_i(s)$ are strictly positive.

(*AD3*): Functions $F_i(N)$, $i=1,2,...,n$, are monotone and linearly bounded, i.e., $R_iN_i>F_i(\mathbf{N})$, where $R_i=\partial_{N_i}F_i(\mathbf{0})>0\ \forall\ i$.

(*AD4*): There are two steady states: $\mathbf{0}=\tilde{Q}[\mathbf{0}]$ and $\mathbf{0}<\mathbf{N}^*=\tilde{Q}[\mathbf{N}^*]$.

(*AD5*): The mutation matrix $\mathbf{L}$ is irreducible.

(*AD6*): The dominant eigenvalue of $\mathbf{LR}$ is larger than unity, where $\mathbf{R}=\operatorname{diag}(R_i)$.

The existence of a spreading speed and its linear determinacy in the discrete case now results from applying the results in [39] to our model.

Theorem 3.3.2. *Given the recursion $\mathbf{N}_{t+1}(x)=\tilde{Q}[\mathbf{N}_t](x)$ and an initial condition $\mathbf{N}_0(x)$ with compact support in x, if $\tilde{Q}$ satisfies assumptions (AD1)-(AD6), then there is an asymptotic spreading speed c^* for $\tilde{Q}$. Moreover, there are travelling wave solutions,*

$\mathbf{N}_t(x) = \mathbf{W}(x - ct)$, *for every* $c \geq c^*$ *and no such solutions otherwise. The system is linearly determinate, with asymptotic speed*

$$c^* = \inf_{s>0} \left\{ \frac{1}{s} \ln(\tilde{\lambda}_s) \right\}, \tag{3.44}$$

where $\tilde{\lambda}_s$ *is the dominant eigenvalue of*

$$\tilde{P}_s[\mathbf{q}] = \mathbf{M_s L R q}. \tag{3.45}$$

The dominant eigenvector of $\tilde{P}_{s^*}$ *is the population distribution at the leading edge, where* s^* *is the value of* s *at which the asymptotic speed is attained.*

Proof. Lui [39] formulated and analyzed an integrodifference equation for a stage-structured population. Assumptions (*AD1*)–(*AD6*) ensure that our trait-structured model satisfies all the conditions in Lui's theory. Hence, by applying Lui's results, we observe that our operator $\tilde{Q}$ has an asymptotic spreading speed; there exist travelling wave solutions; and the speed is linearly determinate.

The claim that the dominant eigenvector is the asymptotic population distribution can be verified in a similar fashion as in the case of a continuous trait space above. The only difference is to replace the eigenfunctions $q_{i,s}(\theta)$ by the eigenvectors $\mathbf{q}_{i,s}$. □

3.4 A Reduction Principle for Asymptotic Spreading Speeds

Having shown that our system admits travelling wave solutions with a linearly determined speed, we would like to understand how some biological mechanisms affect the spreading speed. Here, we explore how the probability of mutation affects the asymptotic spreading speed by considering a mutation kernel and matrix as described in (3.16) and (3.17), respectively. We denote the probability of mutation by μ and indicate the dependence of the next generation operator, the spreading speed and other quantities on mutation by index μ.

For a continuous trait space, we will consider that $T(\theta, \omega)$ is continuous, positive and bounded in Θ^2 and that

$$\int_\Theta T(\theta, \omega) \mathrm{d}\theta = \beta \quad \forall \omega, \tag{3.46}$$

while, for a discrete trait space, we assume that the matrix $\mathbf{T}$ is positive and

$$\mathbf{1}^T \mathbf{T} = \beta \mathbf{1}^T. \tag{3.47}$$

In both cases, i.e., continuous and discrete trait spaces, we assume that $0 < \beta \leq 1$ is a constant. When $\beta = 1$, there are no deleterious mutations, while when $\beta < 1$, there are some. Our assumption implies that all parents, regardless of their trait, have an equal probability of breeding mutant offspring with deleterious traits.

3.4.1 Continuous Trait Space

The mutation kernel in (3.16) does not satisfy the continuity assumption in (*AC5*). Therefore, we rely on the linear conjecture and assume that the linearized projection operator

$$P_{\mu,s}[q](\theta) = (1-\mu) M(\theta, s) R(\theta) q(\theta) + \mu M(\theta, s) \int_\Theta T(\theta, \omega) R(\omega) q(\omega) \mathrm{d}\omega, \tag{3.48}$$

has a simple positive dominant eigenvalue, $\lambda_{\mu,s}$. The asymptotic spreading speed is obtained as before, i.e.,

$$c^*_\mu = \inf_{s>0} \left\{ \frac{1}{s} \ln \lambda_{\mu,s} \right\}. \tag{3.49}$$

Under these assumptions, we use the results by Altenberg [107] and Thieme [108] to show that the asymptotic spreading speed is non-increasing with mutation probabilities.

Theorem 3.4.1. *Assume that the operator $P_{\mu,s}$ has a simple and positive dominant eigenvalue and that the recursion relation $N_{t+1} = P_\mu[N_t]$ has an asymptotic spreading speed, c^*_μ. Then, c^*_μ is non-increasing with mutation probability μ.*

Proof. We define

$$V_s[q](\theta) = M(\theta,s)R(\theta)q(\theta), \tag{3.50}$$

$$A_s[q](\theta) = M(\theta,s)\int_\Theta T(\theta,\omega)R(\omega)q(\omega)\mathrm{d}\omega - V_s[q](\theta), \tag{3.51}$$

and note that

$$P_{\mu,s}[q](\theta) = (V_s + \mu A_s)[q](\theta). \tag{3.52}$$

The operator V_s is an invertible multiplication operator, since $M(\theta,s)R(\theta) > 0$, while A_s is resolvent-positive. We apply theorem 6 in Altenberg [107], to find that for every $\mu > \mu_0 > 0$ we have

$$\gamma(P_{\mu,s}) \leq \gamma(P_{\mu_0,s}) + (\mu - \mu_0)\gamma(A_s), \tag{3.53}$$

where $\gamma(\cdot)$ denotes the spectral bound of an operator. The sign of $\gamma(A_s)$ can be obtained using theorem 3.5 in [108]. We have

$$\mathrm{sign}\{\gamma(A_s)\} = \mathrm{sign}\{\rho(H_s) - 1\}, \tag{3.54}$$

where

$$H_s[q](\theta) = (A_s + V_s)V_s^{-1}[q](\theta) = M(\theta,s)\int_\Theta \frac{T(\theta,\omega)}{M(\omega,s)}q(\omega)\mathrm{d}\omega, \tag{3.55}$$

and $\rho(H_s)$ is the spectral radius of H_s. Since H_s (and its adjoint H_s^*) are compact and positive, $\rho(H_s) = \rho(H_s^*)$ is a simple positive eigenvalue of H_s with corresponding eigenfunction of one sign by the Krein-Rutman theorem [106].

Using equation (3.46), we find that the adjoint operator

$$H_s^*[v](\omega) = \frac{1}{M(\omega,s)}\int_\Theta M(\theta,s)T(\theta,\omega)v(\theta)\mathrm{d}\theta \tag{3.56}$$

has the eigenfunction $v_s(\theta) = 1/M(\theta, s)$, and its corresponding eigenvalue is β. Note that $v_s(\theta)$ is of one sign. Therefore, $\rho(H_s^*) = \rho(H_s) = \beta$.

Since $\beta \leq 1$, we have $\gamma(A_s) \leq 0$. Equality holds when there are no deleterious mutations ($\beta = 1$); strict inequality otherwise. Therefore we have

$$\begin{cases} \gamma(P_{\mu,s}) \leq \gamma(P_{\mu_0,s}), & \text{if} \quad \beta = 1 \\ \gamma(P_{\mu,s}) < \gamma(P_{\mu_0,s}), & \text{if} \quad \beta < 1. \end{cases} \tag{3.57}$$

As we assumed that $P_{\mu,s}$ has a simple and positive dominant eigenvalue, this eigenvalue must equal the spectral bound, hence $\lambda_{\mu,s} = \gamma(P_{\mu,s})$. Taking the logarithm on both sides, dividing by s and taking the infimum in s reveals that

$$\begin{cases} c_\mu^* \leq c_{\mu_0}^*, & \text{if} \quad \beta = 1, \\ c_\mu^* < c_{\mu_0}^*, & \text{if} \quad \beta < 1, \end{cases} \quad \text{for} \quad \mu > \mu_0. \tag{3.58}$$

The first inequality means that asymptotic spreading speed is non-increasing with respect to mutation probability μ when there are no deleterious mutations. The second implies that it is strictly decreasing with mutation probability when deleterious mutations occur. □

3.4.2 Discrete Trait Space

In discrete (finite) trait space, the mutation matrix is irreducible and operator $\tilde{Q}$ satisfies all assumptions in Section 3.3.2. Hence, there is an asymptotic spreading speed and the system is linearly determinate. The linearized next-generation operator is

$$\tilde{P}_{\mu,s}[\mathbf{q}] = (1-\mu)\mathbf{M}_s\mathbf{R}\mathbf{q} + \mu\mathbf{M}_s\mathbf{T}\mathbf{R}\mathbf{q} = \mathbf{P}_{\mu,s}\mathbf{q}. \tag{3.59}$$

Since $\mathbf{P}_{\mu,s}$ is a positive matrix, it has a positive dominant eigenvalue, which we denote as $\tilde{\lambda}_{\mu,s}$. The asymptotic spreading speed is given by the same expression as in equation (3.49), switching $\lambda_{\mu,s}$ for $\tilde{\lambda}_{\mu,s}$.

Theorem 3.4.2. *Let $\tilde{P}_{\mu,s}$ be the linearized operator derived from an operator $\tilde{Q}_\mu$ that satisfies assumptions (AD1)-(AD6). Then, the corresponding asymptotic spreading speed c_μ^* is non-increasing with mutation probability μ.*

Proof. Similarly to the infinite dimensional case, we define

$$\mathbf{V}_s = \mathbf{M}_s\mathbf{R}, \tag{3.60}$$

$$\mathbf{A}_s = \mathbf{M}_s\mathbf{T}\mathbf{R} - \mathbf{V}_s, \tag{3.61}$$

so that

$$\mathbf{P}_{\mu,s} = \mathbf{V}_s + \mu\mathbf{A}_s. \tag{3.62}$$

Since $\mathbf{V}_s$ is invertible and $\mathbf{A}_s$ is essentially positive, Karlin's and Cohen's theorems (see theorem 5.2 in [109] and [110]) can be applied together with lemma 1 in Altenberg [107] to show that

$$\gamma(\mathbf{P}_{\mu,s}) \leq \gamma(\mathbf{P}_{\mu_0,s}) + (\mu - \mu_0)\gamma(\mathbf{A}_s). \tag{3.63}$$

The sign of $\gamma(\mathbf{A}_s)$ can be obtained similarly as in the continuous case. Following theorem 2.3 in Thieme [108], we find

$$\text{sign}\{\gamma(\mathbf{A}_s)\} = \text{sign}\{\rho(\mathbf{H}_s) - 1\}, \tag{3.64}$$

where

$$\mathbf{H}_s = \mathbf{M}_s\mathbf{T}\mathbf{M}_s^{-1}. \tag{3.65}$$

Using equation (3.47), we find that $\mathbf{v_s}^T = 1^T\mathbf{M}_s^{-1}$ is a positive left-eigenvector with eigenvalue β. Noticing that $\mathbf{H_s}$ and $\mathbf{P}_{\mu,s}$ are positive, by Perron-Frobenius [19] we have $\beta = \rho(\mathbf{H}_s)$ and $\gamma(\mathbf{P}_{\mu,s}) = \tilde{\lambda}_{\mu,s}$. By the the same arguments as in the case of continuous trait space, we have the exact same reduction principle for invasion speed as in equation (3.58). □

As the probability of mutation increases, the population cannot remain concentrated at the optimal trait, i.e., the trait that confers the highest speed. Therefore, the spreading speed of the population as a whole is reduced. Note that we did not assume any particular trade-off between growth rate and movement. Hence, the reduction principle is a general principle for any form of correlation between $M(\theta, s)$ and $R(\theta)$.

A similar reduction principle is found in [91] for continuous trait spaces. In our work, however, the principle is generalized for a larger class of mutation kernels. For discrete trait spaces, both Schreiber and Beckman [91] and Morris et al. [90] showed that mutation tends to lead to speed reductions. The model by Morris

et al. [90] consists of reaction–diffusion equations for only two interacting types. Our work shows that this result extends to multiple types as long as the mutation matrices $\mathbf{T}$ are positive and satisfy $\mathbf{1}^T\mathbf{T} = \beta\mathbf{1}^T$.

3.5 Results and Examples

Based on the theoretical results from previous sections, we now explore how mutation rates affect the spreading speed and population distribution at the leading edge under different dispersal kernels and with or without growth-rate trade-offs. In order to investigate trade-offs, we consider a growth rate of the form (3.30), exploring how its curvature affects the results with weak or strong trade-offs. This implies that $F(\theta, N)$ and $R(\theta)$ are nonincreasing with θ. Since we want to explore cases that are compatible with theorems 3.3.1 and 3.3.2, we let the mutation kernels be of the form (3.18), where f is a Gaussian distribution with mean zero and variance $\mu^2 > 0$. We let the compact trait space $\Theta = [\theta_{\min}, \theta_{\max}]$ be rescaled to $[0, 1]$ following equation (3.14). This way, operator Q is compact. For finitely many traits, we formally build the corresponding mutation matrix using equation (3.11). First, we do not consider deleterious mutations, i.e., $L(\theta, \omega)$ is normalized so that it integrates to 1 in θ. Later, we explore the role of deleterious mutations in population distributions and spreading speeds.

In the two extreme cases of no mutations ($\mu \to 0$) and very high mutations ($\mu \to \infty$), we can gain analytical insights; for intermediate cases, we use numerical simulations. In the limit of $\mu \to 0$, the mutation kernel tends to a Dirac delta. The recursion operator loses the necessary properties (compactness) for theorem 3.3.1, since it becomes a multiplication operator, however, the case of discrete trait space can still be investigated. In this case, each type invades the landscape alone. Note that the operator becomes $\mathbf{M}_s\mathbf{R}$, a diagonal matrix. The eigenvalues are $M(\theta_i, s)R(\theta_i)$, and therefore the spreading speed is

$$c^* = \inf_{s>0} \left\{ \frac{1}{s} \ln \left(\max_{\theta_i \in \Theta} (M(\theta_i, s)R(\theta_i)) \right) \right\}, \tag{3.66}$$

while the population distribution is given by the unit vector that points in the direction of the type $\theta_d(s)$ that maximizes $M(\theta_i, s)R(\theta_i)$ and therefore the speed. By continuity, population distributions tend to be concentrated near the optimum trait $\theta_d(s^*)$ at low mutation.

For comparison, we similarly define the single-type spreading speed as

$$c(\theta) = \inf_{s>0} \left\{ \frac{1}{s} \ln \left(M(\theta, s) R(\theta) \right) \right\}. \tag{3.67}$$

This is the speed at which the single type θ will spread if there is no mutation and if no other types are present. Note that the low-mutation limit in (3.66) is not simply the maximum over all the single-type speeds because the maximum over the θ_i is taken inside the infimum over s.

In the limit $\mu \to \infty$, we have $L(\theta, \omega) \to 1/\bar{\Theta}$, where $\bar{\Theta}$ is the size of trait space. In that limit, the eigenvalue problem of P_s is

$$\lambda(s) q_s(\theta) = \frac{M(\theta, s)}{\bar{\Theta}} \int_\Theta R(\omega) q_s(\omega) \mathrm{d}\omega. \tag{3.68}$$

Hence, for each s, $M(\theta, s)$ is an eigenfunction of (3.68) with eigenvalue given by the average

$$\lambda(s) = \langle M(\theta, s) R(\theta) \rangle := \frac{1}{\bar{\Theta}} \int_\Theta M(\theta, s) R(\theta) \mathrm{d}\theta, \tag{3.69}$$

so that by (3.69), the speed is given by

$$c^*_{\mu \to \infty} := \inf_{s>0} \left\{ \frac{1}{s} \ln \langle M(\theta, s) R(\theta) \rangle \right\} = \frac{1}{s^*} \ln \langle M(\theta, s^*) R(\theta) \rangle, \tag{3.70}$$

and the population trait distribution at the leading edge is

$$q^*_s(\theta) = \frac{M(\theta, s^*)}{\| M(\theta, s^*) \|}. \tag{3.71}$$

In the limit of high mutation, the trait distribution at the leading edge depends on individual movement behaviour. The speed, however, depends on the uniform average of the moment generating and the reproduction function $\langle M(\theta, s) R(\theta) \rangle$. In general, this average of the functions is different from the function value at the average trait, $\bar{\Theta}/2$. In fact, if MR is convex in θ, then $\langle M(\theta, s) R(\theta) \rangle \geq M(\bar{\Theta}/2, s) R(\bar{\Theta}/2)$, and since c^* is nonincreasing with mutation, the population always invades with a speed higher or equal to that of the median trait, that is

$$\inf_{s>0} \left\{ \frac{1}{s} \ln M(\bar{\Theta}/2, s) R(\bar{\Theta}/2) \right\} \leq \inf_{s>0} \left\{ \frac{1}{s} \ln \langle M(\theta, s) R(\theta) \rangle \right\} \tag{3.72}$$

$$c(\bar{\Theta}/2) \leq c^*_{\mu \to \infty} \leq c^*_\mu. \tag{3.73}$$

In the first example, we consider no trade-offs between reproduction and dispersal ($R(\theta)$ is constant). Next, we explore weak trade-offs, when all traits/types are viable on their own ($R(\theta) > 1 \; \forall \; \theta$). Finally we investigate strong trade-offs, when some of the traits/types are not viable on their own ($R(\theta) < 1$ for some θ).

Since in our model we consider monotone growth functions that can be linearized at low population densities, spatial selection favours traits θ that are the first to colonize new regions as long as they are able to grow therein, i.e., $R(\theta) > 1$. Hence, we will explore the roles of spatial sorting and selection under different mutation rates in the speed and trait distributions of the invading population.

3.5.1 No Trade-offs

We illustrate how mutation probabilities change the spreading speed, average trait and trait variance for Gaussian and Laplace dispersal kernels, as in (3.12), when there are no trade-offs (see figure 3.1). As mutation increases, the mean trait decreases and trait variance increases. Both speed and trait distribution tend to the asymptotic limits of low and high mutation previewed in equations (3.66) - (3.71). The spreading speed decreases with mutation, as expected by the results from the previous sections. Note, that even though the mutation kernel here differs from the one in section 3.4, we observe the same effect numerically as what we proved using the reduction principle in the previous section.

We plot the trait distribution at the leading edge in figure 3.2. In the limit as $\mu \to 0$, the optimal type/trait is simply the one whose dispersal kernel has the largest variance θ, since this optimizes speed in the absence of trade-offs. Formally, $\theta_d(s) = \max_{\theta \in \Theta} \theta \; \forall \; s$, hence the aggregation at $\theta = \theta_{\max}$. The curve for $M(\theta, s^*)$ shows the distribution obtained in the limit $\mu \to \infty$. While infinitely high mutation rates are not realistic, the analysis is still useful: the distribution in this limit (which can be obtained analytically) is very close to that for $\mu = 1$ (for which no analytical expressions are known). We observe the effect of spatial sorting acting alongside spatial selection on the population: for low mutation rates, the leading edge is eventually inhabited by the most dispersive traits/types; as mutation increases, inheritance decreases, spatial sorting becomes less influential and the distribution is purely governed by the 'arrival densities' at the leading edge, given by $M(\theta, s^*)$ (see below). In both cases, the maintenance of such population distributions is granted by spatial selection favouring first colonizers. We will see below that when there are trade-offs, r-selection (selection for higher growth rates) may prevent

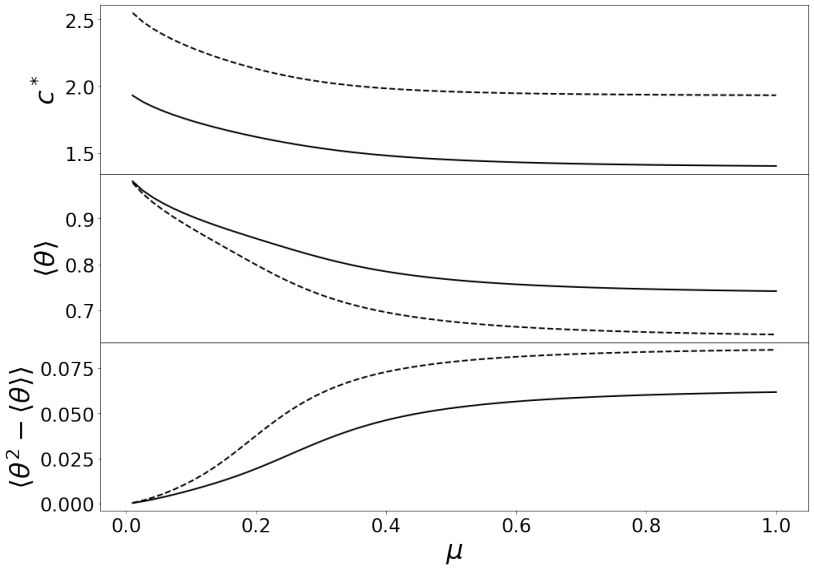

Figure 3.1: Solid (dashed) lines represent the result obtained with Gaussian (Laplace) dispersal kernel. The top plot is the asymptotic spreading speed. The middle and bottom plots are the average trait and trait variance in the leading edge. Trait space $\Theta = [0.1, 1.1]$ is re-scaled to $[0, 1]$ and growth rate to $R(\theta) = 6$.

spatial sorting from shaping population distributions at the front.

To understand how $M(\theta, s^*)$ can be interpreted as 'arrival density', we investigate the outcome of a single dispersal event. We consider that, before dispersal, the trait at the leading edge is distributed uniformly in trait space, i.e., $N \approx e^{-sx}/\bar{\Theta}$. Then after dispersal, the distribution is $e^{-sx}M(\theta, s)/\bar{\Theta}$. Hence, the distribution after dispersal is given by $M(\theta, s)$, i.e., it indicates the frequencies with which the different traits arrive at the leading edge in a single dispersal event. Since we did not include reproduction into these considerations, 'arrival density' does not indicate whether this trait distribution will be maintained at the leading edge.

3.5.2 Weak Trade-offs

We consider weak trade-offs, i.e., a situation where higher dispersal ability implies lower growth rates, but even the types with the lowest growth rates are viable (i.e., $R_{\min} > 1$). When the trade-off is concave (i.e., $\alpha < 1$ in (3.30)), trait distributions behave similarly to the case of no trade-offs (left panel in figure 3.3). The distribution peaks near the trait that maximizes speed. As mutation increases, the distribution tends to the moment generating function. The spreading speed is high when mutation is low and decreases with mutation rates (solid horizontal lines). The assembly of all types never spreads faster than the fastest single-type

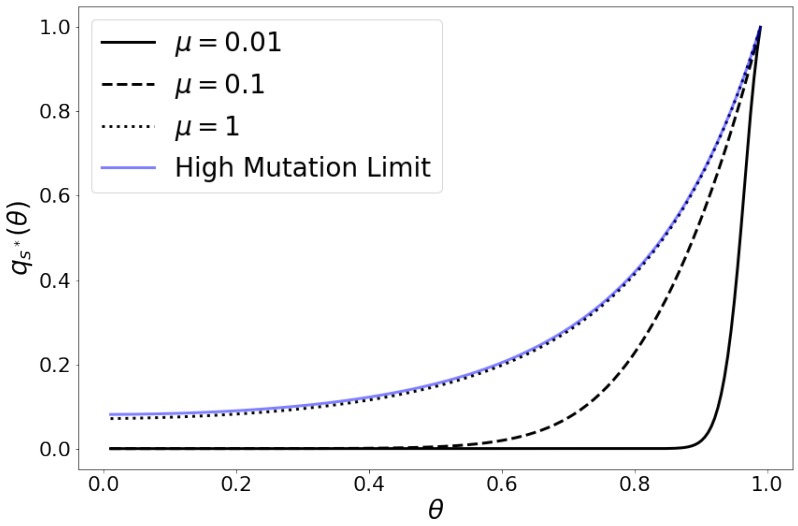

Figure 3.2: Population distributions for different values of mutation kernel variance μ. The blue line represents an approximation of the population distribution by $M(\theta, s^*)$, with s^* obtained from a simulation with $\mu = 10^3$. A Gaussian movement kernel is used.

speed (the horizontal lines are not above the grey curve). Note, however, that the observed behavior differs from spatial sorting in the following sense: at low mutation rates ($\mu \approx 10^{-3}$), the mode of the distribution is located at some $\theta < \theta_{\max}$, a trait that maximizes the speed of individual traits (given by the grey curve), rather than dispersal itself (which would be $\theta_{\max}$). We see that selection can shift the expected trait distributions from the ones obtained solely by spatial sorting (no r-selection).

The right panel of figure 3.3, corresponding to a convex trade-off, shows novel behavior. Trait distributions can now have two modes for some intermediate range of mutation rates (dashed and dotted curves). At low mutation rates, the trait distribution has its maximum densities at $\theta = \theta_{\min}$, so that evolution tends to maximize reproductive outcome (solid black curve in the lower plot). The resulting spreading speed (solid black horizontal line in the upper plot) is nonetheless higher than any of the single-type spreading speeds (3.67), represented by the increasing grey curve. This effect that the assembly of all types spreads at a higher speed than any type in isolation, i.e., $c^* > \sup_\theta c(\theta)$, was called an anomalous spreading speed in Elliott and Cornell [97] and [89][1]. As mutation rate

[1]Note that a more subtle definition of an anomalous spreading speed was first given by Weinberger et al. [111]. An anomalous speed in their sense can only occur when the linearized operator is reducible and system is not linearly determined. Our model does not fall under their definition.

increases, this anomalous speed disappears (i.e., speeds are below the grey solid curve), that is, it only occurs in the case of weak and convex trade-offs in the low mutation limit. With increasing mutation rates, trait distributions can have two modes, one at $\theta_{\min}$ and the other at $\theta_{\max}$. The mode at $\theta_{\min}$ decreases until there remains only a single mode at $\theta_{\max}$, pictured in the limit of high mutation.

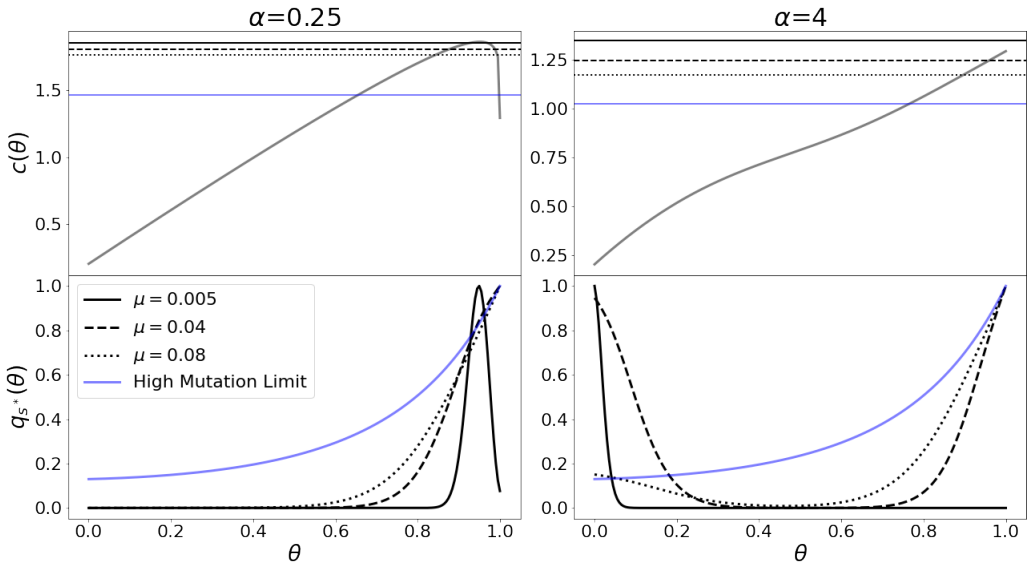

Figure 3.3: The top plots represent spreading speeds of individual traits (grey curves) and the asymptotic spreading speed of the total population for the corresponding values of μ (horizontal lines). When the total population spreads faster than the fastest trait individually (top right plot), we speak of an 'anomalous spreading speed' (see text for details). The bottom plots show the trait distributions at the leading edge for the corresponding values of μ. The left plots are obtained with $\alpha = 0.25$, so that the trade-off curve is concave, while the ones on the right are obtained with $\alpha = 4$, where the trade-off curve is convex. The specific parameter values are $R_{\max} = 6$, $R_{\min} = 2$ and the movement kernel is a Gaussian, with $\theta_{\min} = 0.1$ and $\theta_{\max} = \theta_{\min} + 1$ rescaled to $[0, 1]$.

We observe two evolutionary forces acting simultaneously on the leading edge trait distribution. Natural selection (r-selection) concentrates the traits near the maximal growth rates, at $\theta_{\min}$, but as mutation increases, the reproductive output of these low dispersive traits allows for the most dispersive traits to thrive, so that spatial sorting results in a new mode of the trait distribution at $\theta_{\max}$. As mutation increases, neither r-selection nor spatial sorting is able to dominate, and the trait distribution is simply given by the arrival densities at the leading edge. Clearly, the limit of high mutation is rarely achieved in nature, however, similarly to above, at $\mu = 0.1$, that is, when the Gaussian mutation kernel has a

standard deviation of about a tenth of the trait space, the qualitative behaviour of population distributions at the leading edge is comparable to $\mu \to \infty$: both are asymmetric and highly skewed towards $\theta_{\max}$.

3.5.3 Strong Trade-offs

Next, we consider strong trade-offs, where the most dispersive traits are not viable on their own, i.e., $R_{\min} < 1$. Anomalous spreading speeds occur again when the trade-off curve is convex ($\alpha > 1$); see the top right panel in figure 3.4. We note that such anomalous spreading speeds occur for a larger range of mutation rates as compared to the weak trade-off case. The trait distribution (bottom right plot) can again be bimodal, however, it takes higher mutation rates for the rightmost mode to be dominant. The left panel in figure 3.4 is similar to the case of weak trade-offs as well. Spreading speeds are always below, but close, to the optimum trait speed and decrease with mutation. Trait distributions show only a single mode that shifts from the optimal trait to $\theta_{\max}$ as mutation increases.

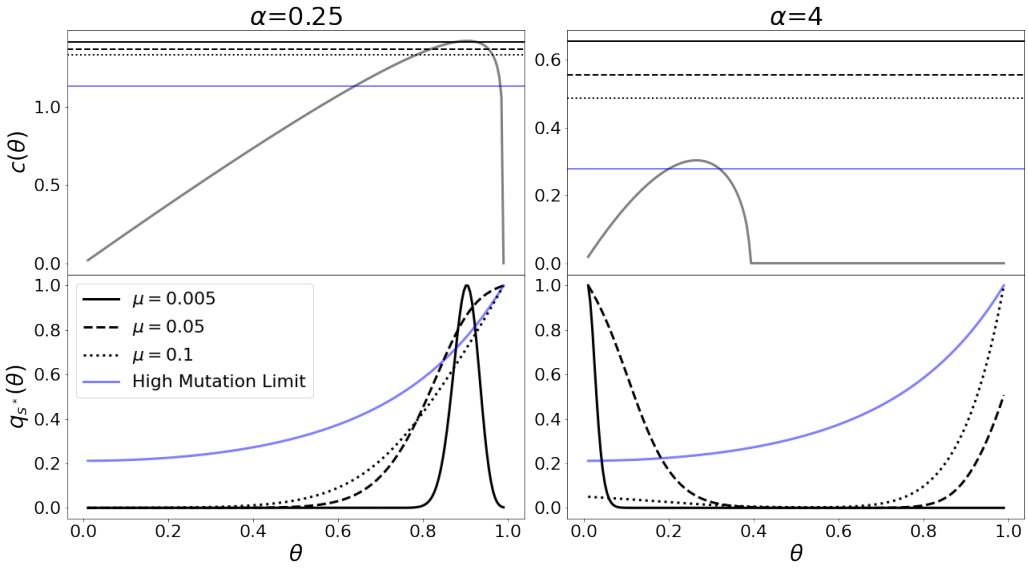

Figure 3.4: Spreading speeds (top) and population distributions (bottom) for a convex ($\alpha = 4$, right panel) and concave ($\alpha = 0.25$, left panel) strong trade off in different mutation levels. The gray solid line in the plots for speed is the speed each trait/type would invade the landscape alone, the horizontal lines are the speeds the population as a whole invade the landscape given the respective mutation rate (μ) value. Parameters used are $R_{\max} = 6$, $R_{\min} = 0.2$, and movement is assumed to be Gaussian, with $\theta_{\min} = 0.1$ and $\theta_{\max} = \theta_{\min} + 1$ rescaled to $[0, 1]$.

Note that, with a strong convex trade-off, speeds of individual traits are positive

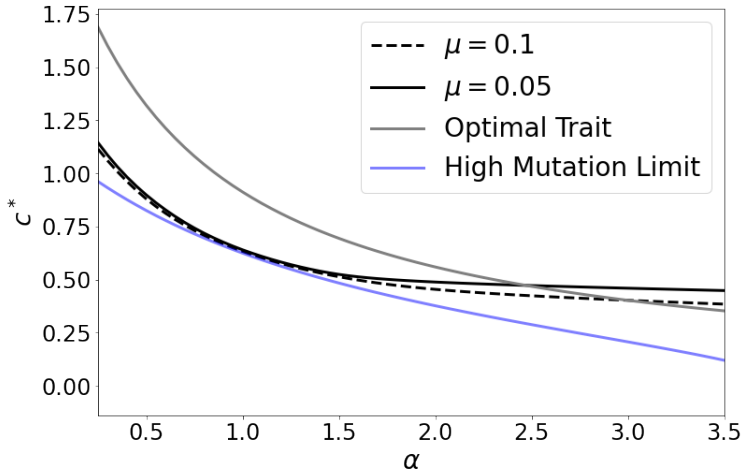

Figure 3.5: Spreading speed in black solid ($\mu = 0.05$) and dashed ($\mu = 0.1$) lines in relation to convexity parameter, α. The speed of the optimal trait/type is given by the gray line, an the limit of high mutation by the blue line. Note that anomalous spreading speeds appear at $\alpha \approx 2.5$ for $\mu = 0.05$, and only at $\alpha \approx 3$ for $\mu = 0.1$, showing that the reduction in speed that we expect from the principle in the previous sections can overshadow anomalous spreading speeds.

only for small enough trait values (top-right plot of figure 3.4). Trait values that are too high are not viable on their own and would not be able to invade individually, but they are present in the population at the leading edge for a range of mutation rates, and they contribute substantially to the overall spreading speed.

We observe that in both weak and strong trade-offs, anomalous spreading speeds do not occur at high mutation rates. This indicates that the speed reduction that results from mutations, as expected from the theoretical results in the previous section, can be strong enough to hinder anomalous spreading speeds. By continuity of the dominant eigenvalue with respect to μ, if for some value of α anomalous spreading speeds appear, we expect that there is a mutation value $\mu = \tilde{\mu}$ for which said anomalous spreading speeds vanish. This expectation is confirmed in figure 3.5, which shows that for $\mu = 5 \cdot 10^{-2}$, anomalous spreading speeds are attained for $\alpha > 2.5$ (roughly), for $\mu = 10^{-1}$, anomalous spreading speeds appear only at $\alpha \approx 3$, and finally, at the high mutation limit, anomalous spreading speeds no longer appear.

3.5.4 Effects of Deleterious Mutations

Finally, we evaluate how deleterious mutations change the results above. Deleterious mutations are those that place offspring outside the trait space so that they are lost from the population and do not contribute to future generations. The equations remain the same as before, but, due to the deleterious mutations, the mutation kernel does not integrate to unity, i.e., the strict inequality (3.19) holds.

In this case, we cannot study the high-mutation limit since the population cannot persist in this limit. We can, however, obtain an upper bound for the spreading speed by comparison. Specifically, for a given mutation kernel $L(\cdot,\cdot)$ with $\int_\Theta L(\theta,\omega)\mathrm{d}\theta < 1$, we define the re-scaled kernel

$$\Lambda(\theta,\omega) \quad = \quad \frac{L(\theta,\omega)}{\int_\Theta L(\theta,\omega)\mathrm{d}\theta}. \tag{3.74}$$

Note that, in contrast to the procedure in section 3.2.3, we do not re-scale the growth function here. We denote by Q_L and Q_Λ the next-generation operators with the respective mutation kernels but otherwise identical growth and dispersal functions. By definition, we clearly have

$$Q_L[N_t](\theta,x) < Q_\Lambda[N_t](\theta,x), \tag{3.75}$$

and therefore the spreading speed of a model with deleterious mutations is no larger than the spreading speed of the corresponding model without, i.e., $c_L^* \leq c_\Lambda^*$.

In addition to the decrease in spreading speeds, expected theoretically from the reduction principle, here, speeds also decrease with mutation rates because mutations lead to an effective loss in reproduction. As mutation increases, more individuals are lost through the boundary of trait space, the dominant eigenvalue of the linearized next-generation operator becomes smaller than unity, and invasion is no longer possible. This effect is highlighted in figure 3.6, where the speed for a model with a Gaussian mutation kernel accounting for deleterious mutations (Q_L, dashed line) is always below the one without deleterious mutations (Q_Λ, solid line), and decays to zero as mutation rates increase.

Figure 3.7 shows that deleterious mutations also affect the occurrence of an anomalous spreading speed. For the model accounting for deleterious mutations, Q_L, anomalous spreading speeds only appear at higher values of α when compared to Q_Λ. Therefore, in the possibility of deleterious mutations, higher α (stronger

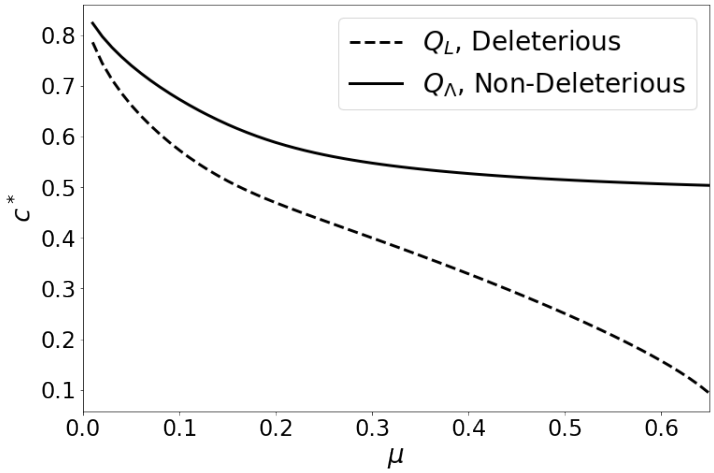

Figure 3.6: Asymptotic spreading speeds as functions of mutation rates, μ, for a model with Gaussian movement and Gaussian mutation kernel with (dashed line) and without (solid line) deleterious mutations. Parameters used are $R_1 = 8$, $R_2 = 0.2$, $\alpha = 4$, which gives a strong and convex trade-off.

convexity in trade-offs) is necessary for an anomalous spreading speed to emerge. This result seems reasonable because the relation $c_L^* \leq c_\Lambda^*$ holds for every α, since the models share the same growth rate functions.

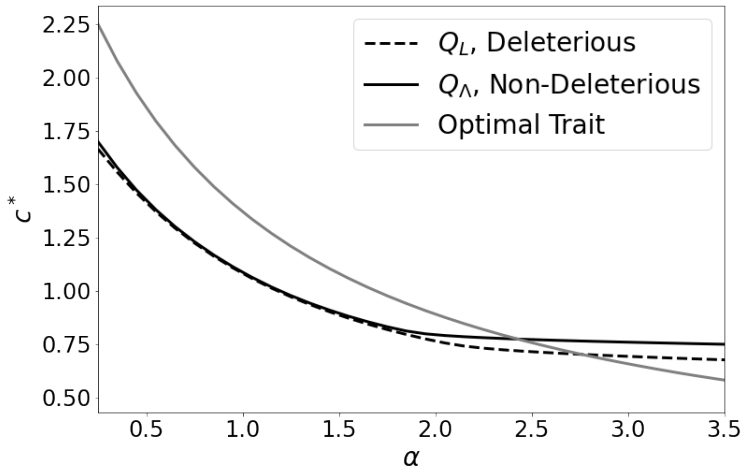

Figure 3.7: Asymptotic spreading speeds as functions of α for models with (dashed line) and without (solid line) deleterious mutations. The grey solid line is the speed with which the optimal trait would invade the landscape alone. Anomalous spreading speeds occur when the solid or dashed black line is above the grey one. Parameters used are $\mu = 5 \cdot 10^{-2}$, $R_1 = 8$ and $R_2 = 0.2$.

The trait distributions at the leading edge change due to deleterious mutations, in particular at the boundaries of trait space where the effects of these mutations is the strongest (see figure 3.8). Since deleterious mutations incur significant loss in growth rates at the edges of trait space, those regions have lower densities than those with fewer deleterious mutations. For concave trade-offs ($\alpha < 1$), the distribution peaks at the optimal trait for speed, and as mutation increases, the distribution becomes wider. For convex trade-off ($\alpha > 1$), the distribution can still be bi-modal, however, the modes are not at $\theta_{\min}$ and $\theta_{\max}$. At low mutation rates, the distribution is centred around low values of θ that are far enough from $\theta_{\min}$, so that the loss through deleterious mutations is small while the growth rate is high enough. For intermediate mutation rates, the distribution is bimodal with modes close to $\theta_{\min}$ and $\theta_{\max}$, maximizing growth and dispersal simultaneously with different proportions depending on μ, but the modes are away from the edges of trait space. Finally, when mutation is high enough, but the population can still persist, dispersal heterogeneity (arrival density) dominates, and pushes the mode to the rightmost part of trait space, i.e., highest dispersal, to $\theta_{\max}$. Again, anomalous spreading speeds tend to occur at high values of α, i.e., when the trade-off is convex.

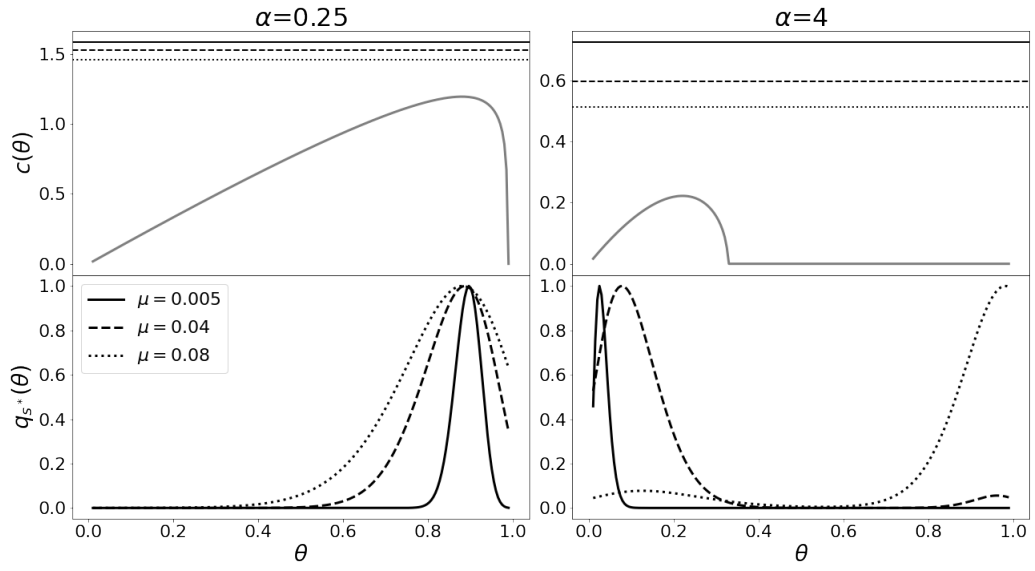

Figure 3.8: Plots on the left are for concave trade-off ($\alpha = 0.25$) and om the right for convex trade-off ($\alpha = 4$). Bottom plots are population distributions, while top ones are spreading speeds of individual traits (gray curve) and the whole population (horizontal lines). Each line style (dashed, solid and dotted) corresponds to the mutation rates indicated. Parameters used are $R_{\max} = 6$ and $R_{\min} = 0.2$ (strong trade-off) and movement is Gaussian.

3.6 Discussion

Within the past decade or two, ecologists became increasingly aware of the role that evolution plays in spatial spread and range expansions [13]. Whereas previous work assumed that the time scale of spatial spread and evolution were quite different, recent examples showed that the two can act simultaneously, with the cane toad being the poster child example [10]. One of the fascinating aspects of evolution during range expansion is that selective forces vary in space and time as the invading population's density changes. This observation has inspired new mathematical models in the form of reaction–diffusion equations and their analysis; see, e.g., Bouin et al. [87]. We presented, analyzed and explored similar questions in the framework of integrodifference equations, which are more realistic for species with discrete non-overlapping generations, and where the dispersal and mutation processes can be modelled more generally than just by diffusion.

We investigated several relevant evolutionary processes that occur during biological invasions. We considered a population structured by a single trait, discrete or continuous. We studied general analytical aspects of the models as well as specific numerical results that can elucidate how spatial sorting and spatial selection may shape range expansions. We considered a single trait that induces individual variability in dispersal and/or growth, and allowed for mutations within a given trait space. We showed that populations at the leading edge can display different trait distributions that give us a hint on which evolutionary forces are dominant in each studied case, as well as how they change population spreading speeds. We first discuss the observations on trait distributions, then their implications for the speed of spread.

Our numerical explorations reveal that when there are no correlations between growth and dispersal, and when mutation is low, spatial selection favours those traits that can colonize new areas first. In this case, spatial sorting is the dominant effect so that only the most dispersive traits are found at the leading edge. As mutation increases, spatial sorting decreases in strength and the population distribution is governed essentially by dispersal heterogeneity. In fact, in the limit of high mutation, the trait distribution at the leading edge approaches the moment generating function, i.e., the order by which traits arrive at the leading edge. This latter result recurs in our numerical simulations independently of any trade-off curve. Our results are similar to those of Bouin et al. [87] in a reaction–diffusion equations. They showed, in the absence of trade-offs, that the trait distribution at

the leading edge is always skewed towards higher dispersal abilities. Hence, our results show that this phenomenon is robust with respect to modelling approach.

When trade-offs are considered, the qualitative behaviour of the trait distributions at the leading edge responds to the curvature of the trade-off relation rather than to its strength. For concave trade-offs ($\alpha < 1$) and at low mutation rates, it is not dispersal or growth that are favoured by spatial selection but rather the combination of the two that maximizes the spreading speed. As mutation rates increase, the trait distributions become wider until they approach the high-mutation limit. In the case of convex trade-offs ($\alpha > 1$), r-selection is the dominant effect at low mutation rates so that the trait distribution is skewed towards high growth rates. Although these traits do not maximize single-trait speeds, they do offer a higher population-level spreading speed. Since spatial selection favours the first colonizers, this trait distribution is maintained. However, as mutation rates increase up to a certain limit, the least fertile/most dispersive traits benefit from the reproductive output of the most fertile/least dispersive individuals. Hence, spatial sorting and selection can exert opposing forces in the population so that a bi-modal trait distribution can appear

Different trait distributions affect the population spread rate differently, depending again on the existence and shape of a trade-off. When there is no trade-off, the skew of the trait distribution towards higher dispersal implies a higher spreading speed, as it does for reaction–diffusion models [87]. This effect, however, depends on the fact that the highest growth rates appear at low density at the invasion front and that the speed is linearly determined. In particular, our modelling assumptions exclude an Allee effect, which we will discuss below. When there is a trade-off, its effect on the spreading speed depends again on the curvature. In concave trade-offs, spreading speeds tend to be close to, but always below, the speed of the optimal trait, i.e., $\max_\theta c(\theta)$. However, under convex trade-offs, anomalous spreading speeds may appear so that the population is able to invade the landscape faster than any of its individual traits would. These anomalous spreading speeds appear at low mutation limits in the case of weak trade-offs ($R_{\min} > 1$). For strong trade-offs, they can occur for a wider range of mutation rates. In all explored cases, spreading speeds decrease with mutation rates, as expected by the reduction principle, and anomalous spreading speeds can disappear as mutation increases.

Anomalous spreading speeds can also arise in corresponding reaction–diffusion equations. Keenan and Cornell [89] use a perturbation argument to show their

existence for finitely many types as long as the trade-off is convex and mutation is low. Here, we recover a similar result numerically and show that regimes of strong trade-offs tend to favour the appearance of anomalous spreading speeds beyond the low mutation limit. Also, we show how different evolutionary factors change asymptotic spreading speeds. Anomalous spreading speeds may not occur even for convex strong trade-offs if mutation rates are high. If deleterious mutations are possible, then that effect can also prevent anomalous spreading speeds. Elliott and Cornell [97] compare two morphs: the establisher (high growth and low dispersion) and the disperser (low growth and high dispersion), and they ask whether anomalous spreading speeds occur because the invading population benefits from the best of its two morphs (high growth and high dispersal). Here, we find that under convex strong trade-offs and a certain range of mutation rates, this might indeed be the case. The evolutionary forces tend to favour high dispersal, but the highest dispersers on their own are not viable. Evolution also favours high growth, but the fastest growing types on their own spread slowly. A combination of the two is both viable and fast. The convex trade-off prohibits intermediate types that could spread faster. Hence a bimodal distribution arises at the leading edge.

Our results point in a similar direction as discussed in Phillips and Perkins [86]. Evolutionary forces act on the invading population trait distribution at the leading edge such that the expression $R(\theta)M(\theta, s)$ is maximized, at least when there is no Allee effect. When trade-offs are concave, simple aggregation at the optimal trait occurs, however, under convex trade-offs, maximizing this expression may involve occupying different regions of trait space, namely regions that contain traits that decrease fitness ($R(\theta)$), but allow for higher spreading speeds. Under convex strong trade-offs, even when trait space contains regions where the growth rate is below one, the population can persist and attain such traits. This highlights how powerful spatial sorting alongside spatial selection can be: it can drive individuals at the leading edge to develop traits that can cost almost all their reproductive capacity. There exist examples of such costs in cane toads, such as reduced ability in males to cling to female partners during amplexus, due to loss of strength in the forelimbs [93], as well as the development of arthritis [10].

Our results on spread with strong trade-offs leads us to reconsider what deleterious mutations are and which role they play during invasions. Clearly, the simple condition $R(\theta) < 1$ (the inability of a single trait to persist and spread) cannot necessarily be regarded as "deleterious" during an invasion from a mathematical

perspective if such traits can be maintained in the population (at the leading edge). In fact, since these traits have high dispersal ability (due to the strong trade-off), they may considerably increase population-level spread rate. Indeed, the growth rate of a particular trait can attain low values due to many factors, such as distinct biotic and climate conditions from the place of origin, which may cause some traits/types of a given species to not thrive on their own. However, those traits can be sustained in the environment if they provide some colonization advantage for the species, as do the most dispersive (hence least reproductive) traits here.

We note that invasions are themselves transients. Once the invasion is complete, traits that are favoured during range expansion are expected to vanish from the population and cede to the most reproductive/competitive and least dispersive traits [85, 86]. In fact, behind the invasion wave, the population is expected to settle at an equilibrium where growth and dispersal balance. The mathematical study of the evolution of dispersal at such an equilibrium has a long and distinguished history, dating back to Karlin and McGregor [112] in an environment consisting of discrete patches and to Hastings [113] in a continuous one-dimensional environment. A recurring finding of these studies is that lower random dispersal rates are favoured in temporally constant but spatially heterogeneous environments; see Cosner [114] for a review. One explanation for this finding is that random movement prevents a resident population from fully utilizing resource peaks. An invading population with sufficiently small random dispersal rate can then exploit whatever the resident population is missing. In our scenario of a spreading population, the most underutilized resource is located ahead of the wave, which is why increased dispersal is often beneficial, but not always, as we show here. A more comprehensive theory of the evolution of dispersal will need to fill in the behavior between the front and the equilibrium.

We mention several avenues for future research that naturally follow from our results. Studying how the steady states at the core of the invasion change according to different choices of the reproduction function is of interest, as some descriptions of non-local competition can create spatial pattern-formation; see e.g., Britton [115], Fuentes et al. [116]. In our framework, this would translate into polymorphism at the core of the range. Trade-offs between competitive abilities, growth rates and dispersal can also lead to different trait distributions throughout space, and Burton et al. [117] shows, in an individual based modelling framework, that competition is selected over dispersal at the core of invasion, while the opposite holds at the leading edge. The model presented here can

account for trade-offs between two traits, but has to be expanded to deal with simultaneously correlated growth rates, competitive abilities and dispersal, as this case would require a bi-dimensional trait space, and, with it, the development of new mathematical analysis.

Here, we focused on showing how trait distributions evolve under Gaussian dispersal, and we expect similar results with Laplace dispersal kernels. However, other movement behaviours are possible and can reveal interesting results. For example, Lutscher [21] (section 12.5) considered a population that can move with two different dispersal kernels (similar to equation (3.15)), one leptokurtic, the other platykurtic, but no trade-offs and no evolutionary forces. In that example, the maximum speed is attained by an optimal mixing of both dispersal modes, instead of uniquely moving with the leptokurtic kernel. This might reveal other mechanisms that prevent spatial sorting to be a dominant evolutionary force, as individuals at the leading edge would, possibly, exhibit the optimal mixing of behaviours.

Other biotic factors, such as Allee effects, interspecific interactions and sex structure need theoretical development and general exploration. Lutscher et al. [92] reveal that, different from what was found here, mutation can speed up invasions in the presence of Allee effects. Including sex structure may allow us to describe assortative mating, either by individual preference or spatial partner availability, such as in Lutscher et al. [92] where mating introduces the Allee effect mentioned before, as well as in [38], where it is shown that spreading speeds are sensitive to various aspects that sex structure introduces. For example, dispersal heterogeneity between sexes may alter the sex ratio at the leading edge and, in turn, reduce or increase speed. The analysis of multi-species systems may give us hints about other sources of eco-evolutionary feed-backs, such as an evolutionary arms race between an invasive predator and a local prey species, specially when such traits under evolution are also correlated with dispersal [13].

In order to obtain a reduction principle for spreading speeds, we considered a mutation kernel that changes linearly with a mutation parameter, the probability of imperfect cloning. This framework follows recent and classic literature on the spectral analysis of these mutation operators, see Schreiber and Beckman [91], Altenberg [107] for integral operators and Morris et al. [90], Karlin [109] for matrices. Our numerical results show that an increase in a measure of spread (e.g., the variance of a mutation kernel) also reduces speed. In both frameworks, the mutation parameter plays the same role, in that it reduces trait inheritance,

however, the properties of the dominant eigenvalues of these integral operators with respect to kernel properties are not fully explored. A future challenge is to uncover a more general relation between spreading speeds and mutation rates. In all the theory, however, we still need to preserve compactness (or ensure weak compactness) of the next generation operators, a fundamental property for the theory developed here to be applied.

The mathematical analysis presented here builds on existing theory for asymptotic spreading speeds and travelling waves for monotone and monostable recursions. These were developed for structured populations of finitely many stages by Lui [39], Neubert and Caswell [40], and for populations with continuous structure in the context of delay equations by Liang and Zhao [105]. Our model is also an example of a 'spatial integral projection model' in the sense of Ellner et al. [118]. We believe that our theory carries over to nonmonotone but monostable recursions, which result from replacing the monotone growth function F by a single-hump function, such as the Ricker function. Using an idea by Thieme [119], one can construct upper and lower bounds of the next-generation operator Q, say $Q_-[u](\cdot,x) \leq Q[u](\cdot,x) \leq Q_+[u](\cdot,x)$, with the property that Q_+ and Q_- are both monotone and monostable and have the same linearly determinate speed $c^*_\pm = c^*_+ = c^*_-$. Then, necessarily, the speed of Q is also linearly determined and equal to $c^*_\pm$; see also Lutscher [21], section 5.4. Difference equations with nonmonotone growth functions may exhibit two-cycles and other oscillating asymptotic behaviour, which appear as fixed points in the corresponding second- or higher iterate operator. Accordingly, integrodifference equations with nonmonotone growth functions can show multiple travelling waves with oscillatory behaviour that correspond to stacked waves in second- or higher order iterations [26]. It is a future challenge to include trait structure in such models and to study the trait distributions in these stacked waves. The case of bistable recursions is much more difficult to address since no linear conjecture is available to study the asymptotic speed and trait distribution. However, even an exploratory numerical study could reveal interesting mechanisms as to how trade-offs and evolution shape spatial spread rates and trait distributions [92].

Chapter 4

Perspectives and Conclusions

In this chapter we cover future directions on mathematical theory for range expansion. Of course, we also highlight some of these directions in the discussion of chapter 3 and 4. Here, however, we try to explain some other ideas in a little more detail and provide some references for them.

4.1 Theory for multiple species interactions

In recent years, the development of theory for single species and two interacting species has been extensively investigated through the scope of RDEs and IDEs as well, although the former is much more present.

In chapter 2 we saw how each species movement behavior can significantly contribute to form different regimes. This highlights how species interactions and their movement behaviors might be too important to neglect in our modeling approaches. Therefore, considering larger networks of interacting species in theoretical spatial ecology is an important step towards understanding these systems and its complicated dynamics in more detail.

In order to do so, of course, we need novel developments in mathematics. Few works look at three species networks in the context of range expansion to formally analyze the existence of traveling wave solutions and asymptotic spreading speeds (see Guo et al. [120], Huang and Lin [121], Lin and Yang [122]), and among these works, either model considerations are restrictive in terms of species interactions, or the studies stay inside a much more mathematical niche, without making it to ecologists to debate their applications and limitations. The latter is a matter not of mathematics *per se*, but a broader problem of science communication in ecology and applied mathematics [123], the former, however, can be quite challenging and require advances in functional analysis and other fields of pure mathematics.

For example, formal mathematical theory for intraguild predation, exploitative and apparent competition, as usually described by classical theoretical ecology

([63, 60, 74]), are lacking in spatial ecology in general, not only in range expansion phenomena, but on persistence problems as well, e.g., in the existence of steady states and critical patch sizes. These classical frameworks are accepted in both mathematical and ecological scientific communities, and with those we can address and formulate questions from and for both communities.

4.2 Sexually structured populations

Formally demonstrating the existence of traveling wave solutions and asymptotic spreading speeds is still a mathematical challenge. Although results for Allee effects are available [29, 28], when mating is explicitly considered in sexually structured populations, the results do not hold. It becomes a two dimensional (male-female) system of equations, which is cooperative, but bi-stable, and therefore classical theory for cooperative systems (Weinberger et al. [41]) no longer applies. Developing theory further will allow us to study taxa in which male-female dispersal are significantly different, and understand the precise conditions in which invasions are successful and at which speed they are expected to occur.

Beyond the mathematical challenge, relevant eco-evolutionary questions rise when considering sexually structured populations. In sexually structured populations, mate finding, mate selection and heritability are all relevant processes that need to be accounted for in order to describe and understand possible evolutionary routes during range expansion phenomena [124]. At the leading edge, as we have shown in chapter 3, sources of selection are different than those at the core, and may drive the invading species in different evolutionary directions. For example, invasive cane toads at the leading edge in northern Australia have much weaker and smaller forelimbs, which turns amplexus [1] much more difficult and reduces egg fertilization success [125], some even mistakenly cling to other males' backs, which in turn avoid emitting sex-identifying sound signals, possibly to avoid alerting predators [126]. Moreover, at the leading edge, males of cane toads have developed longer hindlimbs and smaller gonad mass [126].

The theoretical framework for such phenomena is quite challenging, with increasing levels of complexity. Those with higher dispersal get at the leading edge first, and must find, select and effectively mate with its sexual partners at low population densities, where both inter-specific competition and mate availability are low. Under low mate availability, mate finding and selection can play an

[1] when the male grasps to female's back to fertilize eggs upon their deposition

important role on which traits get transmitted at the leading edge, and how fast the population expands. For example: If females and males are too selective regarding their partners, the invasion is likely to be slower, because mate searching times increase and reproduction might occur at a much smaller rate, since ideal partners might not be available at the leading edge. If they become less selective, reproduction occurs in a faster rate, but the offspring may present traits that do not favor fertility or competition, but dispersal instead. If that is the case, partner selection and search strategies are likely to differ between the core and front of invasion, simply because of density levels [127].

In regards to sexually structured population models that account for evolution, Lutscher et al. [92] reveals that sexually structured populations can exhibit non-monotone invasion speeds with respect to mutation rates. First, although a numerical result, it shows that our reduction principle in chapter 3 is not general (in fact, we expect it to hold only on linearly determinate speeds, which is not the case in sexually structured populations). Secondly, it provides a framework which we can extend to model other processes of interest in sexually structured populations. Another important approach is given in Ochocki et al. [128], through an agent based model. They account for different sources of trait variation within the population: 1) maternal effects, individuals that had larger maternal investments tend to have a better outcome in either dispersal or fertility, 2) environmental variation, individual's are born in different environments and therefore have different life histories, 3) parental additive genetic contributions, how each parent genotypes/phenotypes contributes to offspring's genotypes/phenotypes. Interestingly, this approach reveals scenarios where evolution (governed by parental additive genetic contributions) can either slow down or increase invasion speed (also going against the reduction principle found). Developing theory for such processes in terms of IDEs and PDEs allows us to unify terminology (precisely describing mutation/herdability and inter-specific trait variation), as well as possibly understand how each of these factors contribute to speed in more detail.

4.3 Fragmented Landscapes and the evolution of habitat selection

In chapter 3, we have discussed evolutionary processes that take place throughout biological invasions. There, we have considered that the landscape is homoge-

neous, however, this is usually not the case, and can have various implications for invasion and community formation, as illustrated in chapter 2.

A possible future direction is to investigate what is the role of evolution of habitat selection in biological invasions. Maciel and Lutscher [32] show that there are habitat selection behaviors that are optimal for spreading speeds. However, Maciel et al. [82] show that, at the core of invasion, the Ideal Free Dispersal strategy is the optimal habitat selection behavior [Fretwell [129]] [2]. Therefore, two different evolutionary forces can drive the population habitat selection behavior in opposite directions.

Following our recent work, Poloni and Lutscher [130], we would expect that at the leading edge, either growth, dispersal, or an optimal combination of both is selected, depending on growth-dispersal trade-offs. However, in an heterogeneous landscape, maximizing dispersal and growth involves spending an optimal amount of time in each type of patch. This way, mathematical models that account for individual variability in interface behavior and habitat selection can help unravel important evolutionary drivers in heterogeneous landscapes.

Here we propose using an homogenization technique, following [34, 64], alongside the RDE frameworks of individual variability in dispersal and reproduction (and inherent trade-offs) within an invading population proposed in Elliott and Cornell [97], Keenan and Cornell [89], Morris et al. [90] to study such evolutionary processes.

The homogenization technique is as described in chapter 2. The RDE framework from [89] is qualitatively the same as the one proposed for discrete trait spaces in chapter 3, but in terms of PDEs instead of IDEs. The results are also qualitatively the same: Anomalous spreading speeds appear when growth-dispersal trade-off is convex, while the speed of the fastest type dominates when trade-off is concave. In RDE formulations, we don't have (formally) the exact trait distribution at the leading edge, but it should be given by the dominant eigenvector of the resulting eigenvalue problem for a wavefront profile ($e^{-s(x-ct)}$).

Introducing heterogeneous landscapes and performing homogenization techniques, we expect to arrive at set of equations that are similar to the ones in [89], but now accounting for landscape settings. We can consider that morphs differ in growth-dispersal and patch preference, and then study how those shape effective growth and dispersal ($\langle r \rangle$ and $\langle D \rangle$) curves (convex/concave). With this, we can

[2] Ideal Free Dispersal is the term coined for habitat selection behavior that maximizes fitness across the landscape

explore how different landscapes lead to different selection processes and drive invading populations to different evolutionary outcomes and spreading speeds. For example, if patch preference in populations at the leading edge differs significantly to those at the core, we would expect different distributions between patches at the front and core of range. With that, control strategies drawn with core population behavior might not be as effective at newly colonized regions.

4.4 Conclusions

In this thesis, we revisited classical mathematical formulations of biological invasions and their results. We have focused only on RDE and IDE frameworks, as those are the most present in current literature. Such formulations are focused on determining the speed of spreed of an invading population and the concept of linear determinacy of such speeds. We also showed some classically observed spatial profiles that invading populations form alongside resident communities, e.g., traveling wave solutions that shift local communities into novel equilibria as time passes, joint invasions of competitor species leading into multiple spatial transitions and predators inducing oscillatory regimes through space.

We also obtained novel results and insights for intraguild predation communities through an RDE framework. We numerically verified that speeds of invasion are linearly determinate for a large range of parameters and that the system exhibit traveling wave solutions as well as dynamical stability. Using recent advances and techniques in modeling population in fragmented landscapes, we showed how coexistence regimes can be modulated by each species movement behavior and patch preference, including resource population.

Finally, we developed novel theory for evolutionary processes in biological invasions in IDE framework. We showed that monotone recursions to model trait structured populations present traveling wave solutions and asymptotic spreading speeds, and that these spreading speeds are non-increasing with mutation. We also explored leading edge trait distributions and highlight mechanisms that govern such distributions, such as traded-off shapes and mutation.

All in all, many aspects of biological invasions gets simplified in mathematical formulations. Although slowly, we often need to get past these simplifications to account for more processes that are revealed, through novel empirical observations, to be important in range expansion, such as landscape fragmentation, species interactions and evolution in ecological timescales. By describing these biological

processes in greater detail, mathematical challenges arise, which require advances in different fields, such as function analysis and dynamical systems. In turn, by overcoming such challenges, our results can provide significant insight into ecology again, revealing important aspects of the phenomena that were overlooked and what directions novel experiments and observations could be performed.

Bibliography

[1] Anthony Ricciardi. Are Modern Biological Invasions an Unprecedented Form of Global Change? Conservation Biology, 21(2):329–336, 2007. ISSN 1523-1739. doi: 10.1111/j.1523-1739.2006.00615.x. URL https://onlinelibrary.wiley.com/doi/abs/10.1111/j.1523-1739.2006.00615.x. _eprint: https://onlinelibrary.wiley.com/doi/pdf/10.1111/j.1523-1739.2006.00615.x.

[2] Petr Pyšek, Vojtěch Jarošík, Philip E. Hulme, Ingolf Kühn, Jan Wild, Margarita Arianoutsou, Sven Bacher, Francois Chiron, Viktoras Didžiulis, Franz Essl, Piero Genovesi, Francesca Gherardi, Martin Hejda, Salit Kark, Philip W. Lambdon, Marie-Laure Desprez-Loustau, Wolfgang Nentwig, Jan Pergl, Katja Poboljšaj, Wolfgang Rabitsch, Alain Roques, David B. Roy, Susan Shirley, Wojciech Solarz, Montserrat Vilà, and Marten Winter. Disentangling the role of environmental and human pressures on biological invasions across Europe. Proceedings of the National Academy of Sciences, 107 (27):12157–12162, July 2010. doi: 10.1073/pnas.1002314107. URL https://www.pnas.org/doi/full/10.1073/pnas.1002314107. Publisher: Proceedings of the National Academy of Sciences.

[3] Philip E. Hulme. Climate change and biological invasions: evidence, expectations, and response options. Biological Reviews of the Cambridge Philosophical Society, 92(3):1297–1313, August 2017. ISSN 1469-185X. doi: 10.1111/brv.12282.

[4] John J. Stachowicz, Jeffrey R. Terwin, Robert B. Whitlatch, and Richard W. Osman. Linking climate change and biological invasions: Ocean warming facilitates nonindigenous species invasions. Proceedings of the National Academy of Sciences, 99(24):15497–15500, November 2002. doi: 10.1073/pnas.242437499. URL https://www.pnas.org/doi/10.1073/pnas.242437499. Publisher: Proceedings of the National Academy of Sciences.

[5] Anna Occhipinti-Ambrogi. Global change and marine communities: alien

species and climate change. Marine Pollution Bulletin, 55(7-9):342–352, 2007. ISSN 0025-326X. doi: 10.1016/j.marpolbul.2006.11.014.

[6] Gerardo Ceballos, Paul R. Ehrlich, Anthony D. Barnosky, Andrés García, Robert M. Pringle, and Todd M. Palmer. Accelerated modern human–induced species losses: Entering the sixth mass extinction. Science Advances, 1(5):e1400253, June 2015. doi: 10.1126/sciadv.1400253. URL https://www.science.org/doi/10.1126/sciadv.1400253. Publisher: American Association for the Advancement of Science.

[7] Edward Lowry, Emily J Rollinson, Adam J Laybourn, Tracy E Scott, Matthew E Aiello-Lammens, Sarah M Gray, James Mickley, and Jessica Gurevitch. Biological invasions: a field synopsis, systematic review, and database of the literature. Ecology and evolution, 3(1):182–196, 2013.

[8] Carlos Castillo-Chavez, Bingtuan Li, and Haiyan Wang. Some recent developments on linear determinacy. Mathematical Biosciences & Engineering, 10(5&6):1419–1436, 2013.

[9] Mark A Lewis, Sergei V Petrovskii, and Jonathan R Potts. The mathematics behind biological invasions, volume 44. Springer, 2016.

[10] Gregory P Brown, Cathy Shilton, Benjamin L Phillips, and Richard Shine. Invasion, stress, and spinal arthritis in cane toads. Proceedings of the National Academy of Sciences, 104(45):17698–17700, 2007.

[11] Katriona Shea and Peter Chesson. Community ecology theory as a framework for biological invasions. Trends in Ecology & Evolution, 17(4):170–176, April 2002. ISSN 0169-5347. doi: 10.1016/S0169-5347(02)02495-3. URL https://www.sciencedirect.com/science/article/pii/S0169534702024953.

[12] Nicolas Schtickzelle and Michel Baguette. Behavioural responses to habitat patch boundaries restrict dispersal and generate emigration–patch area relationships in fragmented landscapes. Journal of Animal Ecology, 72(4):533–545, 2003. ISSN 1365-2656. doi: 10.1046/j.1365-2656.2003.00723.x. URL https://onlinelibrary.wiley.com/doi/abs/10.1046/j.1365-2656.2003.00723.x. _eprint: https://onlinelibrary.wiley.com/doi/pdf/10.1046/j.1365-2656.2003.00723.x.

[13] Tom EX Miller, Amy L Angert, Carissa D Brown, Julie A Lee-Yaw, Mark Lewis, Frithjof Lutscher, Nathan G Marculis, Brett A Melbourne, Allison K Shaw, Marianna Sz\textbackslashHucs, and others. Eco-evolutionary dynamics of range expansion. Ecology, 101(10):e03139, 2020.

[14] Ronald Aylmer Fisher. The wave of advance of advantageous genes. Annals of eugenics, 7(4):355–369, 1937.

[15] Kolmogorov A, N, Piscounoff, and I, Petrovsky. Etude de l'equation de la diffusion avec croissance de la quantite de matiere et son application a un probleme biologique. Moscow Univ. Bull. Math., 1:1–25, 1937. URL https://cir.nii.ac.jp/crid/1571980074053692672.

[16] J. G. Skellam. Random Dispersal in Theoretical Populations. Biometrika, 38 (1-2):196–218, June 1951. ISSN 0006-3444. doi: 10.1093/biomet/38.1-2.196. URL https://doi.org/10.1093/biomet/38.1-2.196.

[17] Mark Kot, Mark A. Lewis, and P. van den Driessche. Dispersal Data and the Spread of Invading Organisms. Ecology, 77(7):2027–2042, 1996. ISSN 1939-9170. doi: 10.2307/2265698. URL https://onlinelibrary.wiley.com/doi/abs/10.2307/2265698.

[18] Raymond J. H. Beverton and Sidney J. Holt. On the Dynamics of Exploited Fish Populations. Springer Science & Business Media, 1957. ISBN 978-94-011-2106-4.

[19] Hal Caswell. Matrix Population Models. Sinauer, 2001. ISBN 978-0-87893-121-7.

[20] W. C. Allee. Animal aggregations, a study in general sociology. The University of Chicago Press,, 1931. URL https://doi.org/10.5962/bhl.title.7313.

[21] Frithjof Lutscher. Integrodifference Equations in Spatial Ecology, volume 49 of Interdisciplinary Applied Mathematics. Springer International Publishing, Cham, 2019. ISBN 978-3-030-29293-5 978-3-030-29294-2. doi: 10.1007/978-3-030-29294-2. URL http://link.springer.com/10.1007/978-3-030-29294-2.

[22] H. F. Weinberger. Asymptotic behavior of a model in population genetics. In J.M. Chadam, editor, Nonlinear Partial Differential Equations and

Applications, Lecture Notes in Mathematics, pages 47–96, Berlin, Heidelberg, 1978. Springer. ISBN 978-3-540-35868-8. doi: 10.1007/BFb0066406.

[23] D. G. Aronson and H. F. Weinberger. Nonlinear diffusion in population genetics, combustion, and nerve pulse propagation. In Jerome A. Goldstein, editor, Partial Differential Equations and Related Topics, Lecture Notes in Mathematics, pages 5–49, Berlin, Heidelberg, 1975. Springer. ISBN 978-3-540-37440-4. doi: 10.1007/BFb0070595.

[24] Hans F Weinberger. Long-time behavior of a class of biological models. SIAM journal on Mathematical Analysis, 13(3):353–396, 1982.

[25] Robert Stephen Cantrell and Chris Cosner. Spatial ecology via reaction-diffusion equations. John Wiley & Sons, 2004.

[26] Adèle Bourgeois, Victor LeBlanc, and Frithjof Lutscher. Spreading phenomena in integrodifference equations with nonmonotone growth functions. SIAM Journal on Applied Mathematics, 78(6):2950–2972, 2018.

[27] J. Nagumo, S. Arimoto, and S. Yoshizawa. An Active Pulse Transmission Line Simulating Nerve Axon. Proceedings of the IRE, 50(10):2061–2070, October 1962. ISSN 2162-6634. doi: 10.1109/JRPROC.1962.288235. Conference Name: Proceedings of the IRE.

[28] K. P. Hadeler and F. Rothe. Travelling fronts in nonlinear diffusion equations. Journal of Mathematical Biology, 2(3):251–263, September 1975. ISSN 1432-1416. doi: 10.1007/BF00277154. URL https://doi.org/10.1007/BF00277154.

[29] Roger Lui. Existence and stability of travelling wave solutions of a nonlinear integral operator. Journal of Mathematical Biology, 16(3):199–220, February 1983. ISSN 1432-1416. doi: 10.1007/BF00276502. URL https://doi.org/10.1007/BF00276502.

[30] Nanako Shigesada, Kohkichi Kawasaki, and Ei Teramoto. Traveling periodic waves in heterogeneous environments. Theoretical Population Biology, 30 (1):143–160, 1986.

[31] Otso Ovaskainen and Stephen J Cornell. Biased movement at a boundary and conditional occupancy times for diffusion processes. Journal of Applied Probability, 40(3):557–580, 2003.

[32] Gabriel Andreguetto Maciel and Frithjof Lutscher. How individual movement response to habitat edges affects population persistence and spatial spread. The American Naturalist, 182(1):42–52, 2013.

[33] Gabriel Andreguetto Maciel and Frithjof Lutscher. Allee effects and population spread in patchy landscapes. Journal of biological dynamics, 9(1): 109–123, 2015. Publisher: Taylor & Francis.

[34] Brian P Yurk and Christina A Cobbold. Homogenization techniques for population dynamics in strongly heterogeneous landscapes. Journal of biological dynamics, 12(1):171–193, 2018.

[35] François Hamel, Frithjof Lutscher, and Mingmin Zhang. Propagation phenomena in periodic patchy landscapes with interface conditions. Journal of Dynamics and Differential Equations, pages 1–52, 2022.

[36] Jeffrey Musgrave and Frithjof Lutscher. Integrodifference equations in patchy landscapes: II: Population level consequences. Journal of mathematical biology, 69, August 2013. doi: 10.1007/s00285-013-0715-1.

[37] Jeffrey Musgrave and Frithjof Lutscher. Integrodifference equations in patchy landscapes : I. Dispersal Kernels. Journal of Mathematical Biology, 69(3):583–615, September 2014. ISSN 1432-1416. doi: 10.1007/s00285-013-0714-2.

[38] Tom EX Miller, Allison K Shaw, Brian D Inouye, and Michael G Neubert. Sex-biased dispersal and the speed of two-sex invasions. The American Naturalist, 177(5):549–561, 2011.

[39] Roger Lui. Biological growth and spread modeled by systems of recursions. I. Mathematical theory. Mathematical Biosciences, 93(2):269–295, 1989.

[40] Michael G Neubert and Hal Caswell. Demography and dispersal: calculation and sensitivity analysis of invasion speed for structured populations. Ecology, 81(6):1613–1628, 2000.

[41] Hans F Weinberger, Mark A Lewis, and Bingtuan Li. Analysis of linear determinacy for spread in cooperative models. Journal of Mathematical Biology, 45(3):183–218, 2002.

[42] Mark A. Lewis, Bingtuan Li, and Hans F. Weinberger. Spreading speed and linear determinacy for two-species competition models. Journal of Mathematical Biology, 45(3):219–233, September 2002. ISSN 1432-1416. doi: 10.1007/s002850200144. URL https://doi.org/10.1007/s002850200144.

[43] Yuzo Hosono. The Minimal Speed of Traveling Fronts for a Diffusive Lotka–Volterra Competition Model. Bulletin of Mathematical Biology, 60(3):435–448, May 1998. ISSN 0092-8240. doi: 10.1006/bulm.1997.0008. URL https://www.sciencedirect.com/science/article/pii/S0092824097900082.

[44] Michael G. Neubert and Mark Kot. The subcritical collapse of predator populations in discrete-time predator-prey models. Mathematical Biosciences, 110(1):45–66, June 1992. ISSN 00255564. doi: 10.1016/0025-5564(92)90014-N. URL https://linkinghub.elsevier.com/retrieve/pii/002555649290014N.

[45] C. S. Holling. Some Characteristics of Simple Types of Predation and Parasitism. The Canadian Entomologist, 91 (7):385–398, July 1959. ISSN 1918-3240, 0008-347X. doi: 10.4039/Ent91385-7. URL https://www.cambridge.org/core/journals/canadian-entomologist/article/abs/some-characteristics-of-simple-types-of-predation-and-parasitism19E1E7D2CCC314766A424680444F4EA9F. Publisher: Cambridge University Press.

[46] C. S. Holling. The Functional Response of Invertebrate Predators to Prey Density. The Memoirs of the Entomological Society of Canada, 98(S48):5–86, January 1966. ISSN 0071-075X. doi: 10.4039/entm9848fv. URL https://www.cambridge.org/core/journals/memoirs-of-the-entomological-society-of-canada/article/abs/functional-response-of-invertebrate-predators-to-prey93597109DEB509626DD201D20207D287. Publisher: Cambridge University Press.

[47] J. D. Murray, editor. Mathematical Biology: II: Spatial Models and Biomedical Applications, volume 18 of Interdisciplinary Applied

Mathematics. Springer, New York, NY, 2003. ISBN 978-0-387-95228-4 978-0-387-22438-1. doi: 10.1007/b98869. URL http://link.springer.com/10.1007/b98869.

[48] H. Malchow and S. V. Petrovskii. Dynamical stabilization of an unstable equilibrium in chemical and biological systems. Mathematical and Computer Modelling, 36(3):307–319, August 2002. ISSN 0895-7177. doi: 10.1016/S0895-7177(02)00127-9. URL https://www.sciencedirect.com/science/article/pii/S0895717702001279.

[49] Sergei V Petrovskii and Horst Malchow. Critical phenomena in plankton communities: KISS model revisited. Nonlinear Analysis: Real World Applications, 1(1):37–51, March 2000. ISSN 1468-1218. doi: 10.1016/S0362-546X(99)00392-2. URL https://www.sciencedirect.com/science/article/pii/S0362546X99003922.

[50] MR Owen and MA Lewis. How predation can slow, stop or reverse a prey invasion. Bulletin of mathematical biology, 63(4):655–684, 2001.

[51] Steven R. Dunbar. Traveling Wave Solutions of Diffusive Lotka-Volterra Equations: A Heteroclinic Connection in R4. Transactions of the American Mathematical Society, 286(2):557–594, 1984. ISSN 0002-9947. doi: 10.2307/1999810. URL https://www.jstor.org/stable/1999810. Publisher: American Mathematical Society.

[52] Wenzhang Huang. Traveling Wave Solutions for a Class of Predator–Prey Systems. Journal of Dynamics and Differential Equations, 24(3):633–644, September 2012. ISSN 1572-9222. doi: 10.1007/s10884-012-9255-4. URL https://doi.org/10.1007/s10884-012-9255-4.

[53] Sergei V. Petrovskii and Horst Malchow. Wave of Chaos: New Mechanism of Pattern Formation in Spatio-temporal Population Dynamics. Theoretical Population Biology, 59(2):157–174, March 2001. ISSN 00405809. doi: 10.1006/tpbi.2000.1509. URL https://linkinghub.elsevier.com/retrieve/pii/S0040580900915090.

[54] M. G. Roberts. A pocket guide to host-parasite models. Parasitology Today (Personal Ed.), 11(5):172–177, May 1995. ISSN 0169-4758. doi: 10.1016/0169-4758(95)80150-2.

[55] A. J. Nicholson and V. A. Bailey. The Balance of Animal Populations.—Part I. Proceedings of the Zoological Society of London, 105(3): 551–598, September 1935. ISSN 0370-2774. doi: 10.1111/j.1096-3642.1935.tb01680.x. URL https://onlinelibrary.wiley.com/doi/10.1111/j.1096-3642.1935.tb01680.x.

[56] R. W. Wright and Alan Hastings. Spontaneous Patchiness in a Host-Parasitoid Integrodifference Model. Bulletin of Mathematical Biology, 69(8): 2693–2709, November 2007. ISSN 1522-9602. doi: 10.1007/s11538-007-9236-7. URL https://doi.org/10.1007/s11538-007-9236-7.

[57] Frithjof Lutscher and Tzvia Iljon. Competition, facilitation and the Allee effect. Oikos, 122(4):621–631, 2013. ISSN 1600-0706. doi: 10.1111/j.1600-0706.2012.20222.x. URL https://onlinelibrary.wiley.com/doi/abs/10.1111/j.1600-0706.2012.20222.x. _eprint: https://onlinelibrary.wiley.com/doi/pdf/10.1111/j.1600-0706.2012.20222.x.

[58] Kayla R. S. Hale and Fernanda S. Valdovinos. Ecological theory of mutualism: Robust patterns of stability and thresholds in two-species population models. Ecology and Evolution, 11(24):17651–17671, 2021. ISSN 2045-7758. doi: 10.1002/ece3.8453. URL https://onlinelibrary.wiley.com/doi/abs/10.1002/ece3.8453. _eprint: https://onlinelibrary.wiley.com/doi/pdf/10.1002/ece3.8453.

[59] Daniel R. Amor, Raúl Montañez, Salva Duran-Nebreda, and Ricard Solé. Spatial dynamics of synthetic microbial mutualists and their parasites. PLoS Computational Biology, 13(8):e1005689, August 2017. ISSN 1553-734X. doi: 10.1371/journal.pcbi.1005689. URL https://www.ncbi.nlm.nih.gov/pmc/articles/PMC5584972/.

[60] David Tilman and others. Mechanisms of plant competition for nutrients: the elements of a predictive theory of competition. Mechanisms of plant competition for nutrients: the elements of a predictive theory of competition., pages 117–141, 1990.

[61] RD Holt and ME Hochberg. Indirect interactions, community modules and biological control: a theoretical perspective. Evaluating indirect ecological effects of biological control, pages 13–37, 2001.

[62] G A Polis, C A Myers, and R D Holt. The Ecology and Evolution of Intraguild Predation: Potential Competitors That Eat Each Other. Annual Review of Ecology and Systematics, 20(1):297–330, 1989. doi: 10.1146/annurev.es.20.110189.001501. URL https://doi.org/10.1146/annurev.es.20.110189.001501. _eprint: https://doi.org/10.1146/annurev.es.20.110189.001501.

[63] Robert D Holt and Gary A Polis. A theoretical framework for intraguild predation. The American Naturalist, 149(4):745–764, 1997.

[64] Christina A Cobbold, Frithjof Lutscher, and Brian Yurk. Bridging the scale gap: Predicting large-scale population dynamics from small-scale variation in strongly heterogeneous landscapes. Methods in Ecology and Evolution, 13(4):866–879, 2022.

[65] Renato Andrade and Christina A. Cobbold. Heterogeneity in Behaviour and Movement can Influence the Stability of Predator–Prey Periodic Travelling Waves. Bulletin of Mathematical Biology, 85(1):1, November 2022. ISSN 1522-9602. doi: 10.1007/s11538-022-01101-8. URL https://doi.org/10.1007/s11538-022-01101-8.

[66] Gabriel Andreguetto Maciel and Frithjof Lutscher. Movement behaviour determines competitive outcome and spread rates in strongly heterogeneous landscapes. Theoretical Ecology, 11:351–365, 2018.

[67] Gary A. Polis and Robert D. Holt. Intraguild predation: The dynamics of complex trophic interactions. Trends in Ecology & Evolution, 7(5):151–154, May 1992. ISSN 0169-5347. doi: 10.1016/0169-5347(92)90208-S. URL https://www.sciencedirect.com/science/article/pii/016953479290208S.

[68] Quenton M. Tuckett, Amy E. Deacon, Douglas Fraser, Timothy J. Lyons, Katelyn␣M. Lawson, and Jeffrey E. Hill. Unstable intraguild predation causes establishment failure of a globally invasive species. Ecology, 102 (8):e03411, 2021. ISSN 1939-9170. doi: 10.1002/ecy.3411. URL https://onlinelibrary.wiley.com/doi/abs/10.1002/ecy.3411. _eprint: https://onlinelibrary.wiley.com/doi/pdf/10.1002/ecy.3411.

[69] M. Montserrat, S. Magalhães, M. W. Sabelis, A. M. de Roos, and A. Janssen. Invasion success in communities with reciprocal in-

traguild predation depends on the stage structure of the resident population. Oikos, 121(1):67–76, 2012. ISSN 1600-0706. doi: 10.1111/j.1600-0706.2011.19369.x. URL https://onlinelibrary.wiley.com/doi/abs/10.1111/j.1600-0706.2011.19369.x. _eprint: https://onlinelibrary.wiley.com/doi/pdf/10.1111/j.1600-0706.2011.19369.x.

[70] Thomas H. Fritts and Gordon H. Rodda. THE ROLE OF INTRODUCED SPECIES IN THE DEGRADATION OF ISLAND ECOSYSTEMS: A Case History of Guam. Annual Review of Ecology and Systematics, 29(1):113–140, November 1998. ISSN 0066-4162. doi: 10.1146/annurev.ecolsys.29.1.113. URL https://www.annualreviews.org/doi/10.1146/annurev.ecolsys.29.1.113.

[71] E. D. Grosholz and G. M. Ruiz. Spread and potential impact of the recently introduced European green crab, Carcinus maenas, in central California. Marine Biology, 122(2):239–247, April 1995. ISSN 1432-1793. doi: 10.1007/BF00348936. URL https://doi.org/10.1007/BF00348936.

[72] Gary A. Polis, Wendy B. Anderson, and Robert D. Holt. Toward an Integration of Landscape and Food Web Ecology: The Dynamics of Spatially Subsidized Food Webs. Annual Review of Ecology and Systematics, 28(1):289–316, 1997. doi: 10.1146/annurev.ecolsys.28.1.289. URL https://doi.org/10.1146/annurev.ecolsys.28.1.289. _eprint: https://doi.org/10.1146/annurev.ecolsys.28.1.289.

[73] Peter A Abrams. Habitat choice in predator-prey systems: spatial instability due to interacting adaptive movements. The American Naturalist, 169(5): 581–594, 2007.

[74] C. A. Klausmeier and D. Tilman. Spatial Models of Competition. In Ulrich Sommer and Boris Worm, editors, Competition and Coexistence, Ecological Studies, pages 43–78. Springer, Berlin, Heidelberg, 2002. ISBN 978-3-642-56166-5. doi: 10.1007/978-3-642-56166-5_3. URL https://doi.org/10.1007/978-3-642-56166-5_3.

[75] Min Ming Tang and Paul C. Fife. Propagating fronts for competing species equations with diffusion. Archive for Rational Mechanics and Analysis, 73

(1):69–77, March 1980. ISSN 1432-0673. doi: 10.1007/BF00283257. URL https://doi.org/10.1007/BF00283257.

[76] Horst Malchow. Spatio-temporal pattern formation in nonlinear non-equilibrium plankton dynamics. Proceedings of the Royal Society of London. Series B: Biological Sciences, 251(1331):103–109, January 1997. doi: 10.1098/rspb.1993.0015. URL https://royalsocietypublishing.org/doi/10.1098/rspb.1993.0015. Publisher: Royal Society.

[77] CJ Bampfylde and MA Lewis. Biological control through intraguild predation: case studies in pest control, invasive species and range expansion. Bulletin of Mathematical biology, 69:1031–1066, 2007.

[78] Robert Stephen Cantrell, Chris Cosner, and William F. Fagan. Competitive reversals inside ecological reserves: the role of external habitat degradation. Journal of Mathematical Biology, 37(6):491–533, December 1998. ISSN 0303-6812, 1432-1416. doi: 10.1007/s002850050139. URL http://link.springer.com/10.1007/s002850050139.

[79] Priyanga Amarasekare. Spatial dynamics of communities with intraguild predation: the role of dispersal strategies. The American Naturalist, 170(6): 819–831, 2007.

[80] S. V. Petrovskii and H. Malchow. A minimal model of pattern formation in a prey-predator system. Mathematical and Computer Modelling, 29(8):49–63, April 1999. ISSN 0895-7177. doi: 10.1016/S0895-7177(99)00070-9. URL https://www.sciencedirect.com/science/article/pii/S0895717799000709.

[81] Robert A. Armstrong and Richard McGehee. Competitive Exclusion. The American Naturalist, 115(2):151–170, 1980. ISSN 0003-0147. URL https://www.jstor.org/stable/2460592. Publisher: [University of Chicago Press, American Society of Naturalists].

[82] Gabriel Maciel, Chris Cosner, Robert Stephen Cantrell, and Frithjof Lutscher. Evolutionarily stable movement strategies in reaction–diffusion models with edge behavior. Journal of mathematical biology, pages 1–32, 2018.

[83] Robert D. Holt and Michael B. Bonsall. Apparent Competition. Annual Review of Ecology, Evolution, and Systematics, 48(1):447–

471, November 2017. ISSN 1543-592X, 1545-2069. doi: 10.1146/annurev-ecolsys-110316-022628. URL https://www.annualreviews.org/doi/10.1146/annurev-ecolsys-110316-022628.

[84] Benjamin L Phillips, Gregory P Brown, Justin MJ Travis, and Richard Shine. Reid's paradox revisited: the evolution of dispersal kernels during range expansion. the american naturalist, 172(S1):S34–S48, 2008.

[85] Richard Shine, Gregory P Brown, and Benjamin L Phillips. An evolutionary process that assembles phenotypes through space rather than through time. Proceedings of the National Academy of Sciences, 108(14):5708–5711, 2011.

[86] Ben L Phillips and T Alex Perkins. Spatial sorting as the spatial analogue of natural selection. Theoretical Ecology, 12(2):155–163, 2019.

[87] Emeric Bouin, Vincent Calvez, Nicolas Meunier, Sepideh Mirrahimi, Benoît Perthame, Gaël Raoul, and Raphaël Voituriez. Invasion fronts with variable motility: Phenotype selection, spatial sorting and wave acceleration. Comptes Rendus Mathematique, 350(15):761–766, 2012. ISSN 1631-073X. doi: https://doi.org/10.1016/j.crma.2012.09.010. URL https://www.sciencedirect.com/science/article/pii/S1631073X12002543.

[88] Emeric Bouin, Matthew H Chan, Christopher Henderson, and Peter S Kim. Influence of a mortality trade-off on the spreading rate of cane toads fronts. Communications in Partial Differential Equations, 43(11):1627–1671, 2018.

[89] Vincent A Keenan and Stephen J Cornell. Anomalous invasion dynamics due to dispersal polymorphism and dispersal–reproduction trade-offs. Proceedings of the Royal Society B, 288(1942):20202825, 2021.

[90] Aled Morris, Luca Börger, and Elaine Crooks. Individual Variability in Dispersal and Invasion Speed. Mathematics, 7(9), 2019. ISSN 2227-7390. doi: 10.3390/math7090795. URL https://www.mdpi.com/2227-7390/7/9/795.

[91] Sebastian J Schreiber and Noelle G Beckman. Individual variation in dispersal and fecundity increases rates of spatial spread. AoB Plants, 12(3):plaa001, 2020.

[92] Frithjof Lutscher, Lea Popovic, and Allison K Shaw. How mutation shapes the rate of population spread in the presence of a mate-finding Allee effect. Theoretical Ecology, pages 1–15, 2022.

[93] Gregory S Clarke, Richard Shine, and Benjamin L Phillips. May the (selective) force be with you: spatial sorting and natural selection exert opposing forces on limb length in an invasive amphibian. Journal of evolutionary biology, 32(9):994–1001, 2019.

[94] Matthieu Alfaro, Jérôme Coville, and Gaël Raoul. Travelling waves in a nonlocal reaction-diffusion equation as a model for a population structured by a space variable and a phenotypic trait. Communications in Partial Differential Equations, 38(12):2126–2154, 2013.

[95] Matthieu Alfaro, Henri Berestycki, and Gaël Raoul. The effect of climate shift on a species submitted to dispersion, evolution, growth, and nonlocal competition. SIAM Journal on Mathematical Analysis, 49(1):562–596, 2017.

[96] Matthieu Alfaro, Léo Girardin, Francois Hamel, and Lionel Roques. When the Allee threshold is an evolutionary trait: persistence vs. extinction. Journal de Mathématiques Pures et Appliquées, 155:155–191, 2021.

[97] Elizabeth C Elliott and Stephen J Cornell. Dispersal polymorphism and the speed of biological invasions. PloS one, 7(7):e40496, 2012.

[98] Nathan G Marculis, Maya L Evenden, and Mark A Lewis. Modeling the dispersal–reproduction trade-off in an expanding population. Theoretical population biology, 134:147–159, 2020.

[99] James M Bullock and Ralph T Clarke. Long distance seed dispersal by wind: measuring and modelling the tail of the curve. Oecologia, 124(4):506–521, 2000.

[100] Joseph P Stover, Bruce E Kendall, and Roger M Nisbet. Consequences of dispersal heterogeneity for population spread and persistence. Bulletin of Mathematical Biology, 76(11):2681–2710, 2014.

[101] John FC Kingman. A simple model for the balance between selection and mutation. Journal of Applied Probability, 15(1):1–12, 1978.

[102] Quentin Griette. Singular measure traveling waves in an epidemiological model with continuous phenotypes. Transactions of the American Mathematical Society, 371(6):4411–4458, 2019.

[103] Michael Doebeli. A quantitative genetic competition model for sympatric speciation. Journal of evolutionary biology, 9(6):893–909, 1996.

[104] Robert M May. Stability and complexity in model ecosystems. In Stability and Complexity in Model Ecosystems. Princeton University Press, 2019.

[105] Xing Liang and Xiao-Qiang Zhao. Asymptotic speeds of spread and traveling waves for monotone semiflows with applications. Communications on Pure and Applied Mathematics, 60(1):1–40, January 2007. ISSN 00103640, 10970312. doi: 10.1002/cpa.20154. URL https://onlinelibrary.wiley.com/doi/10.1002/cpa.20154.

[106] Mark Grigor'evich Krein and Mark A Rutman. Linear operators leaving invariant a cone in a Banach space. Uspekhi mat. nauk, 3(1):3–95, 1948.

[107] Lee Altenberg. Resolvent positive linear operators exhibit the reduction phenomenon. Proceedings of the National Academy of Sciences, 109(10): 3705–3710, 2012.

[108] Horst R Thieme. Spectral bound and reproduction number for infinite-dimensional population structure and time heterogeneity. SIAM Journal on Applied Mathematics, 70(1):188–211, 2009.

[109] Samuel Karlin. Classifications of selection-migration structures and conditions for a protected polymorphism. Evol. Biol, 14(61):204, 1982.

[110] Joel E Cohen. Convexity of the dominant eigenvalue of an essentially nonnegative matrix. Proceedings of the American Mathematical Society, 81 (4):657–658, 1981.

[111] Hans F Weinberger, Mark A Lewis, and Bingtuan Li. Anomalous spreading speeds of cooperative recursion systems. Journal of mathematical biology, 55:207–222, 2007.

[112] Samuel Karlin and James McGregor. Towards a theory of the evolution of modifier genes. Theoretical population biology, 5(1):59–103, 1974.

[113] Alan Hastings. Can spatial variation alone lead to selection for dispersal? Theoretical Population Biology, 24(3):244–251, 1983.

[114] Chris Cosner. Reaction-diffusion-advection models for the effects and evolution of dispersal. Discrete & Continuous Dynamical Systems, 34(5):1701, 2014.

[115] Nicholas F Britton. Spatial structures and periodic travelling waves in an integro-differential reaction-diffusion population model. SIAM Journal on Applied Mathematics, 50(6):1663–1688, 1990.

[116] MA Fuentes, MN Kuperman, and VM Kenkre. Nonlocal interaction effects on pattern formation in population dynamics. Physical review letters, 91 (15):158104, 2003.

[117] Olivia J Burton, Ben L Phillips, and Justin MJ Travis. Trade-offs and the evolution of life-histories during range expansion. Ecology letters, 13(10): 1210–1220, 2010.

[118] Stephen P Ellner, Dylan Z Childs, Mark Rees, and others. Data-driven modelling of structured populations. A practical guide to the Integral Projection Model. Cham: Springer, 2016.

[119] Horst R Thieme. Density-dependent regulation of spatially distributed populations and their asymptotic speed of spread. Journal of Mathematical Biology, 8(2):173–187, 1979.

[120] Jong-Shenq Guo, Ken-Ichi Nakamura, Toshiko Ogiwara, and Chin-Chin Wu. Traveling wave solutions for a predator–prey system with two predators and one prey. Nonlinear Analysis: Real World Applications, 54:103111, August 2020. ISSN 1468-1218. doi: 10.1016/j.nonrwa.2020.103111. URL https://www.sciencedirect.com/science/article/pii/S1468121820300298.

[121] Yan-Li Huang and Guo Lin. Traveling wave solutions in a diffusive system with two preys and one predator. Journal of Mathematical Analysis and Applications, 418(1):163–184, October 2014. ISSN 0022-247X. doi: 10.1016/j.jmaa.2014.03.085. URL https://www.sciencedirect.com/science/article/pii/S0022247X14003345.

[122] Jian-Jhong Lin and Ting-Hui Yang. Traveling wave solutions for a diffusive three-species intraguild predation model. International Journal of Biomathematics, 11(02):1850022, February 2018. ISSN 1793-5245. doi: 10.1142/S1793524518500225. URL https://www.worldscientific.com/doi/10.1142/S1793524518500225. Publisher: World Scientific Publishing Co.

[123] Lauren G. Shoemaker, Jonathan A. Walter, Laureano A. Gherardi, Melissa H. DeSiervo, and Nathan I. Wisnoski. Writing mathematical ecology: A guide for authors and readers. Ecosphere, 12(8): e03701, 2021. ISSN 2150-8925. doi: 10.1002/ecs2.3701. URL https://onlinelibrary.wiley.com/doi/abs/10.1002/ecs2.3701. _eprint: https://onlinelibrary.wiley.com/doi/pdf/10.1002/ecs2.3701.

[124] Allison K. Shaw and Hanna Kokko. Mate finding, Allee effects and selection for sex-biased dispersal. The Journal of Animal Ecology, 83(6):1256–1267, November 2014. ISSN 1365-2656. doi: 10.1111/1365-2656.12232.

[125] Cameron M. Hudson, Gregory P. Brown, and Richard Shine. It is lonely at the front: contrasting evolutionary trajectories in male and female invaders. Royal Society Open Science, 3(12):160687, December 2016. doi: 10.1098/rsos.160687. URL https://royalsocietypublishing.org/doi/full/10.1098/rsos.160687. Publisher: Royal Society.

[126] Crystal Kelehear and Richard Shine. Non-reproductive male cane toads (Rhinella marina) withhold sex-identifying information from their rivals. Biology Letters, 15(8):20190462, August 2019. doi: 10.1098/rsbl.2019.0462. URL https://royalsocietypublishing.org/doi/10.1098/rsbl.2019.0462. Publisher: Royal Society.

[127] Luděk Berec, Andrew M. Kramer, Veronika Bernhauerová, and John M. Drake. Density-dependent selection on mate search and evolution of Allee effects. The Journal of Animal Ecology, 87(1):24–35, January 2018. ISSN 1365-2656. doi: 10.1111/1365-2656.12662.

[128] Brad M. Ochocki, Julia B. Saltz, and Tom E. X. Miller. Demography-Dispersal Trait Correlations Modify the Eco-Evolutionary Dynamics of Range Expansion. The American Naturalist, 195(2):231–246, February 2020. ISSN 0003-0147. doi: 10.1086/706904. URL https://www.journals.uchicago.

edu/doi/abs/10.1086/706904. Publisher: The University of Chicago Press.

[129] Stephen Dewitt Fretwell. On territorial behavior and other factors influencing habitat distribution in birds. Technical report, North Carolina State University. Dept. of Statistics, 1969.

[130] Silas Poloni and Frithjof Lutscher. Integrodifference models for evolutionary processes in biological invasions. Journal of Mathematical Biology, 87(1): 10, June 2023. ISSN 1432-1416. doi: 10.1007/s00285-023-01947-z. URL https://doi.org/10.1007/s00285-023-01947-z.